The interaction between melt, deformation and recrystallization within northern Fiordland, New Zealand

James Robert Smith

Presented to the Department of Earth and Planetary Sciences,
Faculty of Science in Partial Fulfillment of the Requirements
for the Degree of

Honours, BSc
Macquarie University, Sydney
November, 2012

Statement of Originality

All the work submitted in this thesis is the original work of the author except were otherwise acknowledged. No part of this thesis has previously been submitted to any other university or institution.

_____ _____

Signed – *James Robert Smith* ***Dated***

Acknowledgements

This year has been incredibly rewarding and it would not have been nearly as enjoyable without everyone who has helped me along the way. Without the continual support from people within the department, work, friends and family, I would not have made it through this year with such enjoyment.

Firstly, I would like to thank my two supervisors, Nathan Daczko and Sandra Piazolo. Nathan, for his endless support, genuine enthusiasm for my topic and advice throughout the year, has been a continual source of motivation. Sandra for her constant advice, support and assistance throughout the year, this has greatly improved my thesis. I am incredibly lucky to have Nathan and Sandra as my supervisors; without them I do not think I would have loved my project as much.

Thank you to James Scott for his help during field work as well as the Department of Conservation for allowing access to the Pembroke Valley. A big thankyou to the department for funding access to GAU. This has greatly improved my skills set.

Thank you to all the academic and laboratory staff that have helped me throughout this year. Thank you to Dick Flood for his help throughout my undergraduate degree and teaching me the basics of geology. Norman Pearson, his continual open door policy throughout this whole year has been greatly appreciated. Norman has helped develop my geochemical skills throughout the whole year. Kevin Grant, his continual help and patience within the lab. Kevin made my time on the instruments a lot more enjoyable and efficient. Thank you to Will Powell for his help with laser ablation. Manal Bebbington for help in making all my thin sections, even if it seemed like I had a never ending supply. Tracy Rushmer, for her interest in my topic and taking the time to discuss problems I could aim to solve. A big thank you to all other academic staff that have played a role throughout my undergraduate degree and this year, if it wasn't for everyone in the department I would not be here writing acknowledgements for an honours thesis.

A special thank you to Rachel. Her continual motivation and captivating passion for geology and research has helped keep me motivated this year. You have put up with all my highs and lows and I thank you for that.

To all the honours students that have helped me this year: Ristch Camille, Alex Tickle, Madeline Kobler, Cait Stuart and Vicki Beecher and everyone else, thank you for all your support. A big thank you to all my non-geology friends for their support and understanding if I was absent for most of this year.

Last but not least, my family. Thank you for supporting me this whole year, I will now come out of hiding! Mum and Dad, I cannot put into words how thankful I am for all their support during my whole academic experience, from school to university. The amount of opportunities you have given me has helped give me the necessary skills to get through a year like this. To Nanny, for continually thinking of me during this whole year, hoping things go well. To my brother and sister, motivating me to get up and swim every morning. Sport has kept me sane this year. For all your love and support, thank you!

It is a good feeling being able to write over a page of acknowledgements with ease. Writing this has made me realise how many people have helped me along the way and I know it would not have been nearly as enjoyable or rewarding if I didn't have so many people to thank. For everyone acknowledged and those that have not been mentioned – Thank you!

Abstract

Well-exposed granulite facies gabbroic rocks from the Pembroke Valley, Fiordland, southern New Zealand provide a unique opportu to study lower crustal processes. Their microstructural and ological evolution has been studied to understand factors resulting in strain localisation. Granulite facies assemblage of two-pyroxene-hornblende transitions to two-pyroxene garnet either side of felsic dyke intrusions resulting in garnet reaction zones. These garnet reaction zones can be further deformed by mylonitic shear zones which are sometimes localised to the outer region of these garnet reaction zones. As such they are termed "paired shear zones". Distinct microstructural changes are essential to result in a rheological contrast promoting strain localization that results in the formation of a paired shear zone. Dykes consist of a similar mineralogy with slight variations of plagioclase, quartz and K-feldspar. Major and trace element analysis indicates subtle variation between dykes. Therefore the degree of garnet reaction zone recrystallization is affected by the ~~time~~ of dyke influence i.e. as a result of melt flowing through an open dyke. Consequently garnet reaction zones can be partially recrystalli due to short dyke influence or extensively recrystallized due to a longer influence. SEM-EBSD analysis provides confirmation that these replacement reactions have occurred under static conditions and garnet mimics the orientation of the pre-existing phase. Therefore lower degrees of static recrystallization will result in partially recrystallized garnet reaction zones which display varied anorthite content due to the presence of relict (igneous) plagioclase grains. ~~Whereas~~ extensively recrystallized garnet reaction zones displays homogenous anorthite content and an increase in garnet abundance close to the dyke. This recrystallization results in the replacement of pre-existing minerals, observed in the trace element patterns. Extensive recrystallization also results in an increased garnet abundance and a harder bulk rock. Later mylonitic shear zones are only localized at the border between extensively recrystallized garnet reaction zones and the surrounding country rock. At these borders a maximum rheological contrast is present resulting in strain localisation, responsible for the formation of paired shear zones.

Abbreviations

Alm	Almandine
An	Anorthite
Ap	Apatite
Bt	Biotite
Cpx	Clinopyroxene
D1	Deformation event 1
D2	Deformation event 2
D3	Deformation event 3
D4	Deformation event 4
EMP	Electron microprobe
GAU	Geochemical Analysis Unit
GEMOC	Geochemical Evolution and Metallogeny of Continents
GLITTER	GEMOC Laser ICPMS Total Trace Element Reduction
Grs	Grossular
Grt	Garnet
GRZ	Garnet Reaction Zone
Hbl	Hornblende
HREE	Heavy rare earth element
Ilm	Ilmenite
Kfs	K-feldspar
LA-ICP-MS	Laser ablation microprobe-inductively coupled plasma mass spectrometry
LLD	Lower Limit of Detection
LPO	Lattice preferred orientation
LREE	Light rare earth element
Opx	Orthopyroxene
Pl	Plagioclase
PPL	Plain Ploarised Light
Pyp	Pyrope
Qtz	Quartz
REE	Rare earth element
Rt	Rutile
Scp	Scapolite
SEM	Scanning Electron Microscope
Sps	Spessertine
St.Dev	Standard deviation
XPL	Cross Polarised Light

Table of Contents

Chapter 1: Regional Geology, Garnet Reaction Zone Formation and Shear zone Phenomena **1**

1.1 Introduction and aim of study 1

1.2 Regional Geology 2

1.3 Garnet Reaction Zones 6

1.4 Paired Shear Zones 8

1.5 Static and Dynamic Recrystallization Microstructures 10

Chapter 2: Field Work and Sample Selection **11**

2.1 Fieldwork 11

Chapter 3: Methods **15**

3.1 Petrography 15

3.2 Major Element Mineral Chemistry: Scanning Electron Microscopy – Energy Dispersive Spectrometry (SEM–EDS) 15

3.3 Trace Element Mineral Chemistry: Laser Ablation Inductively Coupled Plasma Mass Spectrometry (LA-ICP-MS) 16

3.4 Scanning Electron Microscopy – Electron Backscatter Diffraction (SEM-EBSD) 18

Chapter 4: Petrography **19**

4.1 Domain 1: Host two-pyroxene-hornblende gabbroic gneiss 20

4.2 Domain 2: Dyke 24

4.3 Gabbroic gneiss – Garnet Reaction Zones 30

4.3.1 Partially Recrystallized Garnet Reaction Zones 31

4.3.2 Extensively Recrystallized Garnet Reaction Zones 35

4.4 D3 Shear zone 43

4.5 Summary and Interpretation 45

Chapter 5: Major Element Chemistry: Scanning Electron Microscopy – Energy-Dispersive Spectroscopy (SEM-EDS) 47

5.2 Results 48

5.2.1 Plagioclase mineral chemistry 48

5.2.2 Garnet mineral chemistry 60

5.3 Discussion 63

5.4 Summary 67
Chapter 6: Trace Element Mineral Chemistry: Laser Ablation Inductively Coupled Plasma Mass Spectrometry (LA-ICP-MS) **69**
6.1 Introduction 69
6.2 Results 70
6.2.1 Domain 2 70
6.2.2 Domain 3 72
6.2.3 Domain 4 76
6.3 Discussion 79
6.4 Summary 81
Chapter 7: SEM – Electron Back-scatter Diffraction (EBSD) **82**
7.1 Introduction 82
7.2 Results 83
7.3 Discussion 97
7.4 Summary 98
Chapter 8: Summary and Conclusion **99**
Chapter 9: Future Research **102**
References **103**
Appendices **106**
Appendix A: Petrographic descriptions .....
Appendix B: X_{An} transects .....
CD – All major element data .....
Appendix C: Major and trace element data .....
CD – All trace element data .....
Appendix D: EBSD data (maps and pole plots) .....

List of Figures

Chapters 1 and 2:

Figure 1: Example of a paired shear zone in-situ within the Pembroke Valley. A garnet reaction zone has formed either side of the dyke and strain has then localised on the outer regions of this reaction zone. 2

Figure 2: Regional geology of Fiordland displaying the western, median batholith and eastern provinces in detail. Area of study (highlighted yellow and numbered 1) is shown as well as other regions of studied garnet reaction zones. Modified from (Allibone et al., 2009; Clarke et al., 2005)..... 3

Figure 3: Typical garnet reaction zone either side of a felsic dyke. Typical garnet reaction zones are 3 – 10cm in width. Note some without an obvious dyke due to their collapse. 4

Figure 4: Block diagrams of the first three key deformation events within the Pembroke Valley. D1 resulted in gneissic foliation (S1), D2 resulted in fracturing and intrusion of felsic dykes resulting in garnet reaction zones (GRZ) and D3 resulted in east striking mylonite shear zones. Modified from Clarke, et al. (2000)..... 5

Figure 5: Poles to D2 deformation event. Source: Figure 2 Daczko et al. 2001b 7

Figure 6: Pembroke Valley with a view of the creek and in the distance, Milford Sound. Samples were collected within the creek, after looking at in-situ features. ... 11

Chapter 4

Figure 4.1: Field photo (left) with highlighted domains within thin section (right). Thin section comprises of domain 1 (host S1 assemblage), domain 2 (dyke) and domain 3 (garnet reaction zone) 19

Figure 4.1.1: Typical two-pyroxene-hornblende gabbroic gneiss. Photomicrograph of sample 1237AB, PPL and XPL base of photo 4.4mm. Host assemblage with orthopyroxene surrounded by an inner corona symplectite of elongate hornblende grains (green mineral) and quartz (clear mineral). Outer corona is hornblende..... 20

Figure 4.1.2: Typical host assemblage back scatter electron image (BSE) of sample 1234a. Host assemblage corona with clinopyroxene (centre), inner corona symplectite of quartz and hornblende and then an outer corona of hornblende. Note ilmenite exsolutions. 21

Figure 4.1.3: Photomicrograph displaying symplectite of cpx and qtz around orthopyroxene. Photo is from sample 1230 displaying PPL and XPL. Base of photo 4.4mm. 21
Figure 4.1.4: Photomicrograph displaying kyanite disequilibrium texture. Photo is from sample 1237AB displaying PPL (left) and XPL (right). Base of photo 4.4mm. 22
Figure 4.2.1: Typical dyke composition with dyke and wall rock garnet. Note high abundance of quartz and plagioclase. Undulose extinction can be seen within quartz. Photomicrograph of sample PV1222a PPL (left) and XPL (right).
Base of photo 5mm. 25
Figure 4.2.2: SEM photomicrograph of K-feldspar abundance close to the dyke within sample 1230. Light grey colour is K-feldspar with the highest abundance close to the quartz rich dyke. 26
Figure 4.2.3: SEM photomicrograph of K-feldspar between two garnet grains. Red arrows indicate low di-hedral angle. Base of photo is 500µm. 27
Figure 4.2.4: SEM photomicrograph of a typical 'collapsed' dyke within sample 1217c2. Line of scapolite (light grey) and quartz (dark grey) with minor K-feldspar indicating region of previous dyke. 28
Figure 4.2.5: PPL photograph of 'collapsed' dyke within sample PV1230. Slight offsets of garnet reaction zones can be observed during dyke closure. Base of photo is 6.5mm. 28
Figure 4.3.1: Photomicrograph of a typical partially recrystallized garnet reaction zone from sample 1222a, PPL and XPL. Base of photo is 8.6mm. Elongate minerals of orthopyroxene and clinopyroxene with garnet recrystallization around pyroxene. Light coloured minerals consist of kyanite, quartz and powdery plagioclase which comprises of relict and neoblast grains. 31
Figure 4.3.2: SEM photo of a typical garnet reaction zone assemblage. Orthopyroxene (large left mineral) and clinopyroxene (large right mineral) show exsolution of ilmenite. Pyroxenes are surrounded by garnet which contains quartz and clinopyroxene inclusions (dark greys). 32
Figure 4.3.3: Photomicrograph of typical mafic cluster within garnet reaction zones from sample 1217a. PPL (left) and XPL (right) and base of photo is 4.4mm. Clinopyroxene (left green mineral) consisting of opaque inclusions as well as orthopyroxene. Clinopyroxene consists of a mafic cluster and twinning. Both

pyroxenes consist of an outer corona of garnet and an inner corona of clinopyroxene and quartz symplectite. 32
Figure 4.3.4: Photomicrograph of idioblastic grain boundaries of garnet into plagioclase. Photo is from sample 1217c1, PPL and XPL base of photo 4.4mm. 33
Figure 4.3.5: SEM photomicrograph of idioblastic grain boundaries of garnet growing into the plagioclase region. Contains slow growths with no quartz inclusions and inclusion rich fast growths close to pyroxene. Photo is from sample PV1230. ... 33
Figure 4.3.6: Photomicrograph of typical feldspar microstructures. Sample 1217a, PPL and XPL base of photo 0.87mm. Kyanite overgrowths are shown in PPL. Within XPL serrated boundaries can be seen due to grain boundary migration. Kink bands and tapered twins are also present. 34
Figure 4.3.7: Photomicrograph of sample 1217c1 PPL and XPL base of photo 4.4mm. Rutile is overgrown over garnet within the reaction zone. 35
Figure 4.3.8: SEM photo of extensively recrystallised sample PV1216a. Garnet and clinopyroxene rich with no S1 assemblage. 36
Figure 4.3.9: SEM photo of extensively recrystallised sample PV1239 at the intersection of two dykes. Garnet rich with no S1 assemblage 36
Fig 4.3.10: PV1216a garnet grain size and feldspar recrystallization depending on location with the dyke. 37
Figure 4.3.11: Visual estimate of garnet modal percentages depending on distance from the dyke. High abundance of garnet close to the dyke. 38
Figure 4.3.12: Photomicrograph of sample 1217b PPL and XPL base of photo 4.4mm. Lathe like crystals of biotite within the mafic reaction zone assemblage. 39
Figure 4.4.1: Representative paired shear zone sample. High strain is localised on the outer regions of the garnet reaction zone. Red box represents area of thin section from sample PV1234b. Base of photo is 20cm. 43
Figure 4.4.2: Photomicrograph of sample 1217b PPL and XPL base of photo 4.4mm. Lathe like crystals of biotite within the mafic reaction zone assemblage. 44

Chapter 5

Figure 5.2.1: Plagioclase composition between different domains analysed. Data ranges from Oligoclase – Labradorite with an overall 40% spread. 48
Figure 5.2.2: Variation in plagioclase chemistry within domain 2. 50
Figure 5.2.3: Sample PV1211a variation in XAn content within transect PV1211a-T1. Range is 30 – 45%. Note analysis is over large and small plagioclase grains. 51

Figure 5.2.4: Variation of plagioclase between samples within domain 3 52
Figure 5.2.5: Transects within sample PV1222a. Variations in anorthite content from neoblast to relict plagioclase grains. Highlighted region represents relict plagioclase. 53
Figure 5.2.6: Transect within sample PV1230. Variations of anorthite content within sample PV1230 with a range of ~20% XAn. Highlighted region represents the relict plagioclase..... 54
Figure 5.2.7: Transect of sample PV1239 at the intersection of two dykes with ~10% variation in XAn content. 55
Figure 5.2.8: Transect within sample PV1216a. Highlighted region represents 'relict' plagioclase and the overall anorthite content varies by <10%. 56
Figure 5.2.9: Less deformed zone within paired shear zone sample PV1211a. Homogenised XAn content with <10% variation 57
Figure 5.1.10: Variation of plagioclase within shear zone 58
Figure 5.1.11: Homogeneous XAn content within the shear zone of PV1234b. 59
Figure 5.2.12: Ternary diagram of analysed dyke and wall garnet within PV1234b. Dyke garnet are more Grossular + Spessartine rich whereas wall rock garnet are more Pyrope + Almandine rich. 62
Fig 5.2.13: Ternary Diagram of Almandine-Pyrope-Grossular-Spessartine plotting garnet inclusion poor and inclusion rich regions. 63
Figure 5.2.14: Plagioclase composition of all analysed samples compared to literature data. Literature data ranges from Andesine to Oligoclase. 48
Figure 5.2.15: Garnet composition. Data plotted include data produced in this study and data from the previous work (see text for references). 65

Chapter 6

Figure 6.2.1: Varied dyke plagioclase composition between samples PV1234b and PV1222a. PV1234b is enriched in LREE and PV1222a is depleted in LREE. Both samples show a Eu anomaly. 71
Figure 6.2.2: Dyke and wall rock garnet REE signatures. Both samples of dyke garnet are enriched in HREE whereas the wall rock garnet analysed in PV1234b is depleted in HREE. 72
Figure 6.2.3: REE of relict S1 and recrystallized clinopyroxene from PV1222a and PV1234b. Recrystallized cpx has a similar pattern to the relict S1 grain although it is slightly more depleted in all REE. 73

Figure 6.2.4: REE signature of hornblende enriched in middle rare earth elements and depleted in heavy rare earth. 74
Figure 6.2.5: REE signature of plagioclase within the GRZ. All analyses have a similar pattern, enriched in LREE, with a characteristic Eu anomaly and depleted HREE. 75
Figure 6.2.6: REE signature of metamorphic garnet and dyke garnet within PV1222a and PV1234b. Both GRZ garnet samples display a similar pattern of enriched HREE excluding two analyses within PV1234b. 76
Figure 6.2.7: D3 shear zone garnet. Analysed samples are depleted in LREE contain a slight Eu anomaly, consistent with plagioclase and are depleted in the HREE. 77
Figure 6.2.8: Variation of (La/Sm)N vs Eu* [Eu* = EuN/√(SmN*GdN); subscript N indicates chondrite-normalized] presenting an increase in Eu for GRZ grt within PV1222a and post-D3 grt within PV1234b. Recrystallised cpx show no or little variation due to plagioclase (Eu). 78
Figure: 6.2.9: Variation of (Lu/Gd)N vs Eu* [Eu* = EuN/√(SmN*GdN); N indicates chondrite-normalized] presenting an increase in Eu for GRZ grt within PV1222a and post-D3 grt within PV1234b. Recrystallised cpx show no or little variation due to plagioclase (Eu). 79

Chapter 7

Figure 7.2.1: Contour plot of orthopyroxene, preferred alignment in the {001} and {010} planes 85
Figure 7.2.2: Contour plot of clinopyroxene, preferred alignment in the {001} plane. 86
Figure 7.2.3: Scatter pattern of hornblende poles to the {100}, {010} and {001} with two preferred orientations. Different colours represent different euler angles. 86
Figure 7.2.4: Contour plot showing LPO of hornblende to the {100}, {010} and {001} with two preferred orientations. White line indicates S1 foliation. 87
Figure 7.2.5: Alignment of an orthopyroxene grain aligned to the foliation (white line). 89
Figure 7.2.6: clinopyroxene alignment to the NE. White line indicates S1 foliation. 90

Figure 7.2.7: Scatter pattern of garnet poles to the {100}, {110} and {111}. Different colours represent different euler angles. Preferred orientations are present for garnets different planes. Circles represent some key preferred orientations. 90
Figure 7.2.8: Contour plot of garnet poles to the {100}, {110} and {111}. Preferred orientations are present. White line represents S1 foliation. 91
Figure 7.2.9: Contour plot of clinopyroxene. Preferred orientation within the plane {001}. White line indicates S1 foliation. 93
Figure 7.2.10: Scatter pattern of garnet poles to the {100}, {110} and {111}. Preferred orientations are within the three families. 93
Figure 7.2.11: Contour plot of garnet poles {100}, {110} and {111}. Preferred orientations are present. Note preferred orientation within {100} and {111}. White line indicates S1 foliation. 93
Figure 7.2.12: Scatter plot of plagioclase directions <100>, <010> and <001> 95
Figure 7.2.13: Contour plot of plagioclase directions <100>, <010> and <001>. Preferred orientations are present 95
Figure 7.2.14: Scatter plot of syn-D3 garnet. Different colours represent different euler angles. 96
Figure 7.2.15: Contour plot of syn-D3 garnet. No preferred orientation. 96
Figure 7.2.16: Scatter plot of post-D3 garnet within PV1234b 97
Figure 7.2.17: Contour plot of post-D3 garnet within PV1234b 97

Chapter 8

Figure 8: Proposed model for paired shear zone development. A, B and C represent three different deformation events. D1 resulted in the S1 gneissic foliation of two-pyroxene-hornblende gneiss. D2 resulted in felsic dykes and garnet reaction zone formation with different degrees of recrystallization and D3 resulted in east-striking mylonitic shear zones which can sometimes be localised as a paired shear zone. Modified from Clarke et al. (2000) 101

List of Tables

Table 2.1: Collected samples from the Pembroke Valley, detailing if a thin section was made and if yes, the methods used on each sample with their MU numbers. GRZ = garnet reaction zone. 12
Table 3.3: LA-ICP-MS operating conditions..... 16
Table 3.4: expected and obtained BCR2 values 17
Table 4.1: Domain 1 mode and descriptions of each sample..... 22
Table 4.2: Domain 2 (dyke) mode and proportion within each sample. GRZ = garnet reaction zone. 29
Table 4.3: Domain 3 (GRZ) mode and description of samples 39
Table 4.4: Modal proportions and comments for samples undergoing D3 shearing 44
Table 5.1: Minimum, maximum, average and standard deviation of anorthite content between analysed domains 49
Table 5.2: Range of Almandine composition within domains 60
Table 5.3: Range of Pyrope composition within domains..... 60
Table 5.4: Range of Grossular composition within domains..... 61
Table 5.5: Anorthite, albite and orthoclase values from published plagioclase EMP analyses..... 64
Table 5.6: Garnet core analysis from published EMP data..... 64
Table 7.1: Band contrast, euler angles and phases for domain 1 84
Table 7.2: Band contrast, all euler and phases for domain 3 within PV1222a 88
Table 7.3: Band contrast, all euler and phases for domain 3 within PV1216a 91
Table 7.4: Band contrast, all euler and phases for domain 4 within PV1234b..... 94

Chapter 1

Regional Geology, Garnet Reaction Zone Formation and Paired Shear zone Phenomena

1.1 Introduction and aim of study

This chapter introduces the key geological features of the study area in the Pembroke Valley, Fiordland, southern New Zealand, and states the aim of the study. This area of well exposed and preserved high-pressure metamorphic rocks contains spectacular planar domains of garnet granulite overprinting two-pyroxene-hornblende granulite gneisses; these features are called garnet reaction zones. Furthermore, very well developed paired shear zones spatially related to the garnet reaction zones are common in the area (Fig 1). Paired shear zones are a phenomenon resulting from localised strain on the outer regions of garnet reaction zones. The most recent model for the formation of the garnet reaction zones involves the transition to garnet granulite being driven by the interaction of the host two-pyroxene-hornblende gneiss with felsic dykes through dehydration melting. These garnet reaction zones are also present where there is no obvious dyke and these are inferred to have partially to wholly closed (Daczko and Halpin, 2009). This interpretation of dykes is controversial although the most recent publication by Daczko and Halpin (2009) termed these intrusions dykes; therefore this thesis will also use this term. The resulting microstructures with the interaction of these intruded dykes, resulting in paired shear zones has only been studied in general terms within granodiorites within South Tyrol, Italy (Mancktelow and Pennacchioni, 2005; Pennacchioni and Mancktelow, 2007) and requires further analysis and interpretation.

The aim of this thesis is ultimately to construct a model to explain the development of paired shear zones, observed either side of some garnet reaction zones (Fig 1). In order to develop such a model two main aims have to be considered:

1) Mechanism of GRZ formation: evidence for the stated dyke-controlled spatially restricted transition to garnet granulite, and
2) Microstructural and rheological consequence of garnet reaction zones during the subsequent deformation history of the rocks.

When considering these two aims, two minor aims must be considered:

1) Determine if areas with no obvious dyke are due to its collapse, and
2) Determine possible melt extraction textures within the garnet reaction zones

The culmination of all these processes are used to construct a model to explain the development of paired shear zones (Fig 1).

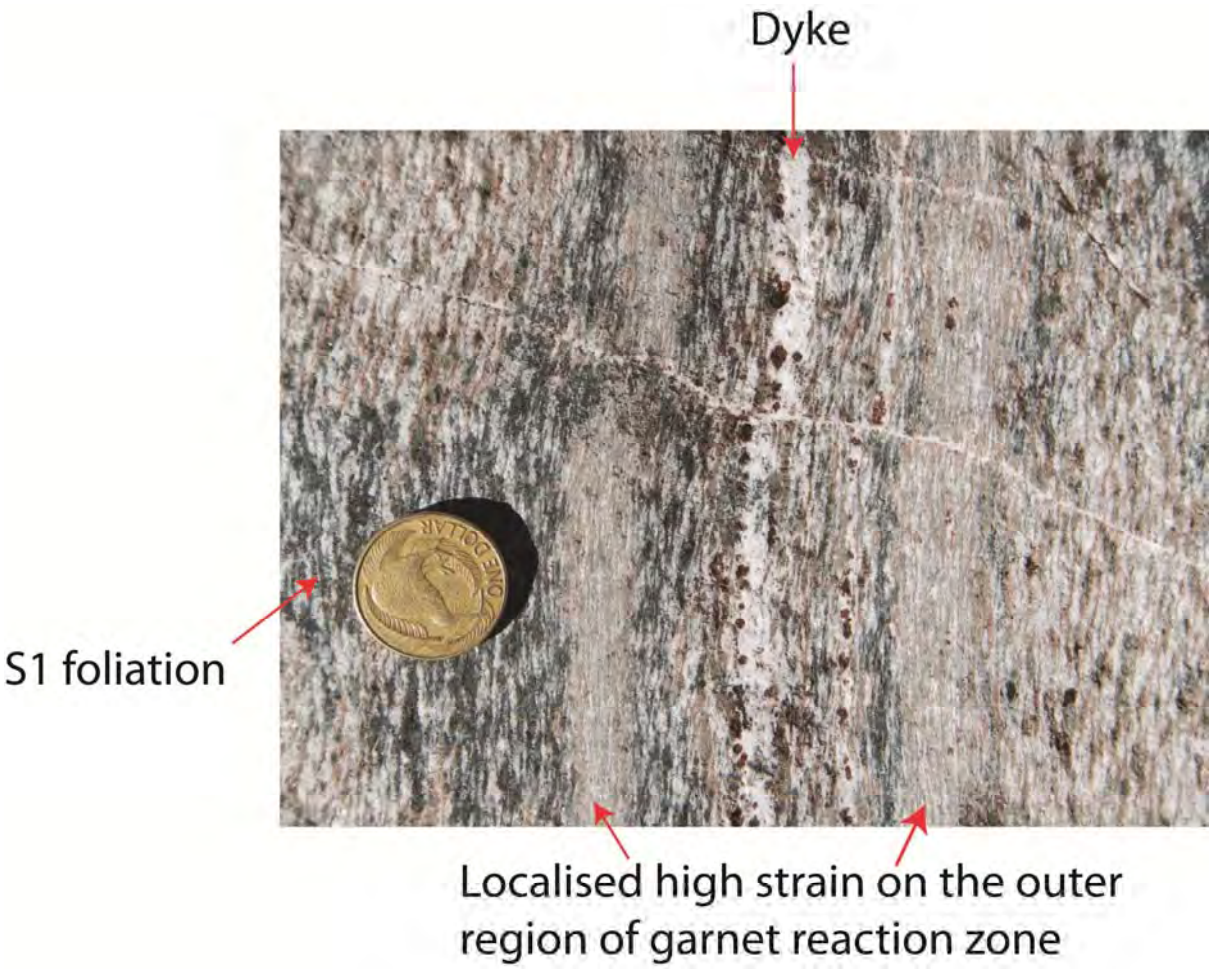

Figure 1: Example of a paired shear zone in-situ within the Pembroke Valley. A garnet reaction zone has formed either side of the dyke and strain has then localised on the outer regions of this reaction zone.

1.2 Regional Geology

The geology of the South Island of New Zealand is divided into three provinces, the volcanic and sedimentary strata of the eastern and western provinces that are divided by the Median Batholith, comprising magmatic arc rocks (Fig 2) (Daczko et al., 2001a; Daczko and Halpin,

2009; Mortimer et al., 1999). The calc-alkaline rocks of the Median Batholith were emplaced and subsequently metamorphosed during arc-continent collision that ceased at ~130 – 125Ma (Bradshaw, 1989a). High-grade metamorphism outlasted the subduction/collision event and continued during the transition to a mid-Cretaceous extension regime which rifted New Zealand away from Gondwana at 105±5Ma (Daczko et al., 2001a).

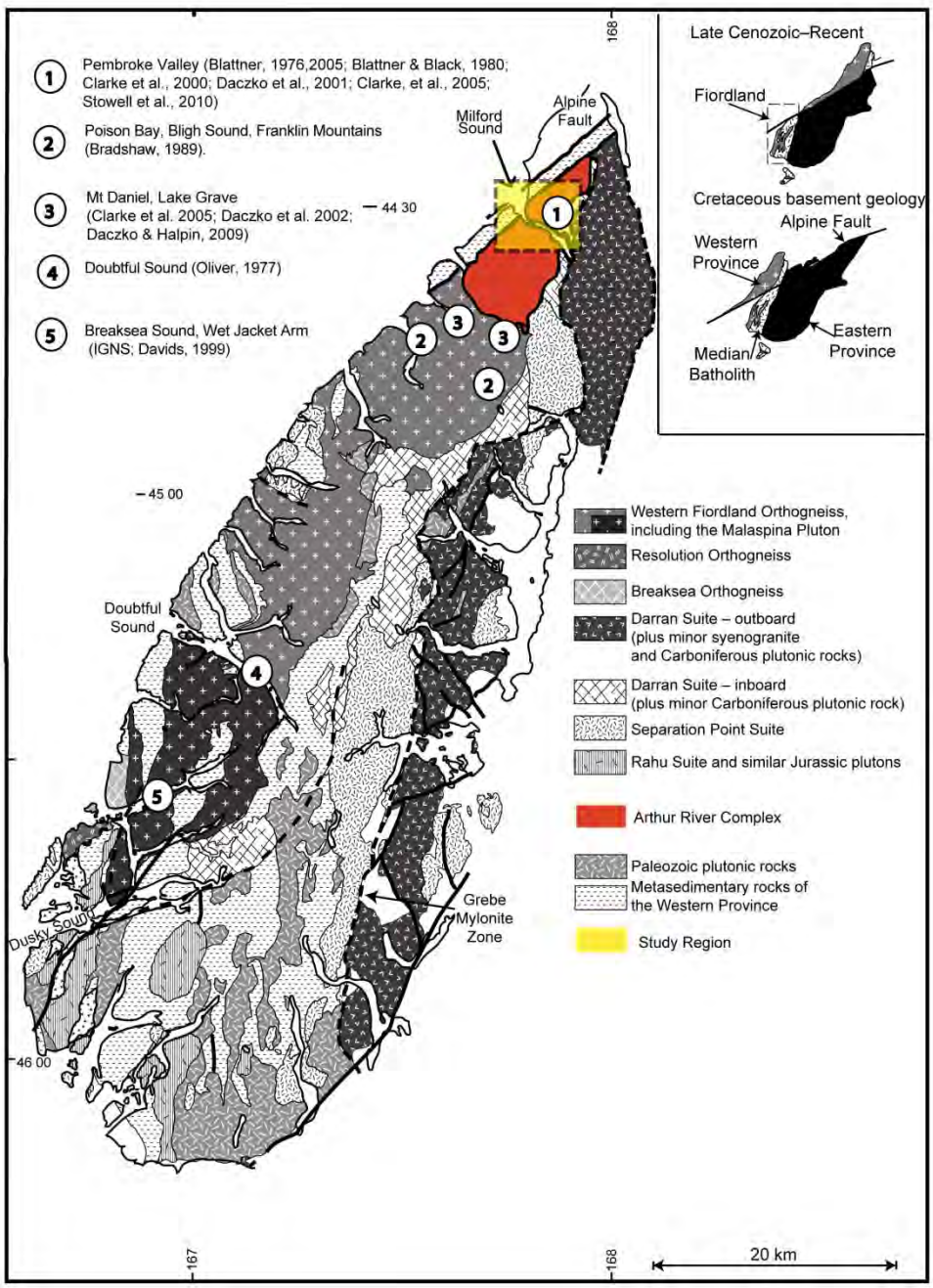

Figure 2: Regional geology of Fiordland displaying the western, median batholith and eastern provinces in detail. Area of study (highlighted yellow and numbered 1) is shown as well as other regions of studied garnet reaction zones. Modified from (Allibone et al., 2009; Clarke et al., 2005).

The Medi atholith is dominated by the voluminous, middle Cretaceous Western Fiordland Othogneiss in western Fiordland (Fig 2); which consists of a two-pyroxene-hornblende gneiss which show a transition to garnet granulite within ~10% of the rocks in the WFO (Daczko and Halpin, 2009). This thesis focuses on similar rocks within the slightly older Arthur River Complex, best exposed in the Pembroke Valley near Milford Sound (Fig 2). The transition to garnet granulite is termed garnet reaction zones and they commonly occur in a thin zone either side of plagioclase-rich dykes which cut the host rocks of two-pyroxene-hornblende assemblage (Fig 3) (Daczko and Halpin, 2009). The mineral assemblage indicates high-P granulite facies metamorphism and mineral chemistry/thermobarometry suggest peak temperatures of ~650 – 700ºC and pressures of ~12 – 13kbar (Daczko et al., 2001a).

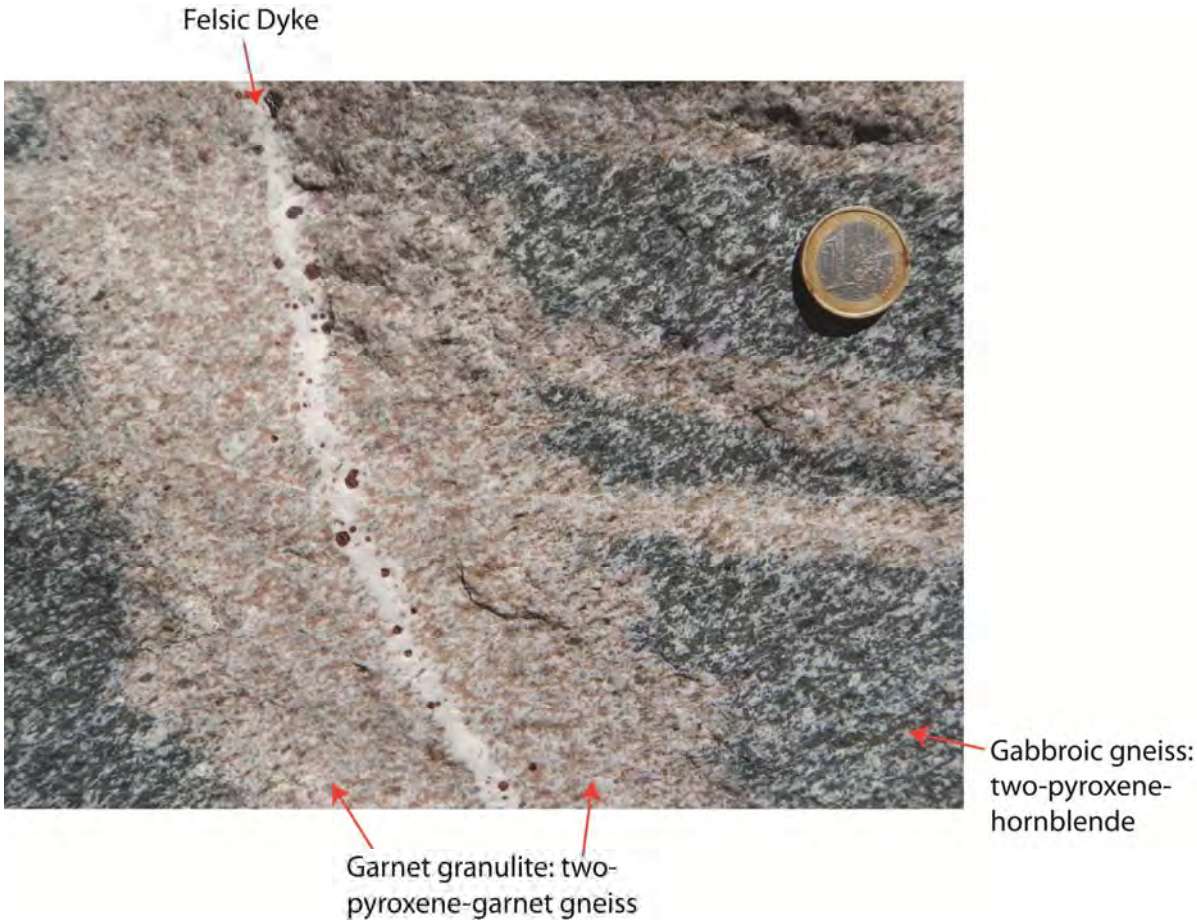

Figure 3: Typical garnet reaction zone either side of a felsic dyke. Typical garnet reaction zones are 3 – 10cm in width. Note some without an obvious dyke due to their collapse.

The Outcrop within the Pembroke Valley comprise two main units: (1) dioritic gneiss which is inferred to have been partially melted on the basis of garnet displaying a peritectic texture (Stowell et al., 2010); and (2) gabbroic gneiss which is the most abundant and is inferred to

have remained at sub-solidus conditions; it consists of two-pyroxene-hornblende gneiss cut by felsic dykes resulting in garnet reactions zones (Fig 3) (Clarke et al., 2005). The gabbroic gneiss generally occurs along the lower reaches of the valley, with up to 20m size lenses of dioritic gneiss interpreted to be xenoliths (pods) (Daczko et al., 2001a). The upper part of the valley consists of a higher abundance of dioritic gneiss (Daczko et al., 2001a).

The gabbroic and dioritic gneisses of the Pembroke Valley have undergone four deformation events (Fig 4) (Clarke et al., 2000). D1 resulted in a pervasive gneissic foliation (S1) containing the metamorphic assemblage of elongated two-pyroxene, hornblende and plagioclase (Daczko et al., 2001a). D2 resulted in brittle deformation resulting in vertical planar fractures, cutting the S1 foliation through the emplacement of felsic dykes together with development of garnet reaction zones (Fig 4) (Clarke et al., 2000). Within garnet reaction zones hornblende from the S1 mineralogy is pseudomorphed by garnet a few centimetres either side of the felsic dykes at pressures at ~14kbar and temperatures of ~750ºC (Daczko et al., 2001a). D3 is defined by narrow (cm – m), east trending, steeply dipping, mylonitic shear zones which can localise either side of garnet reaction zones within the gabbroic gneiss (Fig 1) or they can be up to 3metres in width either side of a dyke (Daczko et al., 2001a). The final deformation event, D4 resulted in shallowly eastward dipping shear zones which variably deform S1 and garnet reaction zones (Clarke et al., 2000). This thesis will focus on the first three events (D1, D2 and D3) ~~on~~ the gabbroic gneiss (Fig 4).

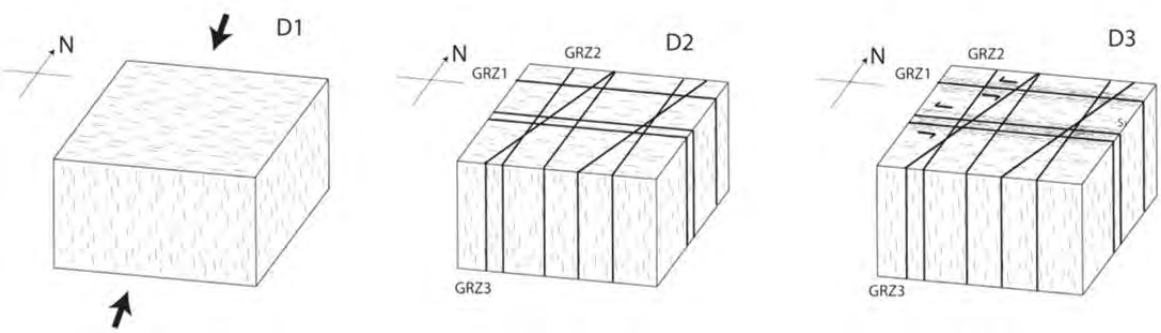

Figure 4: Block diagrams of the first three key deformation events within the Pembroke Valley. D1 resulted in gneissic foliation (S1), D2 resulted in fracturing and intrusion of felsic dykes resulting in garnet reaction zones (GRZ) and D3 resulted in east striking mylonite shear zones. Modified from Clarke, et al. (2000).

1.3 Garnet Reaction Zones

Garnet reaction zones have been extensively studied within Fiordland. These reaction zones are found between Milford Sound and Breaksea Sound (Fig. 2) (Clarke et al., 2005).
Studies of garnet reaction zones in Fiordland have occurred within the Pembroke Granulite (study region) (Blattner, 1976, 2005; Blattner and Black, 1980; Clarke et al., 2005; Clarke et al., 2000; Daczko et al., 2001a; Daczko et al., 2001b; Stowell et al., 2010), the Doubtful Sound area (Oliver, 1977), the Western Fiordland Orthogneiss (Bradshaw, 1989b), Mt Daniel (Clarke et al., 2005; Daczko et al., 2002) and Lake Grave (Daczko and Halpin, 2009). In addition, garnet reaction zones have been studied within the Jijal Complex in Northern Pakistan (Garrido et al., 2006; Padron-Navarta et al., 2008).

The garnet reaction zones form by the replacement of S1 hornblende from the assemblage of hornblende-orthopyroxene-clinopyroxene-plagioclase and ilmenite by garnet resulting in the assemblage of garnet-clinopyroxene-orthopyroxene-plagioclase-quartz and rutile (Daczko et al., 2001a; Oliver, 1977). These reaction zones may be spaced less than 1m apart and are commonly ~1-5cm wide, although this can vary with some zones being up to 10cm wide (Fig 3) (Daczko et al., 2001a). These zones can be traced along strike for at least 50m on subhorizontal surfaces (Daczko et al., 2001a). Daczko et al. (2001b) measured the orientations of garnet reaction zones (GRZ) within the Pembroke Valley and found there are three orientations (Fig 5). Daczko et al (2001b) used the subscript, 1, 2 and 3 to distinguish between the three orientations. GRZ_1 are ESE-striking with near-vertical dips, GRZ_2 intersect GRZ_1 at ~90º, striking NNE with a steep westerly dip (Daczko et al., 2001a). GRZ_3 bisects GRZ_1 and GRZ_2 at ~45º with a NE-strike and a steep south-easterly dip (Daczko et al., 2001a). The garnet reaction zones in some areas within the gabbroic gneiss lack a dyke which could be due to areas of dyke terminations or it could just be sites of previous melt where a dyke has closed (Fig 3) (Clarke et al., 2005).

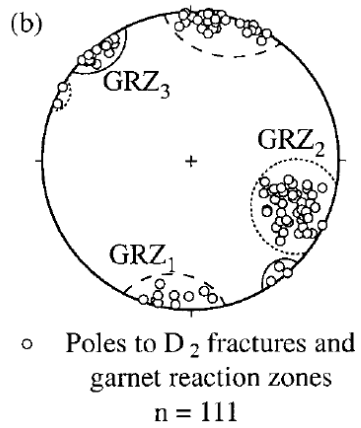

Figure 5: Poles to D2 deformation event. Source: Figure 2 Daczko et al. 2001b

The formation of these planar zones of garnet granulite facies rocks has been continually debated since the discovery of the reaction zones. Previous studies have focused on petrography and field observations and Blattner (1976) developed the theory that these reaction zones formed by CO_2 influx from deep continental crust which moved through a pre-existing fracture network (Blattner, 1976). Within the Doubtful Sound region it has been proposed melt migrated through developed fractures resulting in a loss of H_2O and Na_2O causing dehydration melting of two-pyroxene-hornblende granulite to garnet granulite (Oliver, 1977). The presence of scapolite in reaction zones led Bradshaw (1989) to support the Blattner (1976) CO_2-rich fluid model. However, these reaction zones are not present within the dioritic gneiss even though this unit is also cut by the fracture network and intrusion of felsic melt. Daczko et al. (2001a) suggested that the plagioclase rich dykes originated from local melting of the adjacent dioritic gneiss. Trace-element analysis of garnet in the felsic rich dykes have a REE signature different to garnet from the GRZ, but similar to peritectic garnet in the dioritic gneiss (Schroter et al., 2004). Therefore this garnet seems to have originated as peritectic garnet from the adjacent, partially molten dioritic gneiss (Clarke et al., 2005; Schroter et al., 2004).

A major problem with the felsic dyke hypothesis is that most "dykes" are very thin and are dominated by plagioclase feldspar and garnet (i.e. they don't have a melt composition). Daczko and Halpin (2009) observed true felsic dykes at Lake Grave with limited development of garnet granulite. These authors conclude that magma moving through a fracture/dyke system resulted in extraction of volatiles from the host granulite and caused the

formation of garnet granulite (Daczko and Halpin, 2009). Although this is a controversial model this thesis will term these intrusions dykes.

This garnet reaction zone phenomenon is also found within the Jijal Complex, Northern Pakistan within the Kohistan Paleo-arc Complex (Garrido et al., 2006). This granulite facies complex formed during the subduction of the Neo-Tethys ocean under the Karakoram plate (Garrido et al., 2006). The upper granulite section is comprised of hornblende gabbronorites partially transitioned to garnet granulites, similar to those found within the Pembroke Valley (Garrido et al., 2006). Rare earth element variations support an open system during transition of plutonic rocks to garnet granulite during the early stages of arc formation (Garrido et al., 2006). Trace element variation of La, Th, U and Nb in the granulite excludes dehydration reactions, as these trace elements are insoluble in hydrous fluids (Garrido et al., 2006). This led to the conclusion that dehydration melting played an important role in the transition to garnet granulite (Garrido et al., 2006). Rushmer, (1993) also proposed dehydration melting in the formation of garnet granulite as the presence of a hydrous melt would drastically enhance reactions and garnet growth (Rushmer, 1993).

Electron Backscatter Diffraction (EBSD) studies have also been completed on the Jijal complex granulites in order to study the role of precursor phases on the growth of garnet (Padron-Navarta et al., 2008). Padron-Navarta et al. (2008) proposed from previous studies that in the absence of deformation the crystallographic orientation of product phases should mimic reactants. The results of their EBSD analysis shows orthopyroxene, amphibole and clinopyroxene with strong lattice preferred orientations (LPO) related to the precursor hornblende-gabbronorite (Padron-Navarta et al., 2008). These reactants and precursor phase orientation relationships are also found within garnet, demonstrating the magmatic phases controlled the orientation of garnet within the garnet granulite (Padron-Navarta et al., 2008). This provides evidence that these garnet granulites formed under static conditions.

1.4 Paired Shear Zones

Ductile D3 shear zones occur within the dioritic and gabbroic gneiss in the Pembroke Valley and only paired shear zones form within the gabbroic gneiss, therefore this unit is the focus of this thesis. The types of shear zones include high-strain zones along dyke planes and paired shear zones. These D3 shear zones are representative of ~20 – 25% of the area within the

Pembroke Valley (Daczko et al., 2001a). The mineral assemblage used to define the S3 foliation are garnet-clinopyroxene-quartz-rutle-calcic-amphibole-clinozoisite (Daczko et al., 2001b). There have also been several observations indicating that D3 mineral growth occurred during deformation, including asymmetric amphibole, biotite and clinozoisite fish (Daczko et al., 2001a).

The systematic changes during the history of the gabbroic gneiss must be understood to determine why strain is sometimes localized at the outer regions of garnet reaction zones (paired shear zone). The history of these rocks resulting in the recrystallization and phase changes during development of the S1 gneissosity, garnet reaction zones and D3 shear zones must be interpreted. Understanding mineralogical and microstructural changes during this history is essential as these changes within a rock may localise deformation and explain the development of, for example, paired shear zones (Herwegh et al., 2008). Paired shear zones similar to those identified during fieldwork in the Pembroke Valley are also observed in granodiorites within south Tyrol, Italy (Mancktelow and Pennacchioni, 2005; Pennacchioni and Mancktelow, 2007). Mancketelow and Pennacchioni, (2005) observed strain localisation on the outer regions of alteration haloes (bleached zones symmetric to veins) with a weak foliation, sometimes present between the paired shear zones. Mancketelow and Pennacchioni, (2005) concluded the distribution of strain was due to a rheological contrast as the altered zones close to the vein where rheologically strong, thus resulting in little deformation. Shear was concentrated on the rim of the altered zone implying these regions are rheologically weaker (Mancktelow and Pennacchioni, 2005). Whether a material is rheologically strong or weak depends on composition, modal percentage of hard versus soft phases, pre-existing preferred crystallographic orientation, stored energy within grains, grain boundary network (where interlocking grain boundaries strengthen the material) and grain size (Ranalli, 1995). These parameters are strongly influenced by the microstructure of the rock. This study will examine the microstructure of the garnet reaction zones and paired shear zones to explore which of these parameters may have been important in the development of paired shear zones.

1.5 Static and Dynamic Recrystallization Microstructures

Recrystallization, in its broadest sense, refers to a rearrangement of grain and phase boundaries. ~~Static d~~eformation was highly localized at the edges of brittle fractures (D2) during the development of garnet reaction zones. Therefore, recrystallization took place under very low strain and is termed "static recrystallization". In contrast, dynamic recrystallization occurred in D3 shear zones. Static recrystallization may result in subgrain formation and the rearrangement of dislocations into low energy configurations (Humphreys and Hatherly, 1995). Static recovery will result in a reduction of the stored strain energy of the system by annihilation of dislocations (Borthwick and Piazolo, 2010; Heilbronner and Tullis, 2012). Grain boundary migration will also occur which is mainly driven by stored and surface energy reduction, bulging grain boundaries and grain growth (Heilbronner and Tullis, 2012). Although, if the temperature is not high enough or long enough to allow for mobile grain boundaries and diffusion, static recrystallization will not occur to any significant degree (Herwegh et al., 2008). Static recrystallization may also result in heterogeneous nucleation where in areas of high strain and/or chemical potential, new grains with low stored energy and/or thermodynamically favourable compositions grow (Piazolo et al., 2006).

Dynamic recrystallization will result in new grains nucleating around old grains which can result in the material becoming fully recrystallised (Humphreys and Hatherly, 1995). This process is syn-tectonic and is a continuous process of deformation, nucleation and migration of grain boundaries, resulting in dislocation-free grains which will subsequently deform further (Humphreys and Hatherly, 1995). Dynamic recrystallization will be localised in areas of competency contrast i.e. between rheologically soft and hard domains (Jessel et al., 2005).

This study will examine the static recrystallization within garnet reaction zones and contrast this with the dynamic recrystallization in D3 shear zones. This thesis will aim to determine if a certain degree and type of recrystallization is a required precursor for the development of paired shear zones.

Chapter 2

Field Work and Sample Selection

2.1 Fieldwork

Fieldwork was undertaken during an eight day visit to the South Island of New Zealand between 16th – 24th March 2012. Samples were collected within the Pembroke Valley between 19th – 23rd March 2012, by Nathan Daczko, Sandra Piazolo, James Scott and myself. The camp site was set up within the Pembroke Valley on 19th March, alongside the creek. The Pembroke Valley is only accessible by helicopter and is located north of Milford Sound. The area is maintained by the Department of Conservation who were contacted prior to this study to apply for a visit and sample collection permit within the Pembroke Valley.

The outcrops within the Pembroke Valley are well-exposed due to recent glaciation, although most outcrops are flat surfaces making it difficult to collect in situ samples. The majority of samples were collected from boulders within the creek, a max distance of ~500m from the outcrop (Fig 6).

Figure 6: Pembroke Valley with a view of the creek and in the distance, Milford Sound. Samples were collected within the creek, after looking at in-situ features.

Samples were collected based on in-situ sample observations. All rocks have a well-defined S1 foliation and both dioritic and gabbroic gneisses are cut by felsic dykes. Garnet reaction zones were observed with or without a dyke and these dykes could range up to a width of ~3cms. Dykes were feldspar rich and contained garnet which generally aligned on one side of the dyke's wall. Dykes cutting the gabbroic gneiss resulted in garnet reaction zones which varied in size from ~3cm – 10cm width. Within the dioritic gneiss, dykes did not result in a garnet reaction zone and peritectic garnet was also observed (melt-microstructure), therefore samples of the dioritic gneiss were collected. The diorite varied slightly in composition as some contained more amphibole than others. Mylonitic shear zones were present (D3) and ranged in scale from centimetres to metres in width and were always located either side of a dyke. When shearing occurred at a reaction zone within the gabbroic gneiss, it either sheared either side of the dyke shearing the whole garnet reaction zone. Or shearing was further localised to the outer regions of garnet reaction zones, resulting in a paired shear zone. Samples of interest were determined from in-situ samples and then were found within the creek as boulders. The samples collected are listed in table 2.1.

Table 2.1 lists the samples that have been collected with a field note description, explaining why they are of interest. Samples were collected and identified within the outcrop slab which began at a NZ grid reference of North 0729457 ± 7 and East 5058724 ± 7. Thin sections have been made of selected samples listed within table 2.1. Samples were examined and then described within chapter 4 (petrography).

Table 2.1: Collected samples from the Pembroke Valley, detailing if a thin section was made and if yes, the methods used on each sample with their MU numbers. GRZ = garnet reaction zone.

Field Reference	Field Notes	Thin Section	SEM-BSE	SEM-EDS	Laser Ablation	SEM-EBSD	Mu Number
PV1201a	Top part of shear	-	-	-	-	-	64394
PV1201b	Use for GRZ and Gabbro reference	-	-	-	-	-	64395
PV1201c	Intermediate strain zone	-	-	-	-	-	64396
PV1202	Shear zone. How does the feldspar deform within the dyke?	-	-	-	-	-	64397
PV1203	Metamorphic history, less useful for shear or	-	-	-	-	-	64398

	deformation						
PV1204	Melt veins & distribution of peritectic garnet in country rock. Moderate amount of clinozoisite.	Yes	-	-	-	-	64399
PV1205	Peritectic garnet with less developed melt vein. High amount of clinozoisite. High component of leucosome	-	-	-	-	-	64400
PV1206	Deformed dyke.	-	-	-	-	-	64401
PV1207	Courser grained dioritic gneiss.	Yes	-	-	-	-	64402
PV1208	GRZ and host and into hydrated shear zone. (Four sections)	Yes	-	-	-	-	64403
PV1209	Shear along microdioritie dyke?	-	-	-	-	-	64404
PV1210	Two GRZs. One crystallising and hydrating (surrounded by shear). Second GRZ is collapsed and anhydrous. (three sections)	Yes	-	-	-	-	64405
PV1211	Paired shear zone. Two sections	Yes	Yes	Yes	-	-	64406
PV1212	Owl eyes of garnet. Back reaction has occurred.	-	-	-	-	-	64407
PV1213	Reaction zones in two directions. One with vein and one sheared.	-	-	-	-	-	64408
PV1214	Kyanite grains possible aligned due to melt?	-	-	-	-	-	64409
PV1215	Reference GRZ	-	-	-	-	-	64410
PV1216a and b	Reference dyke reaction zones. Annealing close to dyke for ~1cm.	Yes	Yes	Yes	-	Yes	64411
PV1217	Collapse structure. Four Sections have been made	Yes	Yes	Yes	-	-	64412
PV1218	Flow alignment in dyke?	-	-	-	-	-	64413

PV1219	Collapse structure	Yes	-	-	-	-	64414
PV1220	Melt perculation	-	-	-	-	-	64415
PV1221	Reference	-	-	-	-	-	64416
PV1222	Melt perculation	Yes	Yes	Yes	Yes	Yes	64417
PV1223	Aqueous fluid movement?	-	-	-	-	-	64418
PV1224	Hydration around dyke?	-	-	-	-	-	64419
PV1225	Dyke being partially replaced	-	-	-	-	-	64420
PV1226	High clinozoisite content. GRZ and melt with peritectic garnet	-	-	-	-	-	64421
PV1227	Dyke with only hornblende reacting to pyroxene	-	-	-	-	-	64422
PV1229	Fingering of GRZ	-	-	-	-	-	64423
PV1230	Collapsed dyke	Yes	Yes	Yes	-	-	64424
PV1233	Anorthosite dyke with little deformation due to monomineralic microstructure. Two thin sections	Yes	-	-	-	-	64425
PV1234	Paired shear zone. Two sections)	Yes	Yes	Yes	Yes	Yes	64426
PV1235	Dyke with more reaction zone	-	-	-	-	-	64427
PV1236	Pseudotachylite	-	-	-	-	-	64428
PV1237	Reference reaction zone. Two sections.	Yes	Yes	Yes	-	-	64429
PV1238	Hornblende bearing dyke with reaction zone.	Yes	-	-	-	-	64430
PV1239	Intersecting dyke	Yes	Yes	Yes	-	-	64431
PV1240	Reaction dyke in dioritic rock	Yes	-	-	-	-	64432
PV1241	Peritectic garnet	Yes	-	-	-	-	64433
PV1242	Fingers out of reaction zone. Look for collapsed structures	-	-	-	-	-	64394
PV1243	Dyke with annealing and slight deformation	-	-	-	-	-	64395

Chapter 3

Methods

3.1 Petrography

Eighteen thin sections have been made of the collected field samples. Most samples were cut to a smaller size within the Department of Geology facilities in Dunedin, New Zealand. Samples were examined with the use of a Nikon Eclipse E400 POL petrographic microscope. Photomicrographs were then taken with the PRIOR microscope located within Macquarie University, Sydney, Australia. Area and length measurements were made with this microscope.

Samples were then carbon coated for the Zeiss EVO MA15 Scanning electron microscope (SEM) within the GEMOC National Key Centre within Macquarie University, Sydney, Australia. Back-scattered electron (BSE) images were collected to categorize samples. The SEM operated at an accelerating voltage of 20kV, with a ~8 - 10 nA beam current and a working distance of 10 - 13mm.

3.2 Major Element Mineral Chemistry: Scanning Electron Microscopy – Energy Dispersive Spectrometry (SEM-EDS)

Samples were coated by Kevin Grant for the Zeiss EVO MA15 scanning electron microscope within the GEMOC National Key Centre within Macquarie University. Energy Dispersive Spectrometry values were obtained for plagioclase and garnet end members. The element compositions were acquired using energy X-ray dispersive spectroscopy. Garnet grains were analysed for major element oxides (SiO_2, TiO_2, Al_2O_3, FeO, MnO, MgO and CaO) and plagioclase was analysed for major element oxides (Na_2O, K_2O, CaO, Al_2O_3 and SiO_2). The obtained element spectrum was quantified using the EDS software Aztec 2.0 by Oxford Instruments. Major elements were analysed at an accelerating voltage of 20kV, a beam current of 8-10nA and a counting time of ~10 – 20seconds (auto setting - acquisition continues until enough counts are collected in the spectrum for quantification). Acquisition occurred with a working distance of 11 – 13mm, 1024 no. of channels; 10Kev energy range

and 10eV energy per channel. When data was obtained for absolute values of garnet, copper was used as a calibration instrument. Calibration was undertaken every 15 minutes in order to avoid drift during instrument use. All SEM-EDS data has been normalised to 100%. Plagioclase end-member anorthite and garnet end-member components for pyrope (Pyp), almandine (Alm), grossular (Grs) and spessartine (Sps) were calculated from the method described by Deer, et al. (1966).

3.3 Trace Element Mineral Chemistry: Laser Ablation Inductively Coupled Plasma Mass Spectrometry (LA-ICP-MS)

Two polished 30µm thin sections, prepared by Manal Bebbington were examined with the LA-ICP-MS. Analysis was undertaken within the Australian Research Council (ARC) National Key Centre for Geochemical Evolution and Metallogeny of Continents (GEMOC), located within the Department of Earth and Planetary Sciences at Macquarie University. Analysis was undertaken under the operating conditions listed within table 3.3.

Table 3.3: LA-ICP-MS operating conditions

Instrument information	**Type**
ICP-MS type	Quadrupole
Model	Photon Machines Excite 193nm
Laser type	Eximer
Beam Diameter	30 - 50µm with He in cell
Ablation Gas in cell	He
Carrier gas	Ar
Gas flow rate	0.8L/min
Laser pulse rate	5Hz
External Standard	STD610
Reference sample for accuracy	BCR2 – Basaltic glass
Data reduction software	GLITTER
Background count time	60s
Signal count time	120s
Scan speed	1µm/s or 2µm/s depending on run
Dwell time	30milliseconds per isotope

Analysis was conducted within small runs consisting of: 2 analysis of STD610, 1 of BCR2, 11 – 18 of samples and 2 analysis of STD610. Data is corrected for instrument drift to STD610 and BCR2 which are also used for accuracy of acquired data. Calcium oxide weight percentage values have been used as an internal standard which were obtained from the SEM-EDS and the clinopyroxene run method was used.

The expected and obtained BCR2 values are compiled within table 3.4. Expected values have been obtained for BCR2 by published data from Norman et al. (1998).

Table 3.4: expected and obtained BCR2 values:

Element	**Average BCR2 value (ppm) (n=4)**	**Average 1σ (ppm) (n=4)**	**STD610 Expected values (ppm)**	**1σ (ppm)**
La139	25.38	0.84	24.5	0.7
Ce140	50.85	1.66	50.5	1.6
Pr141	6.43	0.21	6.8	0.3
Nd146	28.76	0.97	29	1.1
Sm147	6.45	0.26	6.6	0.4
Eu153	2.00	0.08	1.92	0.12
Gd157	6.30	0.26	6.5	0.4
Tb159	0.98	0.04		
Dy161	5.95	0.24	6.5	0.4
Ho165	1.19	0.05	3.6	0.2
Er167	3.35	0.14	3.5	0.2
Tm169	0.47	0.02		
Yb173	3.37	0.15	3.5	0.2
Lu175	0.46	0.02	0.51	0.03

During analysis the lower limit of detection (99% confidence) and 1 sigma error are calculated and the data is checked and optimum background and signal ranges are detected using GLITTER (Appendix C). The optimum signal is chosen to avoid inclusions, poor signal or high background. This filtered data is then ready to be exported.

3.4 Scanning Electron Microscopy – Electron Backscatter Diffraction (SEM-EBSD)

Polished thin sections of 30µm were mechanically polished by Manal Bebbington within Macquarie University. Samples were then chemically etched with colloidal silica in alkali solution in order to remove any bubbles on the surface. A thin carbon coat of 2 – 5nm (barely visible) was applied within the GEMOC National Key Centre within Macquarie University. They were then analysed with the Zeiss EVO MA15 scanning electron microscope - EBSD. EBSD and EDS maps were obtained with an accelerating voltage of 20kV and a beam current of 8.0nA. Samples were tilted to 70° and the EBSD was moved to a working distance of ~12 – 15mm from the tilted stage. Once the beam position was determined, electron backscatter occurs due to the interaction with the electron beam and the arrangement of atoms within the crystal. These backscattered patterns are detected on a fluorescent screen and are called kikuchi bands which directly relate to specific minerals crystal structure (Bestmann and Prior, 2003). In order to index kikuchi bands, knowledge of expected minerals is required for correct phase identification. This is completed by adding expected phases into the Aztec 2.0 software by Oxford Instruments and determining the amount of reflectors necessary to identify each phase. The exposure time was set to auto, bin mode is between 4x4 or 8x8 and the gain is kept low to avoid noise. Automatic indexing occurred with a step size of 2µm and full crystallographic orientation data was collected using HKL Channel 5 software from Oxford Instruments HKL Technology.

The gathered data is then processed to remove non-indexed points through the Tango component within the HKL Channel 5 software which allows a three step noise reduction to occur (Prior et al., 2002). These steps include the removal of nonsystematic data points, termed wild spikes, replacing zero solutions by an algorithm to expand the nearest neighbour and the removal of systematic miss-indexing (Humphreys, 2001). This data can then be displayed as a band contrast image which shows the data acquisition and image quality (Bestmann and Prior, 2003). This is displayed through grey scales with the lighter colours displaying good indexing and the poor indexing in dark. Different features of the data can also be displayed in maps. These include euler angles which are angles from one point in the grains chosen to be the reference and the deviation 0-10° from this point is calculated and visualized by a rainbow colour scheme. The Mambo component of HKL Channel 5 allows projection of microstructure orientations onto pole figures.

Chapter 4

Petrography

Introduction

This chapter examines the petrography of the gabbroic gneiss within the Pembroke Valley, Milford Sound, southern New Zealand. The aim of this chapter is to distinguish domains of the gabbroic gneiss on the basis of mineralogy. Eighteen thin sections were examined and four rock domains have been determined: 1) host two-pyroxene-hornblende gneiss 2) felsic dykes 3) garnet reaction zones with different degrees of recrystallization and 4) D3 shear zones. As thin sections have been cut to comprise of different rock domains, one section can be categorised into more than one domain (Fig 4.1). This chapter will describe key features of each domain, while overall individual sample descriptions are presented in Appendix A.

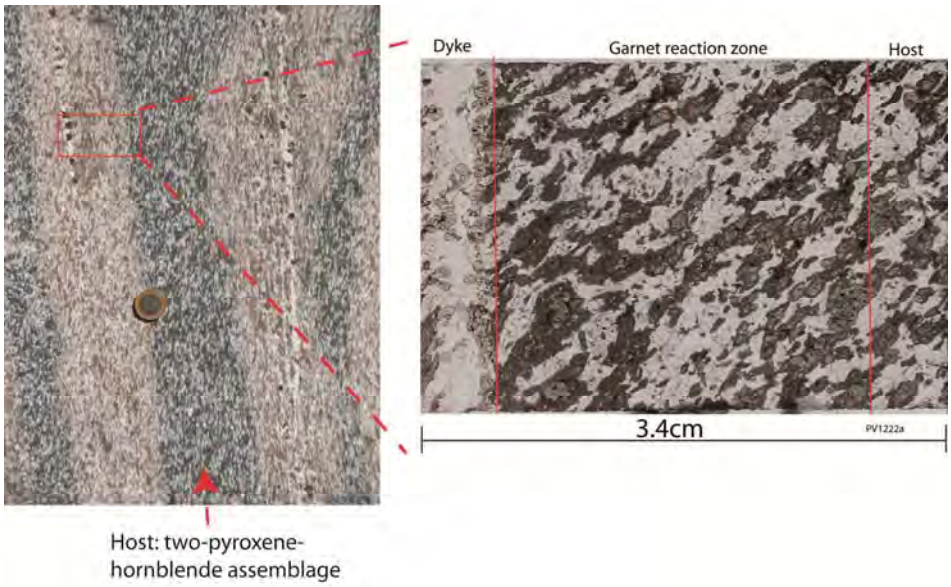

Figure 4.1: Field photo (left) with highlighted domains within thin section (right). Thin section comprises ~~of~~ domain 1 (host S1 assemblage), domain 2 (dyke) and domain 3 (garnet reaction zone)

4.1 Domain 1: Host two-pyroxene-hornblende gabbroic gneiss

The host gabbroic gneiss consists of a well-developed gneissose texture (S1 foliation) defined by the assemblage of two-pyroxene-hornblende. This gneiss is plagioclase rich which consists of relict (large igneous plagioclase grains) and neoblasts (small metamorphic plagioclase grains).

Hornblende is typically found in the host two-pyroxene-hornblende assemblage as a ~~developed~~ corona surrounding pyroxene. It is pleochroic from light green to dark green. The inner co[illegible] consists of elongate grains of hornblende seen as a symplectite with quartz (Fig 4.1.1~~) and~~ (Fig 4.1.2). The outer corona consists of anhedral crystal faces with embayed edges. Cleavage and twinning is rare.

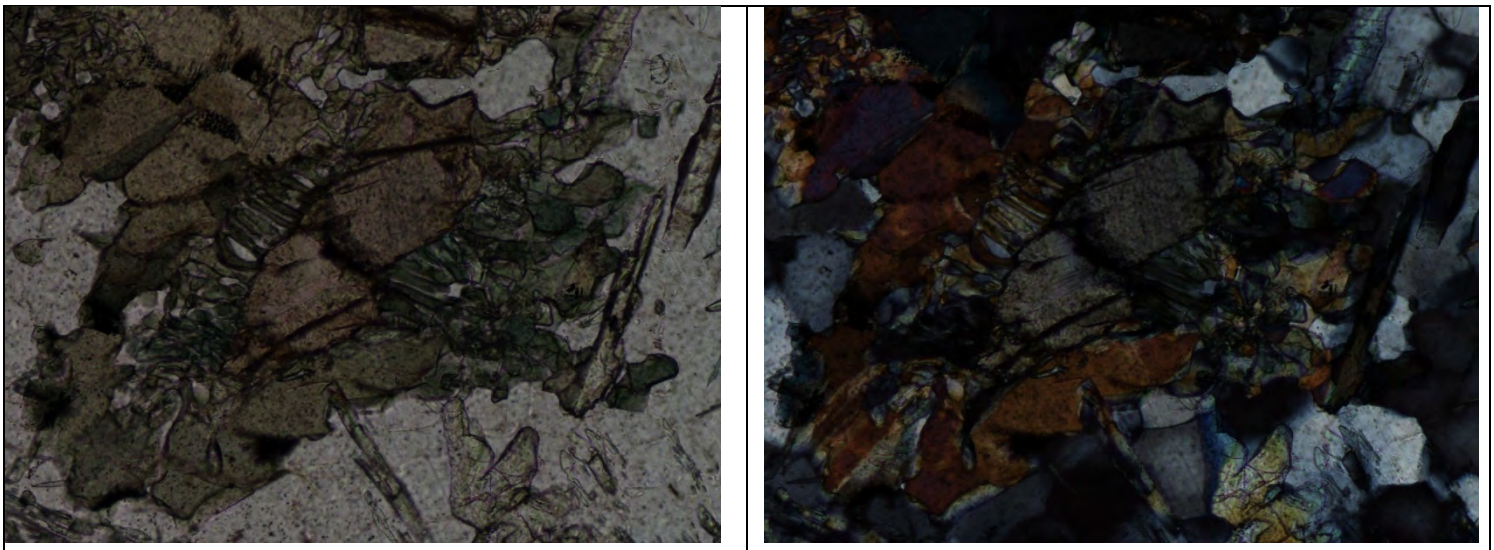

Figure 4.1.1: Typical two-pyroxene-hornblende gabbroic gneiss. Photomicrograph of sample 1237AB, PPL and XPL base of photo 4.4mm. Host assemblage with orthopyroxene surrounded by an inner corona symplectite of elongate hornblende grains (green mineral) and quartz (clear mineral). Outer corona is hornblende.

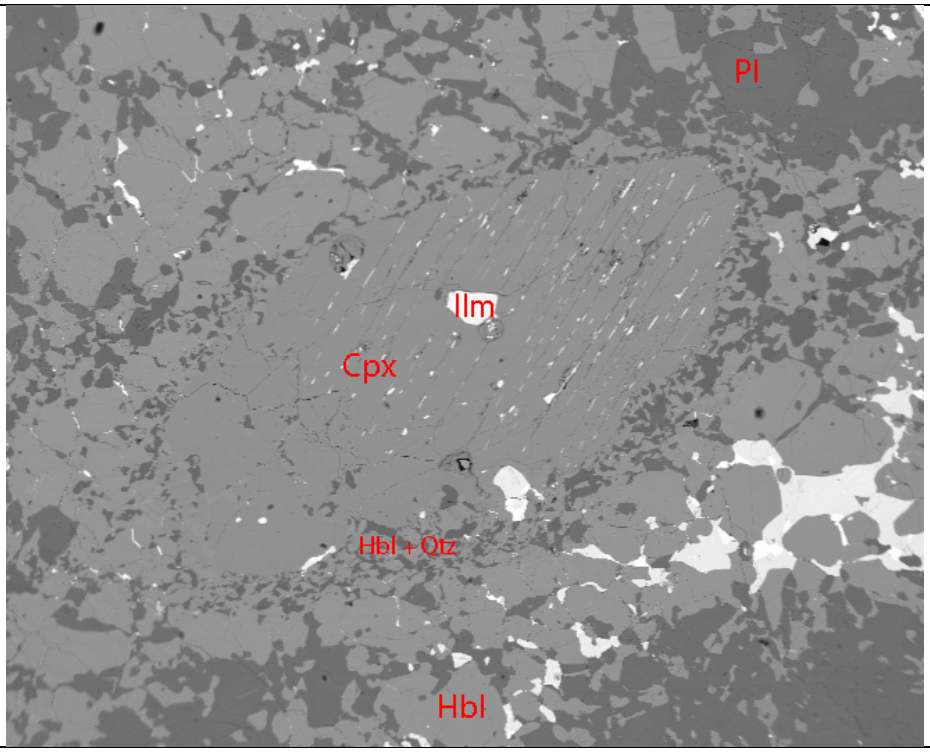

Figure 4.1.2: Typical host assemblage back scatter electron image (BSE) of sample 1234a. Host assemblage corona with clinopyroxene (centre), inner corona symplectite of quartz and hornblende and then an outer corona of hornblende. Note ilmenite exsolutions.

Pyroxene is commonly found as clinopyroxene or orthopyroxene within the host, as subhedral grains with a poorly developed cleavage. Pyroxenes commonly develop an inner corona of a symplectite texture of quartz and pyroxene (Fig 4.1.3). Pyroxenes also consist of well-defined euhedral faces and are commonly found in a mafic cluster.

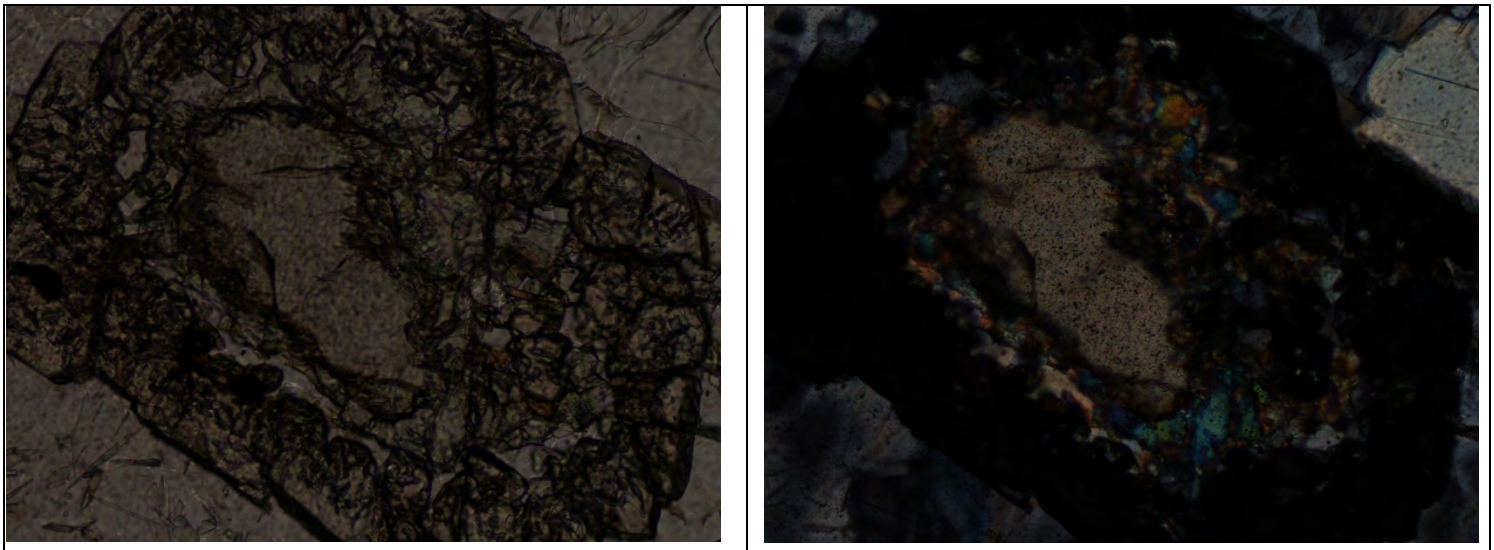

Figure 4.1.3: Photomicrograph displaying symplectite of cpx and qtz around orthopyroxene. Photo is from sample 1230 displaying PPL and XPL. Base of photo 4.4mm.

Kyanite is abundant within the plagioclase rich regions as acicular minerals which can grow in a high abundance within close proximity to each other. Figure 4.1.4 is an example from within a garnet reaction zone. This texture has been termed a disequilibrium texture.

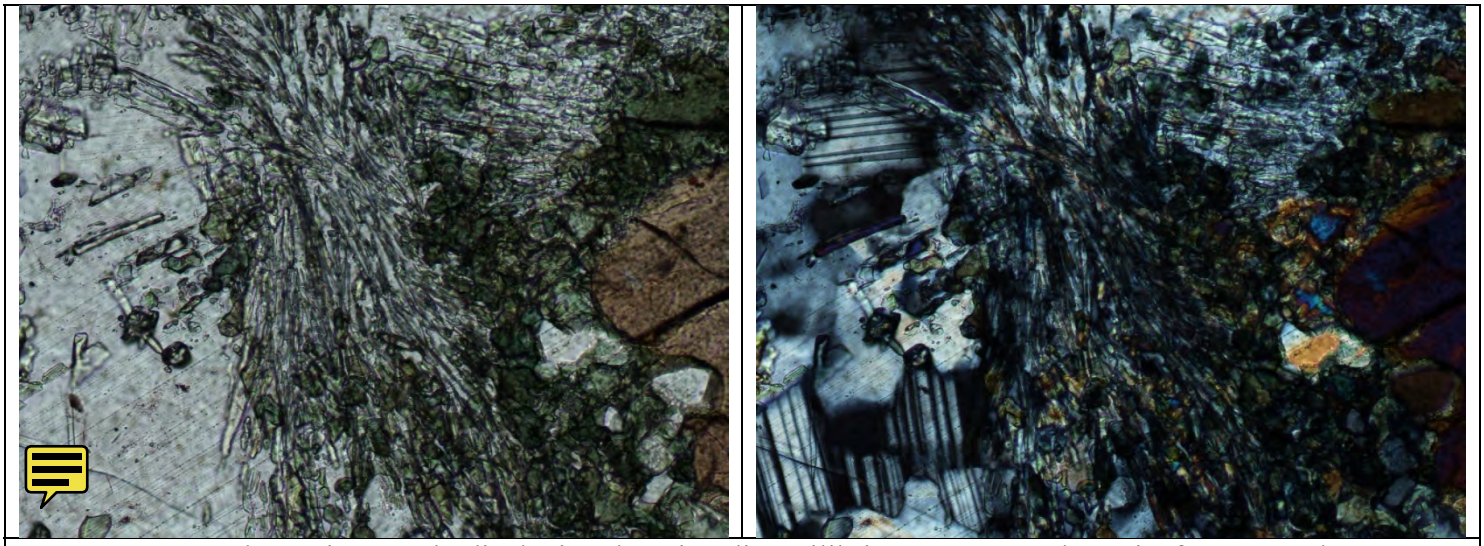

Figure 4.1.4: Photomicrograph displaying kyanite disequilibrium texture. Photo is from sample 1237AB displaying PPL (left) and XPL (right). Base of photo 4.4mm.

Plagioclase is of a high abundance within this domain and displays deformation textures such as kink bands, tapered twins and bulging grain boundaries. Plagioclase has a powdery texture. Biotite and epidote are also common in small proportions. Biotite is lathe-like with anhedral crystal faces and pleochroic from dark brown/ light brown. Epidote is commonly circular with a yellow colour and a high birefringence, commonly located close to the dyke.

Table 4.1 describes domain 1 within different samples, providing modal proportions and descriptions.

Table 4.1: Domain 1 mode and descriptions of each sample

GNS	Major Minerals and Estimated Mode	Minor	Structure/ Comments
PV1230	Plagioclase 40% Orthopyroxene 5% Hornblende 25% Clinopyroxene 10% Kyanite 5% Quartz 5% Epidote 5% Biotite ~5%	Oxides Rutile	Medium grained foliated gabbroic gneiss. Hornblende is euhedral with poorly defined cleavage and twinning. Plagioclase has a variety of grain sizes, sutured grain boundaries, kink bands and deformation twins. Pyroxene consists of an inner corona disequlibrium texture of quartz and pyroxene symplectites and is common

			within mafic clusters. Quartz commonly contains undulose extinction. Well defined S1 foliation.
PV1237aa	Plagioclase 30% Hornblende 30% Clinopyroxene 10% Orthopyroxene 5% Epidote 5% Kyanite 10% Quartz 10%	Rutile Oxides Biotite	Typical host assemblage of two-pyroxene-hornblende gneiss. Typical dis-equilibrium corona texture of pyroxene, inner corona of quartz and hornblende surrounded by hornblende. Plagioclase twin boundary migration and lobate grain boundaries. Clinopyroxene consists of exsolutions of ilmenite. Kyanite disequilibrium texture is present. Large epidote grains are present.
PV1237AB	Plagioclase 35% Hornblende 30% Clinopyroxene 10% Orthopyroxene 5% Kyanite 10% Epidote 5% Quartz 5%	Oxides Rutile	Host two-pyroxene-hornblende assemblage. Plagioclase, irregular grain boundaries. High proportion of mantle porphyroblasts (deformed and recrystallized). Clinopyroxene typically consists of an exsolution of ilmenite. Kyanite disequilibrium texture.
PV1234a	Hornblende 35% Plagioclase 40% Ilmenite 5% Clinopyroxene 10% Epidote 5% Kyanite 5%	Orthopyroxene	Strained host assemblage and well-foliated due to later D3 shear zone. Increased abundance of epidote due to shear. Typical dis-equilibrium corona texture surrounding pyroxene. Plagioclase typically homogenised ~0.25mm in diameter and contains undulose extinction, deformation twins and bulging grain boundaries.
PV1239	Plagioclase 35% Garnet 20% Hornblende 15% Quartz 10% Clinopyroxene 10% Epidote 5% Biotite 5%	Scapolite Rutile Oxides ilmenite	Further recrystallized host two-pyroxene-hornblende assemblage. Recrystallization of clinopyroxene, resulting in a higher abundance of quartz. Plagioclase has homogenised grain size ~0.5mm with tapered twins and bulging grain boundaries. High abundance of inner corona of quartz and hornblende symplectites within this domain.
PV1216b	Plagioclase 40% Hornblende 35% Clinopyroxene 5% Biotite 5% Epidote 5% Quartz 5% Ilmenite 5%	Rutile	Pyroxene is typically extensively recrystallized removing the S1 texture. High abundance of quartz and hornblende symplectites. Recrystallised plagioclase grains resulting in serrated boundaries and bulging grain boundaries, typically ~0.25mm in diameter. Biotite lathes present.
PV1219	Plagioclase 35% Hornblende 25% Clinopyroxene 10% Orthopyroxene 10% Ilmenite 5% Epidote 5%	Rutile Kyanite	Poorly foliated sample. Varied plagioclase grain size from 0.1mm up to 2.5mm. Plagioclase consists of bulging grain boundaries, deformation twins and kink bands. Amphibole and quartz symplectites are common. Pyroxenes are highly

	Quartz 10%		deformed and exsolved with opaques.
PV1233a	Hornblende 40% Plagioclase 30% Quartz 10% Clinopyroxene 10% Epidote 10%	Rutile Oxides	Hydrous sample with amphibole and epidote. Symplectites of amphibole and quartz are common. Clinopyroxene porphyroblasts have pressure solution tails of recrystallised hornblende. Clinopyroxenes consist of deformation tails and exsolution due to chemical mixing, common in pyroxenes. Plagioclase tapered twin edges.

4.2 Domain 2: Dyke

D2 resulted in the cutting of the S1 assemblage by moderately to steeply dipping felsic dykes and has resulted in domain 2 (Daczko and Halpin, 2009). These dykes can be seen at the centre of most garnet reaction zone textures, although sometimes this is not the case. Therefore garnet reaction zones with no obvious dyke are termed 'collapsed' dykes (Daczko and Halpin, 2009).

Dykes commonly consist of plagioclase (powdery texture), garnet, quartz (clear) and minor K-feldspar with different modal proportions. Plagioclase and quartz commonly have granoblastic – ~~seriate~~ grain boundaries. Plagioclase commonly exhibits deformation textures such as tapered twins, kink banding and bulging grain boundaries whereas quartz displays undulose extinction. Garnet is typically found within the dyke as large grains (up to 1mm in diameter) and as wall rock garnet. Dyke garnet is a lighter pink colour than garnet reaction zone garnet. The wall rock garnet is texturally different as they appear to be growing into clinopyroxene of the garnet reaction zone assemblage (Fig 4.2.1).

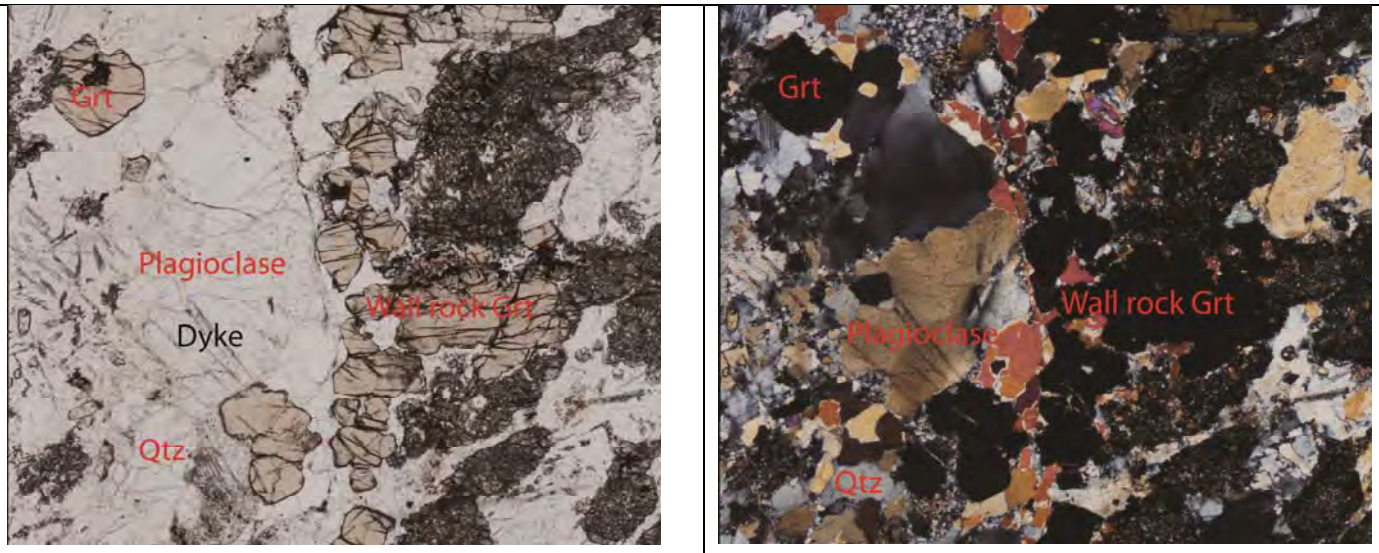

Figure 4.2.1: Typical dyke composition with dyke and wall rock garnet. Note high abundance of quartz and plagioclase. Undulose extinction can be seen within quartz. Photomicrograph of sample PV1222a PPL (left) and XPL (right). Base of photo 5mm.

K-feldspar is most easily seen ~~within back-scatter electron images (BSE) from the scanning electron microscope~~. Figure 4.2.2 displays K-feldspar abundance which can be seen on the outer edges of the dyke and garnet reaction zones. This dyke is quartz rich and contains two zircon grains (bright white grain within quartz rich dyke).

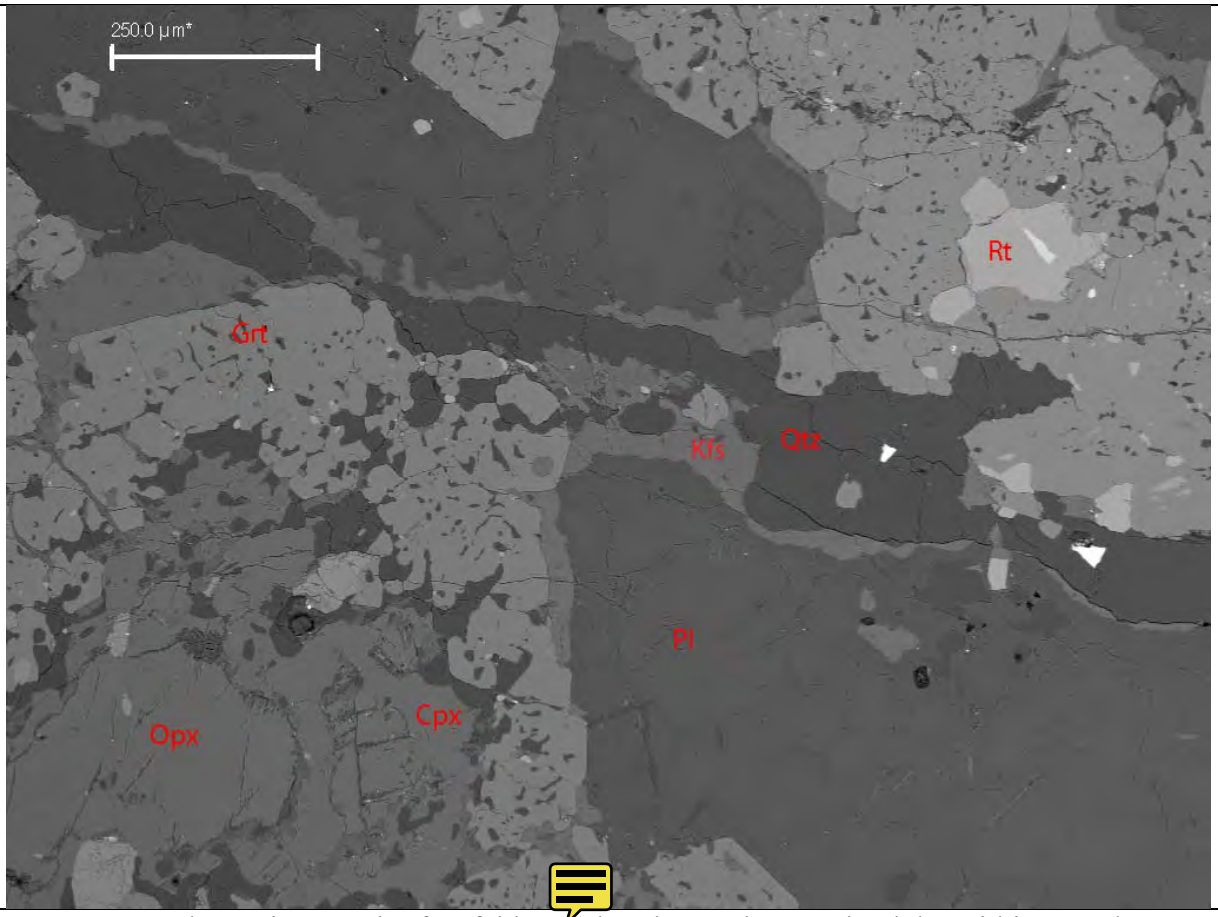

Figure 4.2.2: SEM photomicrograph of K-feldspar ~~abundance close to~~ the dyke within sample 1230. ~~Light grey colour is K-feldspar with the highest abundance close to the quartz rich dyke.~~

Detailed analysis of K-feldspar displays garnet grains becoming increasingly rounded with a low dihedral angle ~~of K-feldspar~~ at grain boundaries (Fig 4.2.3).

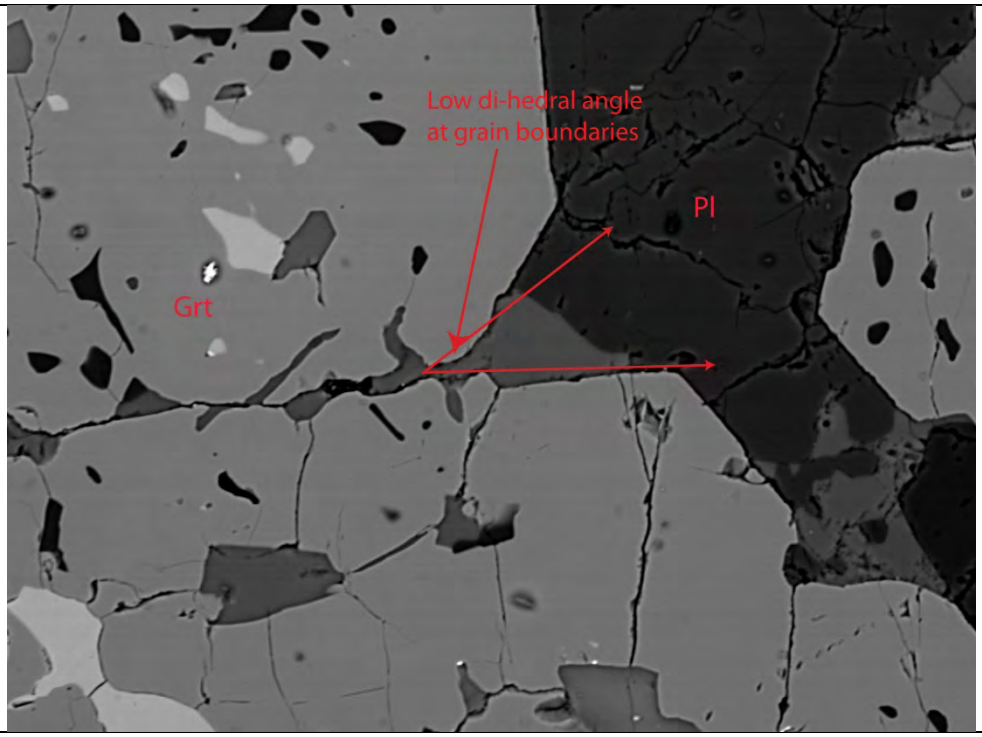

Figure 4.2.3: SEM photomicrograph of K-feldspar between two garnet grains. Red arrows indicate low di-hedral angle. Base of photo is 500µm.

Some dykes have also been termed 'collapsed' and these dykes commonly consist of remnant dyke garnet (lighter coloured than garnet reaction zone garnet), quartz, and K-feldspar and/or scapolite ~~alignment~~ (Fig 4.2.4).

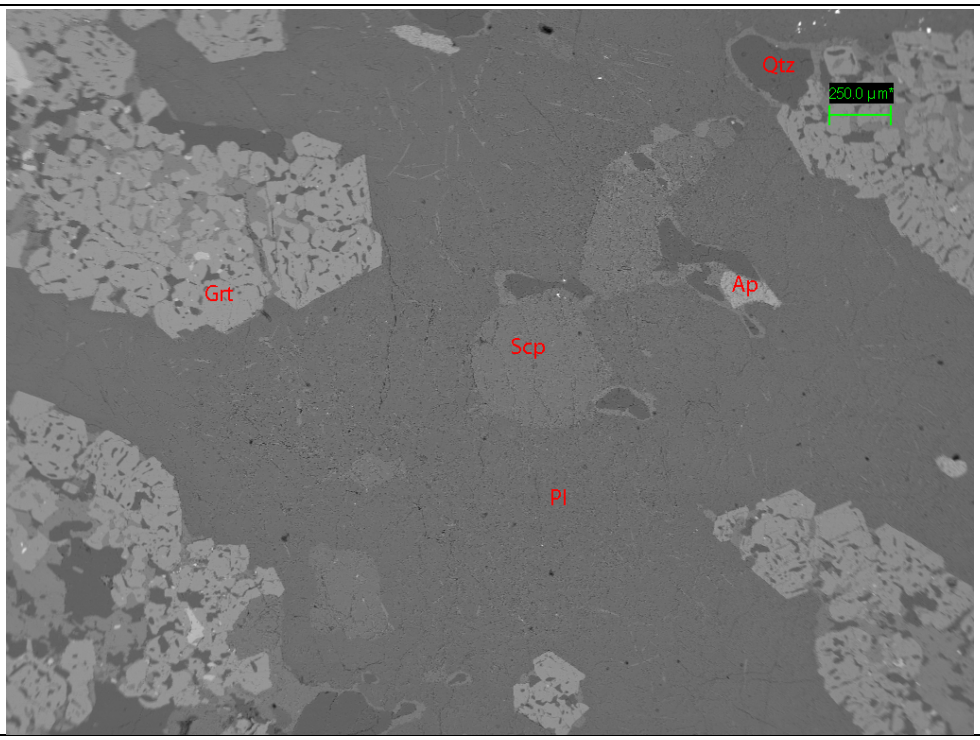

Figure 4.2.4: SEM photomicrograph of a typical 'collapsed' dyke within sample 1217c2. Line of scapolite (light grey) and quartz (dark grey) with minor K-feldspar indicating region of previous dyke.

Small offsets of garnet reaction zones can be seen within some samples. Offsets appear to of formed during the closer of a dyke, resulting in slight offsets (Fig 4.2.5).

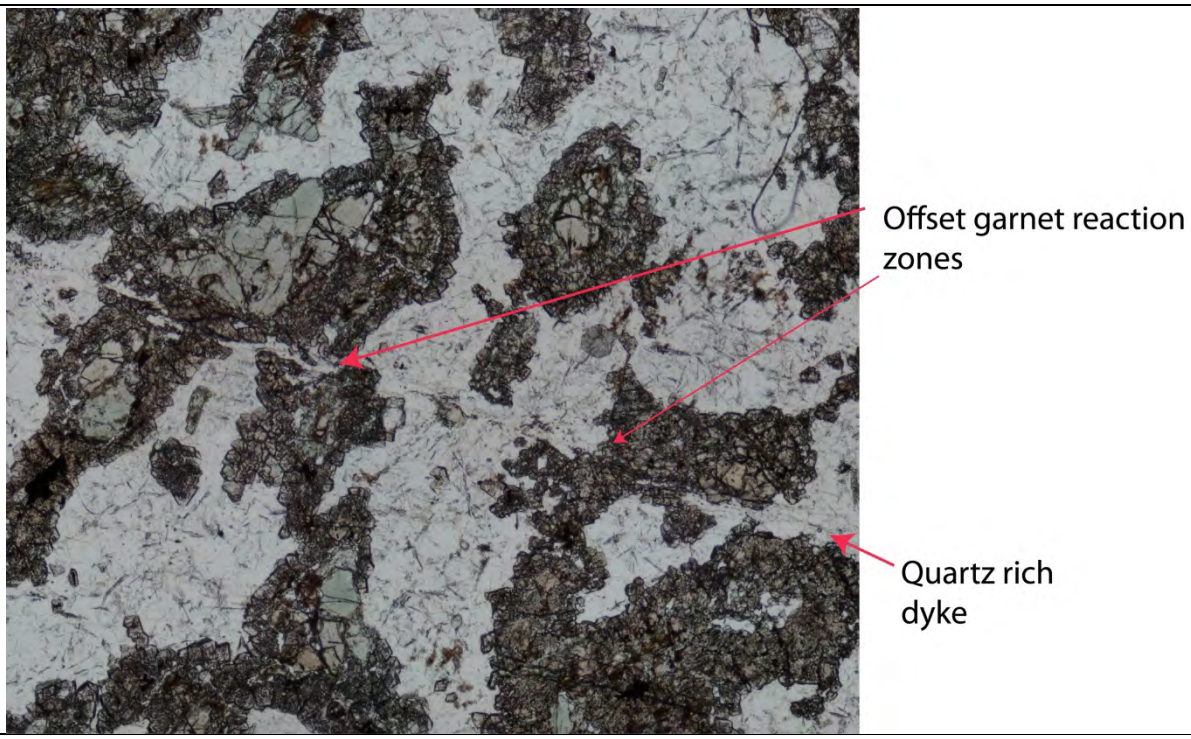

Figure 4.2.5: PPL photograph of 'collapsed' dyke within sample PV1230. Slight offsets of garnet reaction zones can be observed during dyke closure. Base of photo is 6.5mm.

Table 4.2 presents the modal proportions and descriptions of dykes within different samples. Dyke boundaries are diffused therefore table 4.2 distinguishes dyke boundaries at the transition from felsic to mafic garnet reaction zone assemblage.

Table 4.2: Domain 2 (dyke) mode and proportion within each sample. GRZ = garnet reaction zone.

GNS	Major Minerals and Estimated Mode	Minor	Structure/ Comments
PV1222A	Plagioclase 45% Quartz 35% Garnet 15% K-feldspar 5%		Granoblastic grain boundaries. Plagioclase commonly consists of bulging grain boundaries, undulose extinction and tapered twins. Commonly ranges in size from 0.25mm – 4mm in diameter. Quartz commonly forms a mortar texture around plagioclase and ranges in size from <0.1mm – 0.25mm. Garnet is found within the dyke and on the wall of the dyke. Minor K-feldspar present.
PV1217c2	Plagioclase 50% Quartz 40% Garnet 10%		'Collapsed dyke' sample. Modal proportions are from the region where the dyke collapsed. Line of dyke garnet (light coloured compared to GRZ) and quartz is present. Line of scapolite is also present and is interpreted as a product of dyke recrystallization.
PV1230	Quartz 90% K-feldspar 10%		'Collapsed dyke' sample. Consists of offset garnet reaction zones either side of the dyke, interpreted due to a collapse. Quartz consists of undulose extinction. Zircon grain with high birefringence is observed within the dyke.
PV1216A	Plagioclase 45% Quartz 40% K-feldspar 10% Garnet 5%		Seriate grain boundaries. Homogenised grain size ~0.25mm with a high proportion of plagioclase and quartz. Quartz and plagioclase commonly consist of bulging grain boundaries and undulose extinction.
PV1237AA	Quartz 80% Garnet 10% Plagioclase 5% K-feldspar 5%		Granoblastic grain boundaries. Quartz rich dyke with anhedral faces and commonly displays undulose extinction. Garnet is commonly found on the wall rock.
PV1237AB	Quartz 60% Plagioclase 30% K-feldspar 5% Garnet 5%		Granoblastic grain boundaries. Quartz average grain size of ~0.25mm with undulose extinction. Plagioclase commonly <0.2mm with tapered twins, kink bands and bulging grain boundaries.
PV1208A	Quartz 80%		Highly recrystallized dyke. Common quartz

	Garnet 10% K-feldspar 10%		grain size <0.1mm. Pods of large quartz grains are common, surrounded by mortar texture of quartz. Dyke and wall rock garnet are present.
PV1234b	Plagioclase 55% Quartz 25% K-feldspar 15% Garnet 5%		Seriate grain boundaries. Varied plagioclase grain size of <0.1mm to ~6mm. Common kink bands and deformation twins. Quartz is commonly small grained (~<0.1mm) and contains undulose extinction.
PV1239	Quartz 50% Plagioclase 40% Garnet 5% K-feldspar 5%		Common granoblastic grain boundaries of quartz and plagioclase. Plagioclase and quartz have varied grain sizes (~0.1mm – 2mm). Quartz commonly forms a mortar texture around plagioclase. Deformation twins and bulging grain boundaries are present within plagioclase. Quartz commonly contains undulose extinction.
PV1211a	Plagioclase 60% Quartz 25% K-feldspar 10% Garnet 5%		Common seriate grain boundaries. Plagioclase is commonly highly deformed with bulging grain boundaries and deformation twins. Quartz commonly consists of undulose extinction. Some large plagioclase grains, up to ~2mm in diameter.

4.3 Gabbroic gneiss – Garnet Reaction zones

Garnet reaction zones are commonly observed either side of felsic dykes and are amphibole-, biotite- and epidote-poor with a well-defined S1 fabric of elongate clusters of mafic minerals (clinopyroxene, orthopyroxene ± garnet) in a plagioclase-rich rock (Fig. 4.3.1). Minor phases include quartz, rutile, ilmenite and K-feldspar. Garnet reaction zones are further divided on the basis of recrystallization, which generally increases closer to the dyke from partial to extensive recrystallization. A partially recrystallized garnet reaction zone consists of an S1 assemblage whereas an extensively recrystallized sample ~~has been termed this on the basis of wide spread recrystallization, with no S1 assemblage present.~~

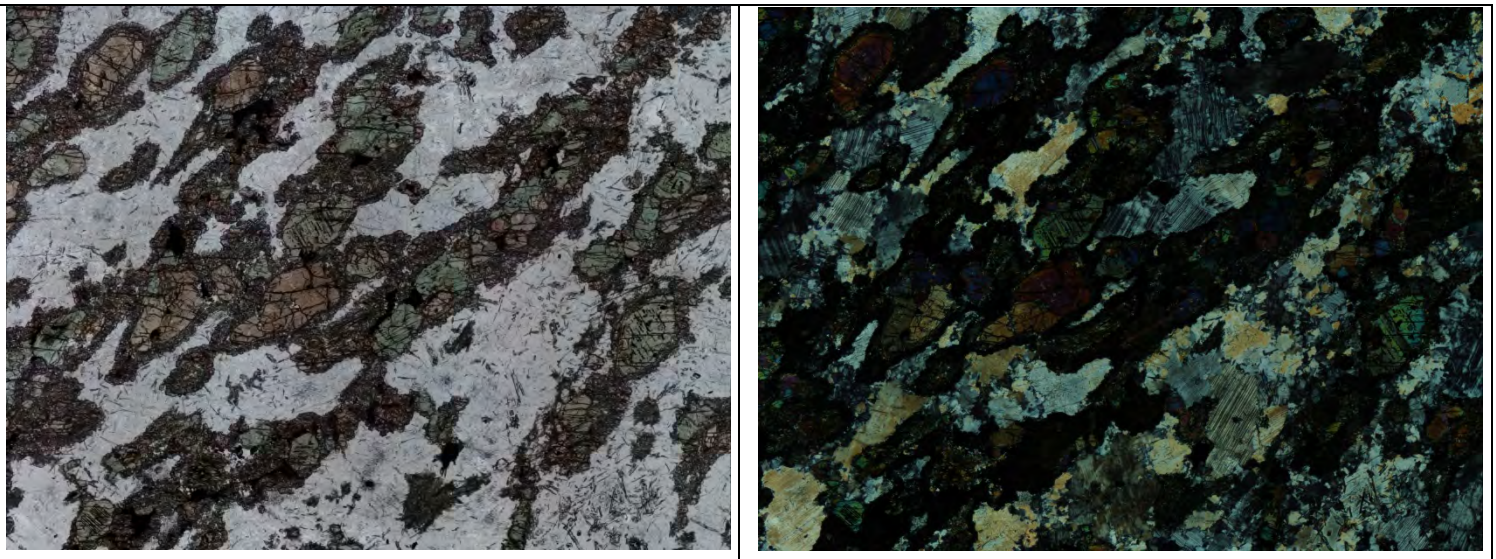

Figure 4.3.1: Photomicrograph of a typical partially recrystallized garnet reaction zone from sample 1222a PPL and XPL. Base of photo is 8.6mm. Elongate minerals of orthopyroxene and clinopyroxene with garnet ~~recrystallization~~ around pyroxene. Light coloured minerals consist of kyanite, quartz and powdery plagioclase which comprises of relict and neoblast grains.

4.3.1 Partially Recrystallized Garnet Reaction Zones

Clinopyroxene and orthopyroxene are common primary S1 mafic minerals with common exsolutions of ilmenite (Fig 4.3.2). Frequently found as ~~a~~ mafic cluster. Clinopyroxene commonly contains orthopyroxene inclusions with a poorly developed cleavage (Fig 4.3.3). Clinopyroxene is commonly found in a reaction zone inner corona of a symplectite with quartz and pyroxene.

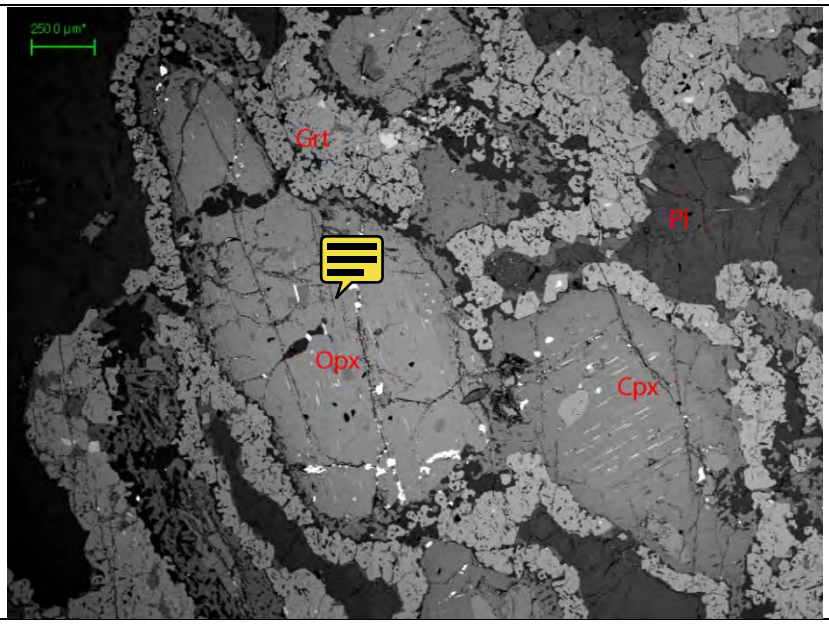

Figure 4.3.2: SEM photo of a typical garnet reaction zone assemblage. Orthopyroxene (large left mineral) and clinopyroxene (large right mineral) show exsolution of ilmenite. Pyroxenes are surrounded by garnet which contains quartz and clinopyroxene inclusions (dark greys).

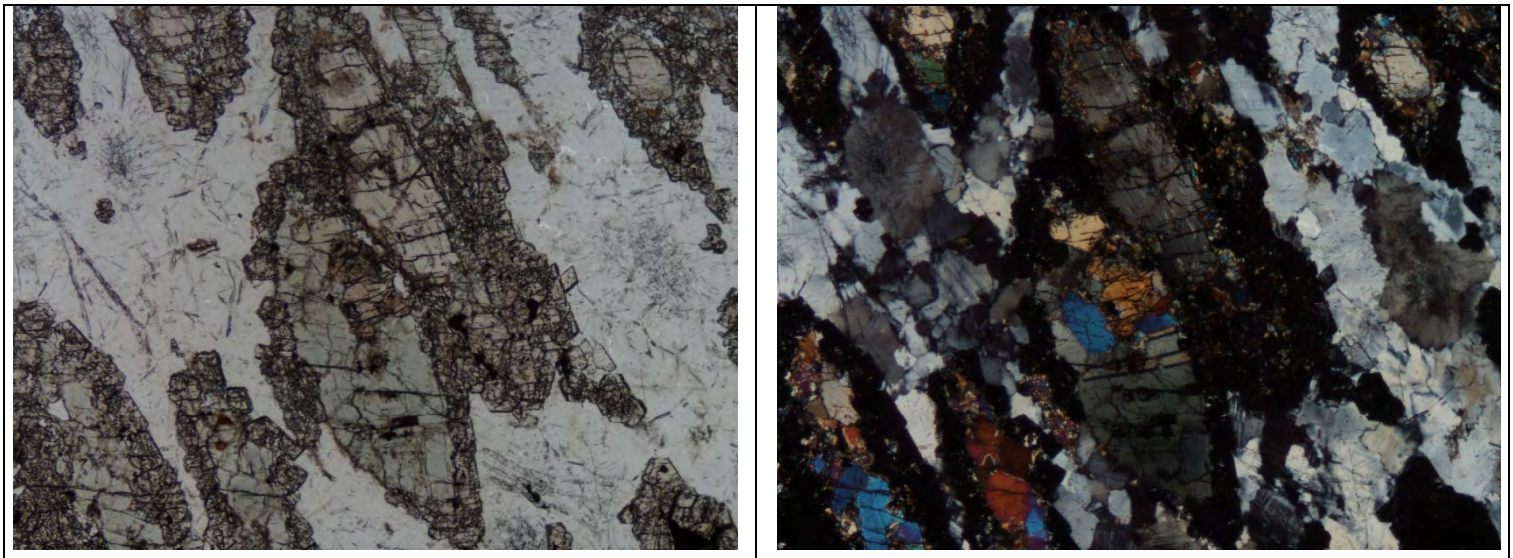

Figure 4.3.3: Photomicrograph of typical mafic cluster within garnet reaction zones from ple 1217a. PPL (left) and XPL (right) and of photo is 4.4mm. Clinopyroxene (left green min consisting of opaque inclusions as well as orthopyroxene. Clinopyroxene consists of a mafic cluster and twinning. Both pyroxenes consist of an outer corona of garnet and an inner corona of clinopyroxene and quartz symplectite.

Garnet can be found within two different textural settings, (1) as coarse idioblastic grains with straight grain boundaries growing into the plagioclase domain (Fig 4.3.4) or (2) porphyroblast garnet from the dyke (dy wall rock) (Fig 4.2.1), sometimes containing overgrowths of rutile and/or ilmenite. Symplectite textures are common in garnet within the

garnet reaction zones, resulting in a garnet/quartz symplectite. Garnet within garnet reaction zones psuedomorphs hornblende from the S1 two-pyroxene-hornblende assemblage (domain 1).

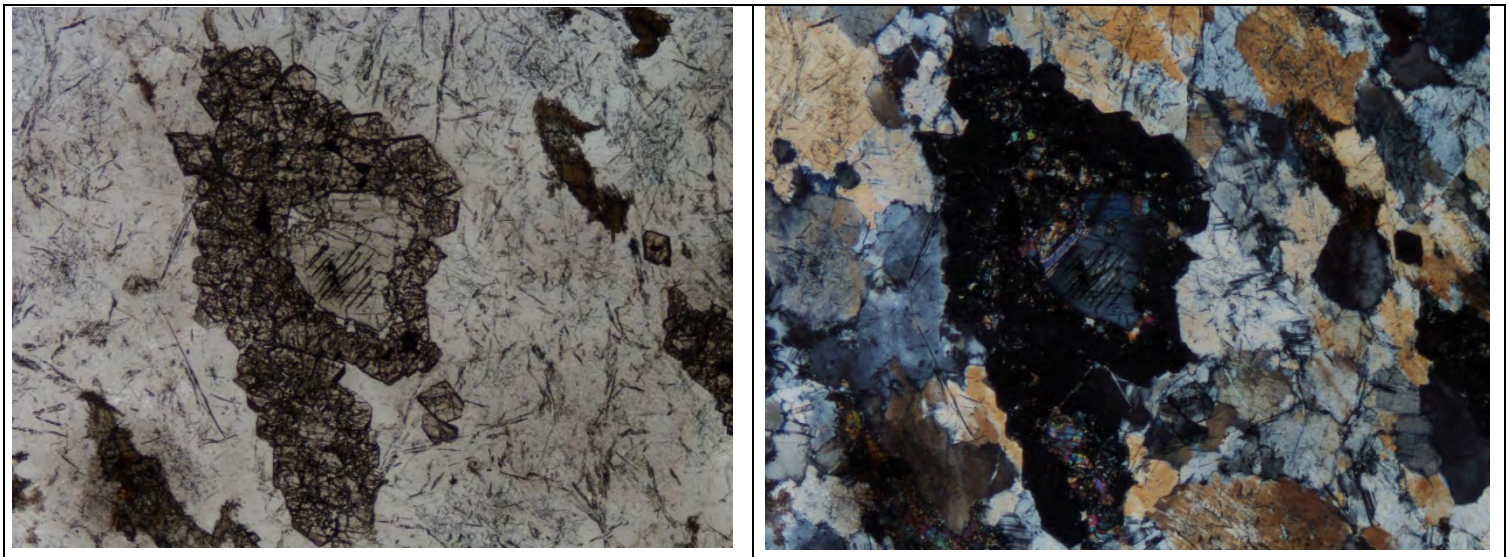

Figure 4.3.4: Photomicrograph of idioblastic grain boundaries of garnet into plagioclase. Photo is from sample 1217c1, PPL and XPL base of photo 4.4mm.

Symplectites of garnet and quartz can be further divided into inclusion rich (close to pyroxene) or inclusion poor (close to plagioclase) due to different growth rates (Fig 4.3.5).

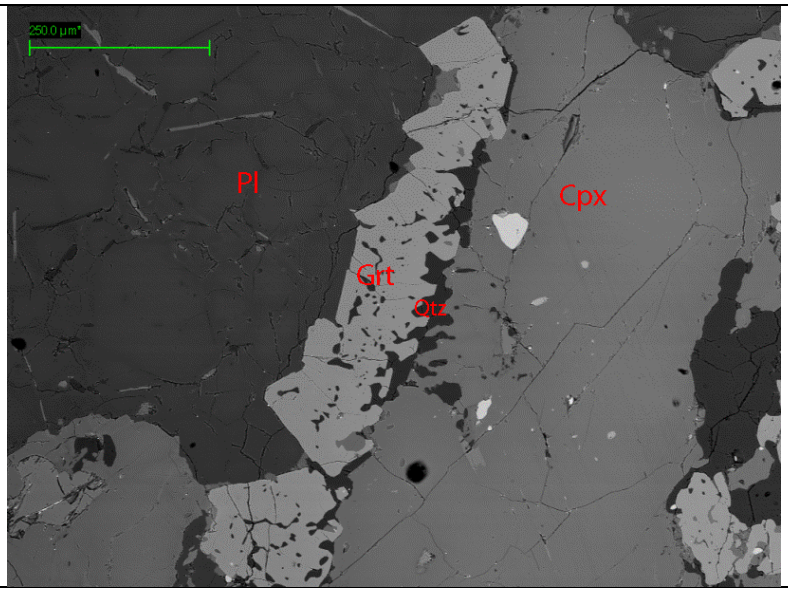

Figure 4.3.5: SEM photomicrograph of idioblastic grain boundaries of garnet growing into the plagioclase region. Contains slow growths with no quartz inclusions and inclusion rich fast growths close to pyroxene. Photo is from sample PV1230.

Plagioclase is commonly inequigranular – interlobate with undulose extinction, deformed twins, tapered twins and serrated boundaries. Kink bands and deformation twins are also common (Fig 4.3.6). Relict plagioclase grains are of a higher abundance within partially recrystallized samples.

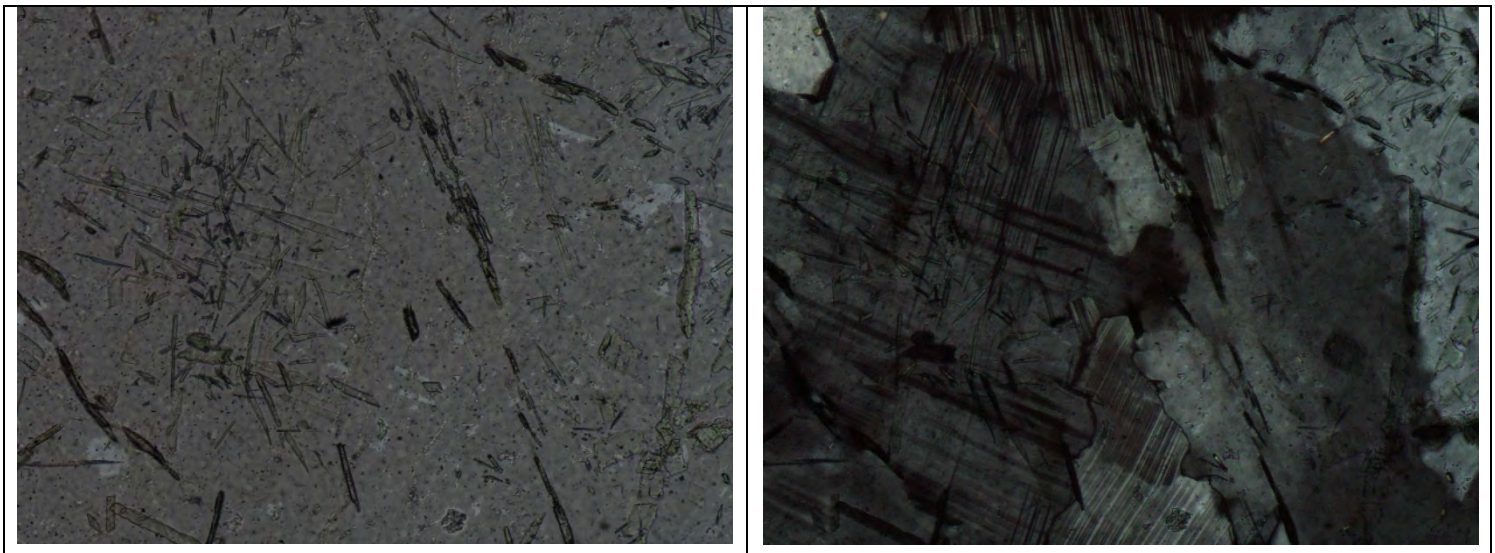

Figure 4.3.6: Photomicrograph of typical feldspar microstructures. Sample 1217a, PPL and XPL base of photo 0.87mm. Kyanite overgrowths are shown in PPL. Within XPL serrated boundaries can be seen due to grain boundary migration. Kink bands and tapered twins are also present.

Biotite is found in a small abdundance within some garnet reaction zones with a lath~~e~~-like texture. Biotite is pleochroic from light to dark brown. Kyanite is acicular and can be found within plagioclase ~~regions~~, indicating high P-T. Epidote can also be found as acicular – spherical poikiloblasts and is common close to recrystallised dykes with an anomalous blue birefringence. Scapolite is also common close to dykes with a powdery texture and low birefringence colours.

Rutile is commonly subeuhedral to anhedral appearing as overgrowths of pyroxene and garnet (Fig 4.3.7). Rutile can also be seen associated with plagioclase. Ilmenite is black and commonly found as an exsolution ~~with~~ clinopyroxene, most easily seen within BSE images.

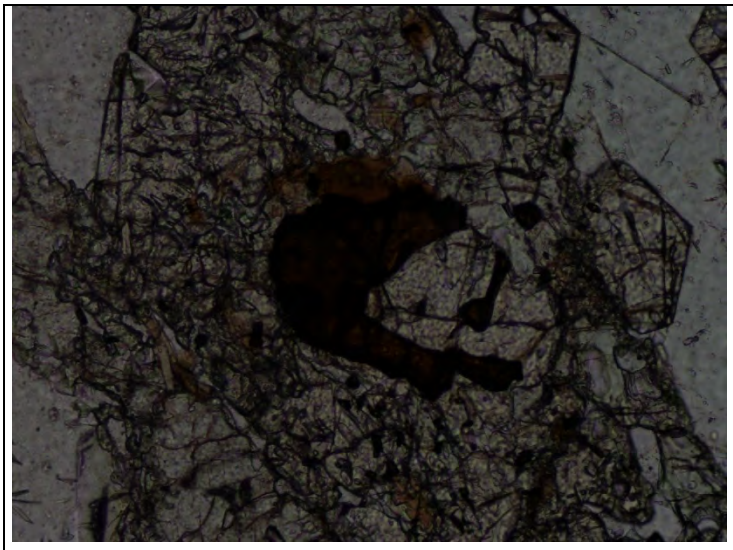

Figure 4.3.7: Photomicrograph of sample 1217c1 PPL and XPL base of photo 4.4mm. Rutile is overgrown over garnet within the reaction zone.

4.3.2 Extensively Recrystallized Garnet Reaction Zones

Extensive recrystallization results in the removal of the S1 assemblage (two-pyroxene-hornblende) and is developed within most garnet reaction zones close to the dyke. Samples are termed this if there has been large scale recrystallization throughout the whole garnet reaction zone. Within these samples large pyroxene grains have been fully recrystallized and there is no obvious corona texture. Sample PV1216a is a representative extensively recrystallized sample (Fig 4.3.8).

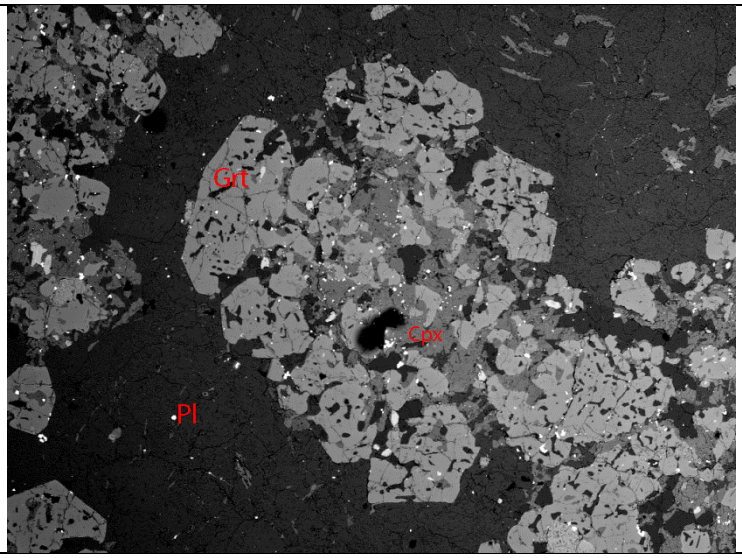

Figure 4.3.8: SEM photo of extensively recrystallised sample PV1216a. Garnet and clinopyroxene rich with no S1 assemblage.

Extensive recrystallization is also observed within sample PV1239 at the intersection of two dykes. This sample has undergone further deformation and therefore further recrystallization from dyke interaction (Fig 4.3.9).

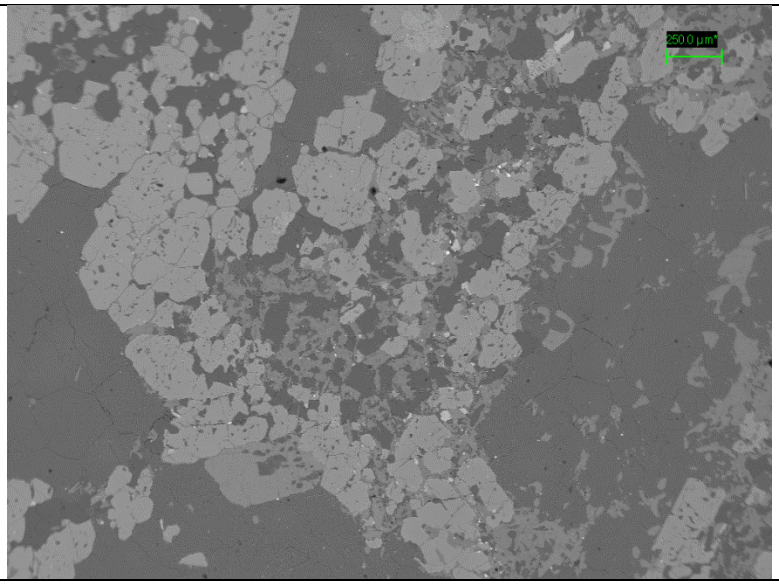

Figure 4.3.9: SEM photo of extensively recrystallised sample PV1239 at the intersection of two dykes. Garnet rich with no S1 assemblage.

Garnet and dyke interaction varies across samples, although there is a general trend of increased garnet grain size closer to the dyke and an increase in the degree of feldspar recrystallization. Statistics have been completed through measuring grain areas from the

PRIOR microscope showing the dyke interaction effect on grain size and recrystallization within sample PV1216a (Fig 4.3.10).

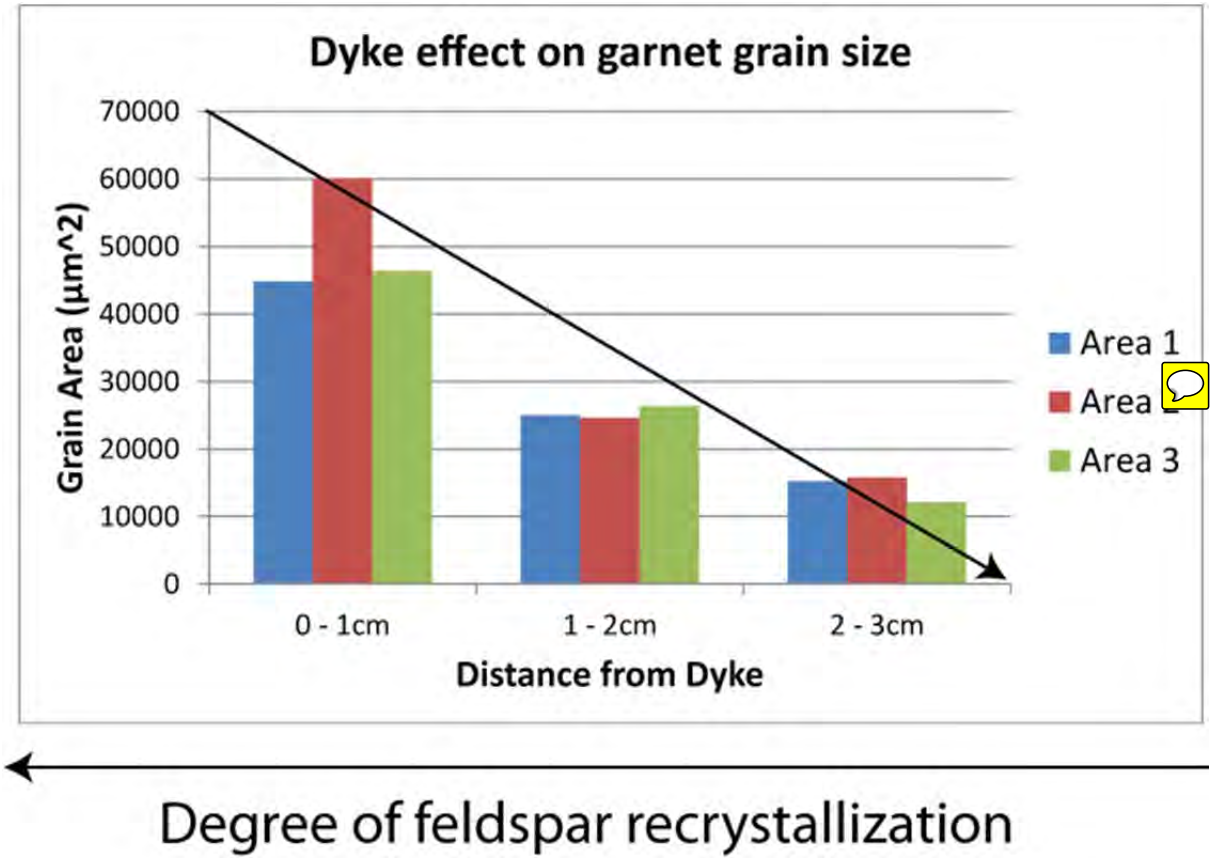

Fig 4.3.10: PV1216a garnet grain size and feldspar recrystallization depending on location with the dyke.

Garnet modal abundance has been visually estimated within mafic clusters of two-pyroxene-garnet with respect to the dyke. There is a general increase in garnet abundance close to the dyke (Fig 4.3.11).

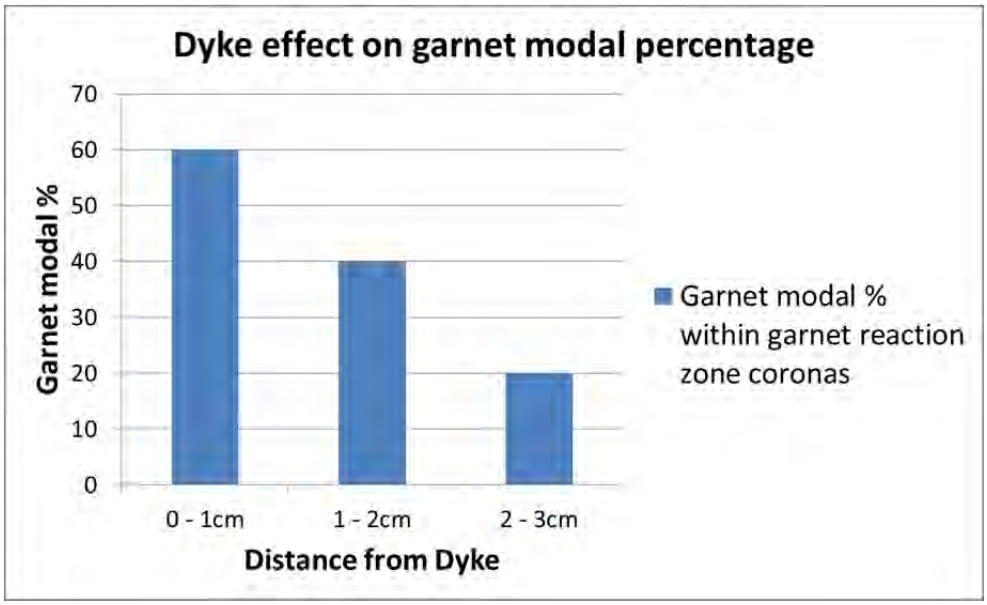

Figure 4.3.11: Visual estimate of garnet modal percentages depending on distance from the dyke. High abundance of garnet close to the dyke.

Plagioclase consists of sutured grain boundaries, bulging grain boundaries, deformation twins and kink banding. Relict and neoblast grains are still present although the proportions of neoblasts are higher within extensively recrystallized samples.

Minor biotite is present within extensively recrystallized garnet reaction zones. Biotite consists of lathe like crystals and pleochroic from light to dark brown (Fig 4.3.12). Some garnet reaction zones have been deformed further by D3 shear zones which have brought in hydrous minerals into the extensively recrystallized garnet reaction zone region.

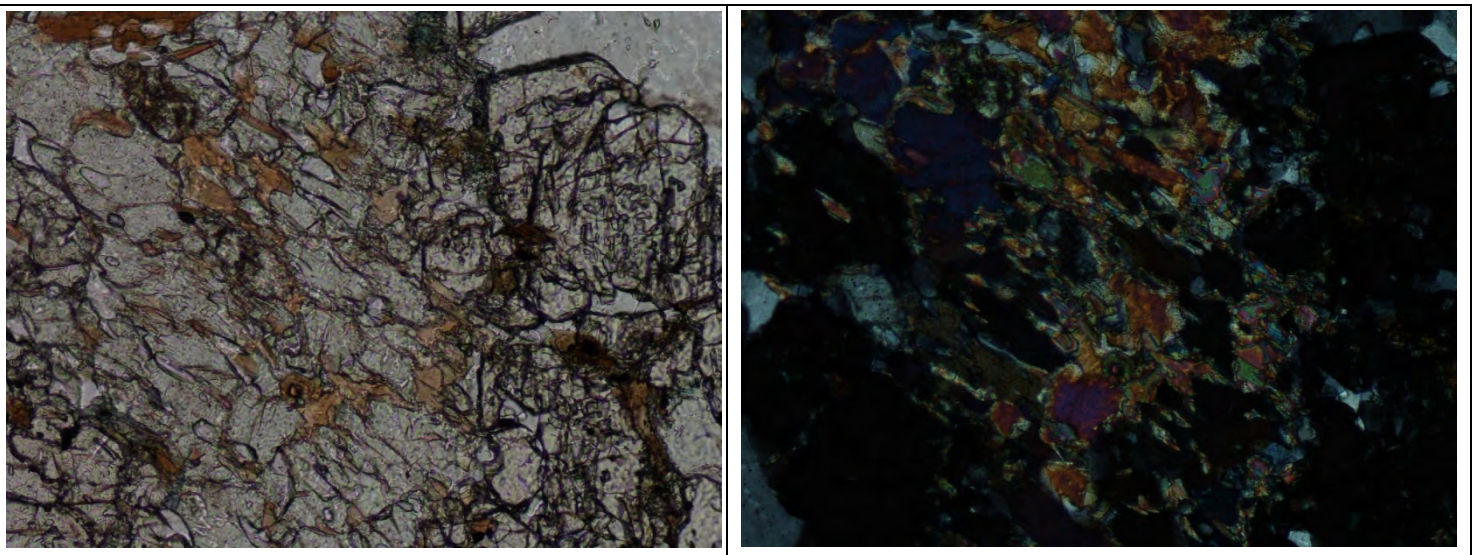

Figure 4.3.12: Photomicrograph of sample 1217b PPL and XPL base of photo 4.4mm. Lathe like crystals of biotite within the mafic reaction zone assemblage.

The visually estimated mode of each sample and a description is summarised in Table 4.3. Table 4.3 segregates garnet reaction zones on the basis of recrystallization, which generally increases closer to the dyke.

Table 4.3: Domain 3 (GRZ) mode and description of samples

GNS	Recrystallization Degree	Major Minerals and Estimated Mode	Minor	Structure/ Comments
PV1222A	Partially	Plagioclase 40% Garnet 30% Clinopyroxene 15% Orthopyroxene 10% Quartz 5%	Epidote Rutile Ilmenite Scapolite	Common texture of garnet and quartz symplectite surrounding pyroxenes. Exsolution texture of ilmenite within cpx. Plagioclase with anhedral grain boundaries, kink banding, tartan twinning and bulging grain boundaries. Quartz commonly contains undulose extinction.
PV1217a	Partially	Plagioclase 40% Garnet 25% Clinopyroxene 15% Orthopyroxene 10% Biotite 5% Kyanite 5%	Rutile Ilmenite Hornblende Epidote Quartz	GRZ garnet displays little variation in grain size. Plagioclase deformed twins and serrated boundaries. Plagioclase also consists of strain induced grain boundary migration (kink

				bands and deformation twin boundaries). Pyroxene grains are commonly found as mafic clusters.
PV1217b	Partially	plagioclase 40% Garnet 20% Clinopyroxene 15% Orthopyroxene 10% Kyanite 5% Quartz 5% Scapolite/epidote 5%	Biotite Rutile Ilmenite	Typical anhydrous two-pyroxene-garnet assemblage. Clinopyroxene and quartz symplectites are within reaction zone coronas. Mafic clusters of pyroxenes. Plagioclase inequigranular – interlobate with bulging grain boundaries and mortar textures.
PV1217c1	Partially	Plagioclase 45% Garnet 30% Clinopyroxene 15% Orthopyroxene 5% Quartz 5%	Scapolite Hornblende Rutile Ilmenite	Large relict plagioclase grains and bulging grain boundaries with deformation textures. Mafic clusters of pyroxenes. Garnet reaction zone garnet with bulging grain boundaries. Dyke garnet is present at collapsed dyke location. Close to previous dyke, there is extensive recrystallization.
PV1217c2	Partially	Plagioclase 40% Garnet 30% Clinopyroxene 15% Orthopyroxne 5% Quartz 5% Kyanite 5%	Rutile Hornblende Biotite Scapolite Ilmenite	Line of scapolite at previous dyke location. Varied plagioclase grain size, relict grains which are large with lobate grains. Increased recrystallization of reaction zone close to previous dyke.
PV1230	Partially	Plagioclase 30% Orthopyroxene 15% Garnet 20% Clinopyroxene 15% Quartz 10% Epidote 5% Biotite ~5%	Ilmenite Rutile	Medium grained foliated gabbroic gneiss. Plagioclase has a variety of grain sizes, sutured grain boundaries, kink bands, deformation twins. Pyroxene consists of quartz as a symplectite. Quartz commonly displays undulose extinction. Well defined S1 foliation.
PV1237aa	Partially	Plagioclase 35% Garnet 25% Clinopyroxene 15% Quartz 10% Epidote 5% Biotite 5% Kyanite 5%	Rutile Ilmenite	Plagioclase twin boundary migration, lobate grain boundaries. Clinopyroxene consists of exsolutions of ilmenite. Large epidote grains close to the dyke.

PV1237AB	Partially	Plagioclase 45% Garnet 25% Clinopyroxene 15% Orthopyroxene 10% Kyanite/epidote 5%	Ilmenite Rutile	Plagioclase, irregular grain boundaries from strain induced grain boundary migration. High proportion of mantle porphyroblasts (deformed and recrystallized). Clinopyroxene commonly found as mafic cluster.
PV1208a	Partially	Hornblende 25% Plagioclase 20% Garnet 20% Clinopyroxene 10% Epidote 10% Biotite 10% Quartz 5%	Scapolite Rutile	Hydous sample with high abundance of amphibole and epidote. Garnet quartz symplectites. Highly strained sample.
PV1219	Partially	Plagioclase 45% Garnet 35% Clinopyroxene 5% Orthopyroxene 5% Quartz 5% Epidote 5%	Rutile ilmenite Kyanite	Large relict plagioclase grains with bulging grain boundaries. Amphibole and quartz symplectites are common within GRZ coronas. Garnet and quartz exsolutions are also common. Pyroxenes are highly deformed and exsolved with opaques.
PV1211a	Extensively	Plagioclase 40% Garnet 40% Clinopyroxene 10% Quartz 5% Biotite 5%	Epidote Ilmenite Rutile	Extensively recrystallized sample. High abundance of garnet and no S1 assemblage.
PV1216a	Extensively	Plagioclase 40% Garnet 40% Clinopyroxene 15% Quartz 5%	Epidote Kyanite Rutile Biotite Ilmenite	Extensively recrystallised garnet reaction zone where the S1 mineralogy is no longer present. Plagioclase sutured grain boundaries, bulging grain boundaries, deformation twins, kink banding. Increased abundance of garnet. Pyroxene mafic clusters and twinning.
PV1216b	Extensively	Plagioclase 40% Garnet 35% Clinopyroxene 10% Biotite 5% Epidote 5% Quartz 5%	Rutile Ilmenite	Garnet and quartz poikiloblasts during the pseudomorph of hornblende. Symplectites of amphibole and quartz forming a corona texture around pyroxenes. Recrystallised plagioclase grains resulting in serrated

				boundaries and bulging grain boundaries. Garnet small grains and rounded. No obvious S1 assemblage. Biotite lathes.
PV1239	Extensively	Plagioclase 40% Garnet 30% Quartz 10% Clinopyroxene 10% Epidote 5% Biotite 5%	Scapolite Rutile ilmenite	Extensively recrystallised sample. Plagioclase tapered twins and bulging grain boundaries. High abundance of clinopyroxene and quartz symplectites within reaction zone. At dyke intersection there is no S1 assemblage present and highly recrystallized.
PV1234b	Extensively	Plagioclase 30% Garnet 30% Hornblende 15% Clinopyroxene 10% Quartz 5% Biotite 5% Epidote 5%	Apatite Ilmenite Rutile Scapolite	Hydrous sample texturally in equilibrium. Extensively recrystallised sample which has also been deformed by D3 at the outer region of garnet reaction zone. Plagioclase deformed twins and serrated boundaries due to grain boundary migration. Plagioclase also consists of bulging grain boundaries (kink bands and deformation twin boundaries).

4.4 D3 shear zone

Two key samples have undergone further deformation by D3 shear zones (PV1234b and PV1211b). These samples are paired shear zone samples which consist of an extensively recrystallized garnet reaction zone with localized strain on the outer regions (Fig 4.4.1).

Figure 4.4.1: Representative paired shear zone sample. High strain is localised on the outer regions of the garnet reaction zone. Red box represents area of thin section from sample PV1234b. Base of photo is 20cm.

Shear zones are plagioclase, clinopyroxene and garnet rich and consist of a homogenised plagioclase grain size (~0.25mm in diameter) with minor biotite and kyanite grains. Garnet can be found as two types, 1) deformed garnet (syn-D3) due to the shear zone or 2) post-D3 which are growing into plagioclase with idioblastic grain boundaries (Fig 4.4.2).

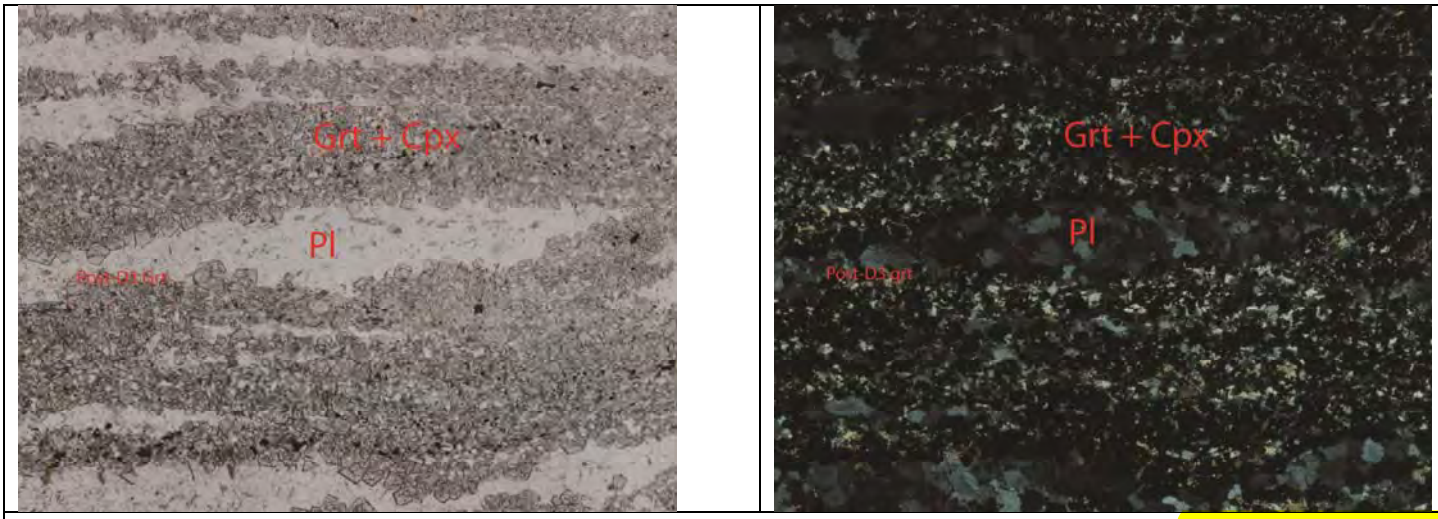

Figure 4.4.2: Photomicrograph of sample 1217b PPL and XPL base of photo 4.4mm. Lathe like crystals of biotite within the mafic reaction zone assemblage.

Table 4.4 presents modal proportions, common textures and comments for D3 strained zones.

Table 4.4: Modal proportions and comments for samples undergoing D3 shearing

GNS	Recrystallization Degree	Major Minerals and Estimated Mode	Minor	Structure/ Comments
PV1234b	Extensively	Garnet 50% Plagioclase 20% Quartz 10% Clinopyroxene 15% Biotite, kyanite and ilmenite 5%	Rutile	Homogenised plagioclase grain size with ~0.25 diameter. Granoblastic grian boundaries with deformation twins. Quartz displays undulose extinction. Two texturally different garnets, 1) small rounded grains (syn-D3 ~0.25mm diameter max) and 2) large post-D3 garnet grains (~1mm diameter) with idioblastic grain boundaries. Cpx is highly recrystallized.
PV1211b	Extensively	Garnet 40% Plagioclase 25% Clinopyroxene 15% Quartz 20%	Rutile Ilmenite Biotite	Highly recrystallized sample. Homogenised plagioclase and quartz grain size of ~0.1mm in diameter. Garnet has small syn-D3 grains ~0.1mm diameter and larger ~0.2mm post-D3 grains. Clinopyroxene is extensively recrystallized.

4.5 Summary and Interpretation

Garnet reaction zones have formed due to the dehydration reaction of hornblende + pyroxene + plagioclase → garnet + pyroxene + quartz + H_2O (Schroter et al., 2004). The typical garnet reaction zone metamorphic assemblage of garnet-clinopyroxene-orthopyroxene-hornblende-biotite-plagioclase-rutile and quartz ~~which all~~ indicate high P-T of ~12 – 16kbar and ~720 – 890°C during garnet granulite formation (Daczko and Halpin, 2009).

This reaction has resulted in the development of four rock domains in the gabbroic gneiss and these are distinguished from the petrography. Domain 1 consists of a well-foliated (S1) two-pyroxene-hornblende assemblage where hornblende forms a well-defined corona texture around pyroxene. This texture comprises an inner corona of hornblende and quartz symplectite, indicating a time of dis-equilibrium. Domain 2 consists of felsic dykes that cut S1. Variable modes of plagioclase, garnet, quartz and minor K-feldspar with a variable grain size are observed. This domain also contains hydrous minerals (epidote and scapolite) which have been concluded to of formed due to the crystallization of the dyke (Harte et al., 1993). K-feldspar abundance increases closer to the dyke with low dihedral angles, suggesting K-feldspar represents melt filled pores and a pathway of melt extraction (Holness and Sawyer, 2008). Domain 3 consists of garnet granulite, commonly developed adjacent to the dykes. These are divided into two types on the basis of the degree of recrystallization of S1 minerals. Garnet reaction zones that preserve relict S1 minerals are termed partially recrystallised, whereas those interpreted to have largely recrystallised most S1 mineralogy are termed extensively recrystallised. The partially recrystallised type of garnet reaction zone contains plagioclase feldspar with core-mantle microstructure and garnet forms a well-developed corona. All samples with collapsed dykes have a partially recrystallized texture and some consist of offsets, supporting the conclusion of dyke close~~r~~ by Dackzo & Halpin (2009). The extensively recrystallised type of garnet reaction zones contains homogeneous grain sizes of feldspar, lack corona textures or relict S1 minerals. Garnet is also coarser grained compared with partially recrystallised samples. Garnet abundance increases within extensively recrystallized garnet reaction zones creating a rheologically strong region as garnet commonly behaves as a rigid object during deformation (Muramoto et al., 2011). Domain 4 consists of well-foliated (S3) garnet-clinopyroxene-hornblende-biotite gneiss with homogeneous grain size within D3 high strain zones.

On the basis of the observed increased intensity of recrystallization and removal of the S1 assemblage in sample PV1239 at the intersection of two dykes, it is inferred the duration of dyke interaction with the host rock is an important variable resulting in extensively recrystallised samples. This implies a relationship between the duration that a dyke is open (and melt migration continues) and the development of the garnet reaction zone microstructure. Extensively recrystallised samples may be interpreted as developing adjacent to dykes that were open longer than dykes near partially recrystallised samples. On the basis of a lack of preferred orientation of minerals or any other deformation textures in garnet granulite, recrystallization and grain coarsening occurred in a static environment. The common driver of recrystallization in static environments is temperature (Herwegh et al., 2008). Though dykes of different compositions (and therefore temperature; (Gibson and Walker, 1963)) may explain the variable intensity of recrystallization, the similar mineralogy observed in all dykes argues against this possibility.

All paired shear zones examined have developed adjacent to extensively recrystallised garnet reaction zones. This observation implies a microstructural control on the localisation of D3 strain. In the most extensively recrystallised garnet reaction zone sample (PV1216a), grain size and the mode of garnet increases with proximity to the dyke. These characteristics develop a rheological contrast, with strong coarse grained garnet rich rock adjacent to weak, finer grained less garnet rich rock (Kleinschrodt and McGrew, 2000; Ranalli, 1995). It is inferred that D3 strain was localised within rock domain boundaries between maximum rheological contrasts.

Chapter 5

Major Element Mineral Chemistry: Scanning Electron Microscopy – Energy-Dispersive Spectroscopy (SEM-EDS)

5.1 Introduction

Four key domains were identified for the gabbroic gneiss in chapter 4: (1) host two-pyroxene-hornblende-gabbroic gneiss; (2) dyke; (3) variably recrystallised garnet reaction zones; and (4) D3 shear zones including paired shear zones. The degree of recrystallization is variable in each of these domains. A focus of this study is to explore the relationship between recrystallization in garnet reaction zones and the subsequent development of D3 paired shear zones. A prediction developed from chapter 4 is that garnet reaction zones with extensive recrystallization develop a pronounced rheological contrast at the boundary between the extensively and partially recrystallised textures. D3 strain is localised at each rheological contrast resulting in a paired shear zone. To explore this hypothesis, the mineral chemistry of ten key samples has been analysed using SEM-EDS at Macquarie University, Sydney. These key samples include partially recrystallised garnet reaction zone samples with or without a dyke (PV1222a, PV1237aa, PV1217c1, PV1217c2 and PV1230), the intersection of two reaction zones resulting in extensive recrystallization (PV1239), an extensively recrystallised garnet reaction zone sample (PV1216a) and paired shear zone samples (PV1211a, PV1211b and PV1234b). The approach involved individual spot analysis of garnet and plagioclase was analysed by transects of 20 analyses. The main aim is to determine to what degree recrystallization homogenises mineral chemistry in extensively recrystallised garnet reaction zones and D3 shear zones. A secondary aim is to compare the mineral chemistry between samples of different domains.

The anorthite ($CaAl_2Si_2O_8$) end-member (X_{An} = Ca/(Ca+Na) is calculated for all plagioclase data and the end-member proportions of pyrope (X_{Pyp} = 100*Mg/(Fe+Mg+Ca+Mn)), almandine (X_{Alm} = 100*Fe/(Fe+Mg+Ca+Mn)), grossular (X_{Grs} = 100*Ca/(Fe+Mg+Ca+Mn)) and spessartine (X_{Sps} = 100*Mn/(Fe+Mg+Ca+Mn)) are calculated for garnet data. All major element analysis and end-member calculations are present in Appendix B. The minimum,

maximum, average and standard deviation of plagioclase and garnet end-members have been determined for each sample (Tables 5.1, 5.2, 5.3 and 5.4).

5.2 Results

Analysis of plagioclase and garnet has been undertaken within domain 2 (dyke), domain 3 (garnet reaction zones, partially and extensively recrystallized) and domain 4 (D3 shear zones). Major element chemical analysis has not focused on D1 (host two-pyroxene-hornblende assemblage) as the development of paired shear zones are the result of the subsequent deformation during D2 – D3.

5.2.1 Plagioclase mineral chemistry

Several distinct differences in the plagioclase chemistry can be observed between analysed plagioclase within and between different domains (domain 2 (dyke), domain 3 (GRZ) and domain 4 (D3 shear zones)). The data from all domains ranges from Oligoclase – Labradorite (Fig 5.2.1). Domain 3 has a large range of X_{An} of ~40% whereas domains 2 and 4 ranges by ~20% X_{An} (Fig 5.2.1).

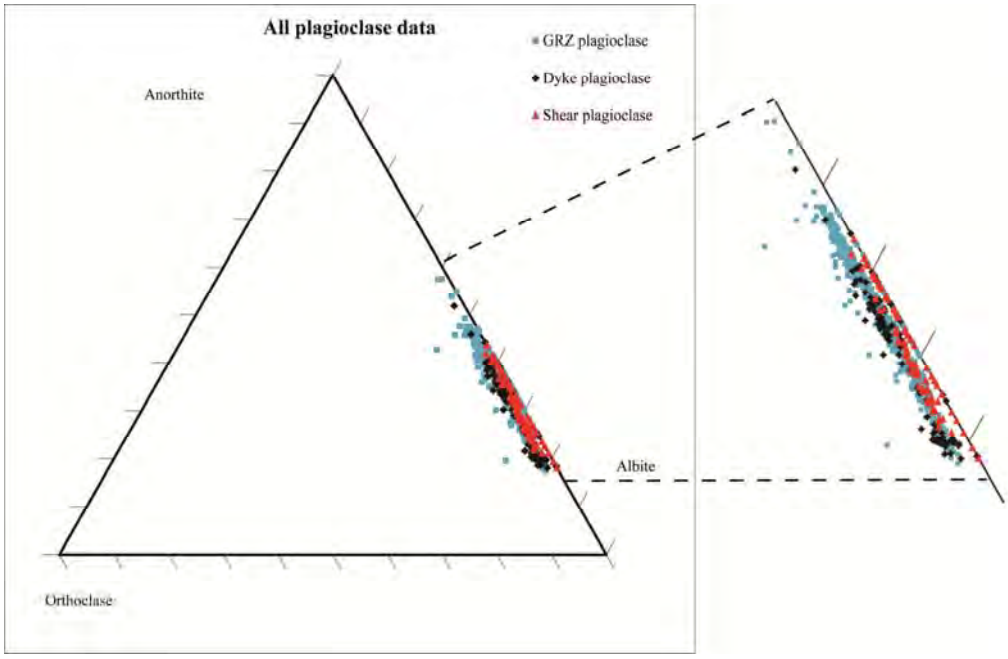

Figure 5.2.1: Plagioclase composition between different domains analysed. Data ranges from Oligoclase – Labradorite with an overall 40% spread.

This variation between domains is displayed within table 5.1 which presents the range and variation of anorthite content between analysed samples and their domains. Plagioclase analysis of samples from domain 2 (dyke) have a low standard deviation 0.3 – 0.5 between samples. The range of anorthite content between samples is also variable, producing the ~20% spread in figure 5.2.1.

Domain 3 (GRZ) has been categorised as partially or extensively recrystallised (cf. Chapter 4). Extensively recrystallized samples display the lowest average standard deviation of X_{An} (0.04), opposed to the partially recrystallized samples with a higher standard deviation of 0.054. This domain displays variable X_{An} content between samples, producing the ~40% spread in figure 5.2.1.

Domain 4 (D3 shear zone) presents a low standard deviation of measured anorthite, 0.4 – 0.6 between samples. Sample PV1234b displays more homogenisation of X_{An} with a lower range (16% X_{An}) and standard deviation (0.04), whereas PV1211b presents a higher range (26% X_{An}) and standard deviation (0.06).

Table 5.1: Minimum, maximum, average and standard deviation of anorthite content between analysed domains

Domain	**Sample**	**An Content**			
		Min	Max	Avg.	St.Dev
Domain 2: Dyke	PV1222a	0.08	0.30	0.20	0.03
	PV1234b	0.18	0.35	0.29	0.05
	PV1211a	0.32	0.52	0.37	0.05
	PV1216a	0.36	0.46	0.37	0.04
Domain 3: GRZ: Partially Recrystallized	PV1222a	0.20	0.46	0.35	0.07
	PV1230	0.26	0.49	0.40	0.05
	PV1237aa	0.20	0.57	0.29	0.08
	PV1217c1	0.35	0.57	0.42	0.04
	PV1217c2	0.37	0.47	0.43	0.03
Domain 3: GRZ: Extensively Recrystallized	PV1216a	0.25	0.55	0.35	0.05
	PV1234b	0.20	0.39	0.30	0.04
	PV1239	0.17	0.36	0.22	0.04
	PV1211a	0.27	0.47	0.36	0.04

	PV1211b	0.28	0.41	0.36	0.03
Domain 4: D3 Shear Zone	PV1234b	0.21	0.37	0.28	0.04
	PV1211b	0.18	0.44	0.34	0.06

This variability of anorthite content between analysed domains is further explored by transects of X_{An}. Complete transects analysed and their locations within different thin sections are located within Appendix B as well as major element chemistry for each analysed transect. Ternary diagrams have also been created for each domain from all gathered transect data.

Domain 2 (dyke) displays variation within samples and between samples, with an overall range of 30% between the four analysed samples (Fig 5.2.2).

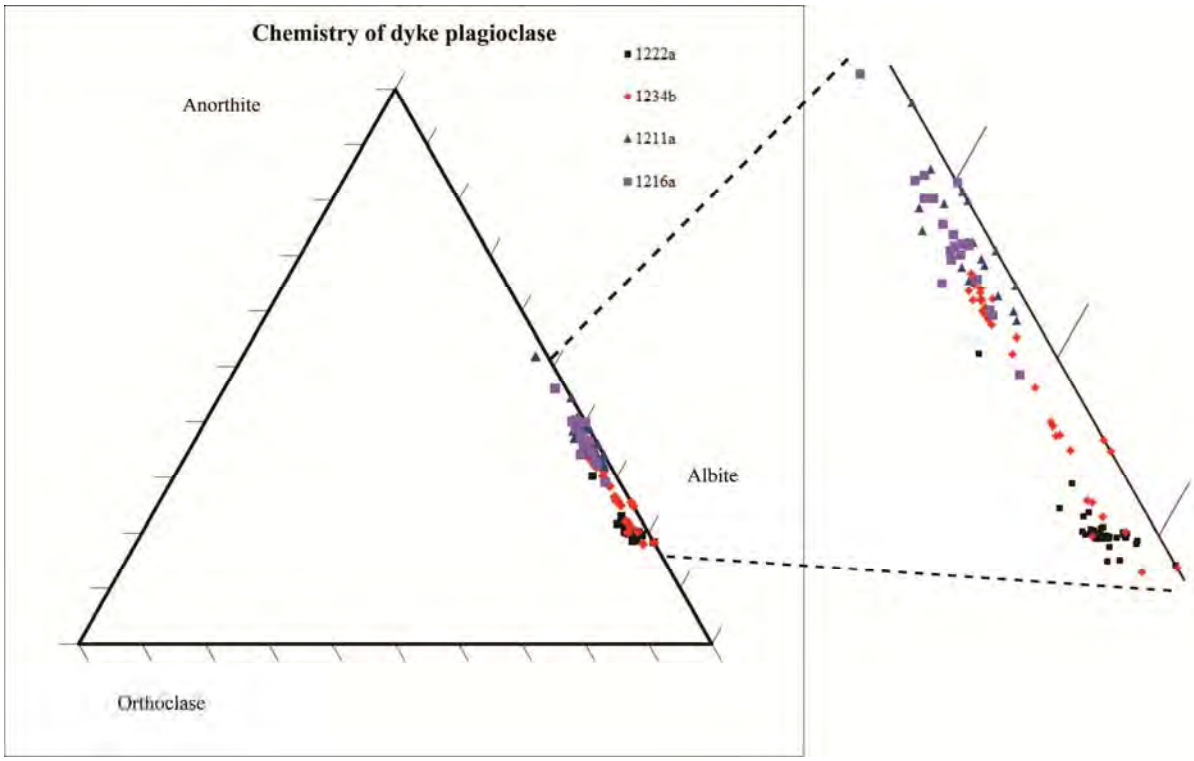

Figure 5.2.2: Variation in plagioclase chemistry within domain 2.

Transects have been completed to determine local differences in anorthite content. Transect PV1211-T1 is a representative transect of domain 2, with a range in X_{An} content from 30% - 45%. Dykes have varied plagioclase grain sizes which show no significant variation in X_{An} (Fig 5.2.3).

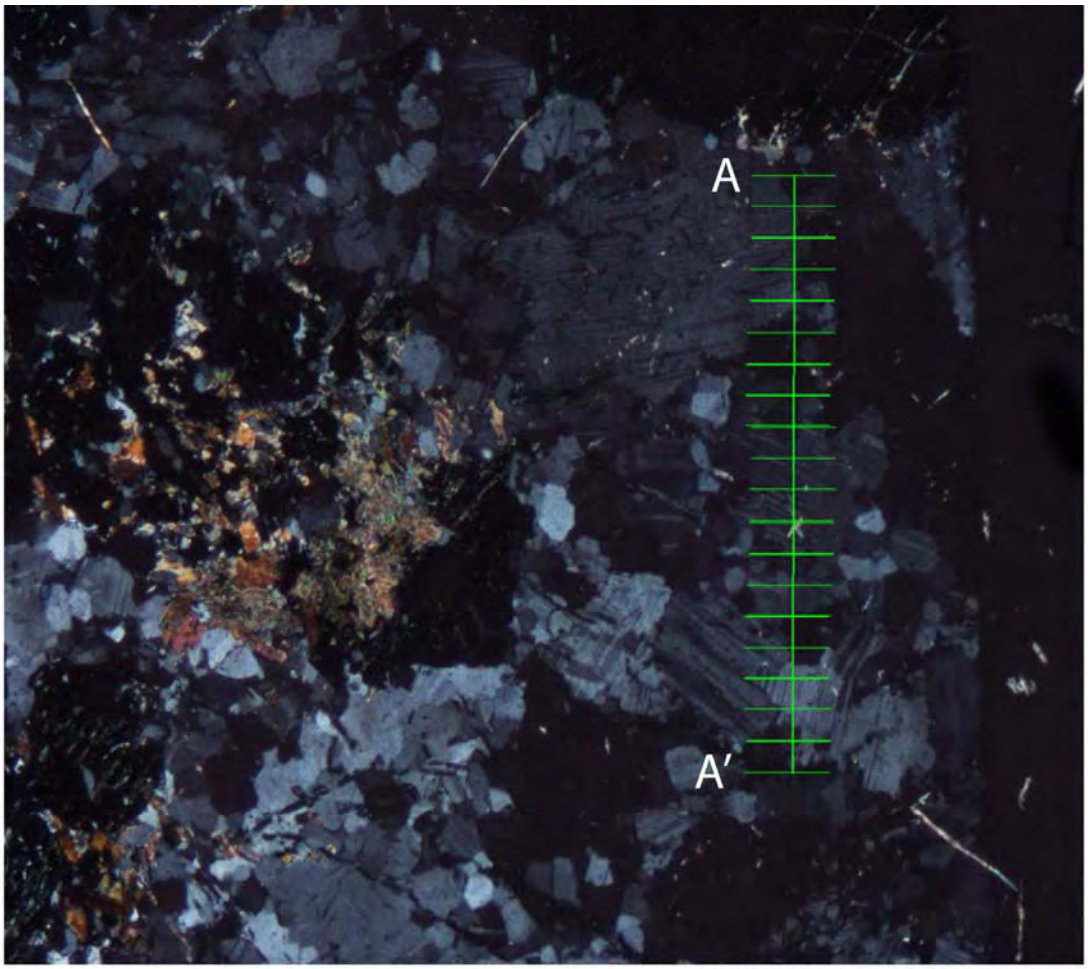

PV1211a-T1. Base of photo is 4.4mm

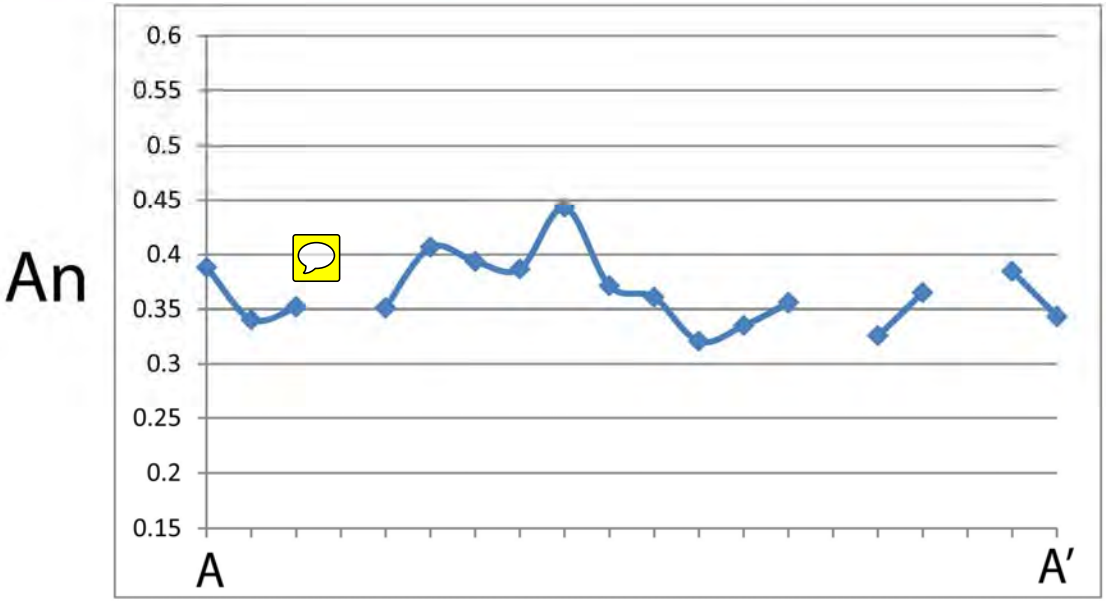

Figure 5.2.3: Sample PV1211a variation in X_{An} content within transect PV1211a-T1. Range is 30 – 45%. Note analysis is over large and small plagioclase grains.

Domain 3 (GRZ) displays a 40% variation in anorthite content and there is variation within and between samples (Fig 5.2.4).

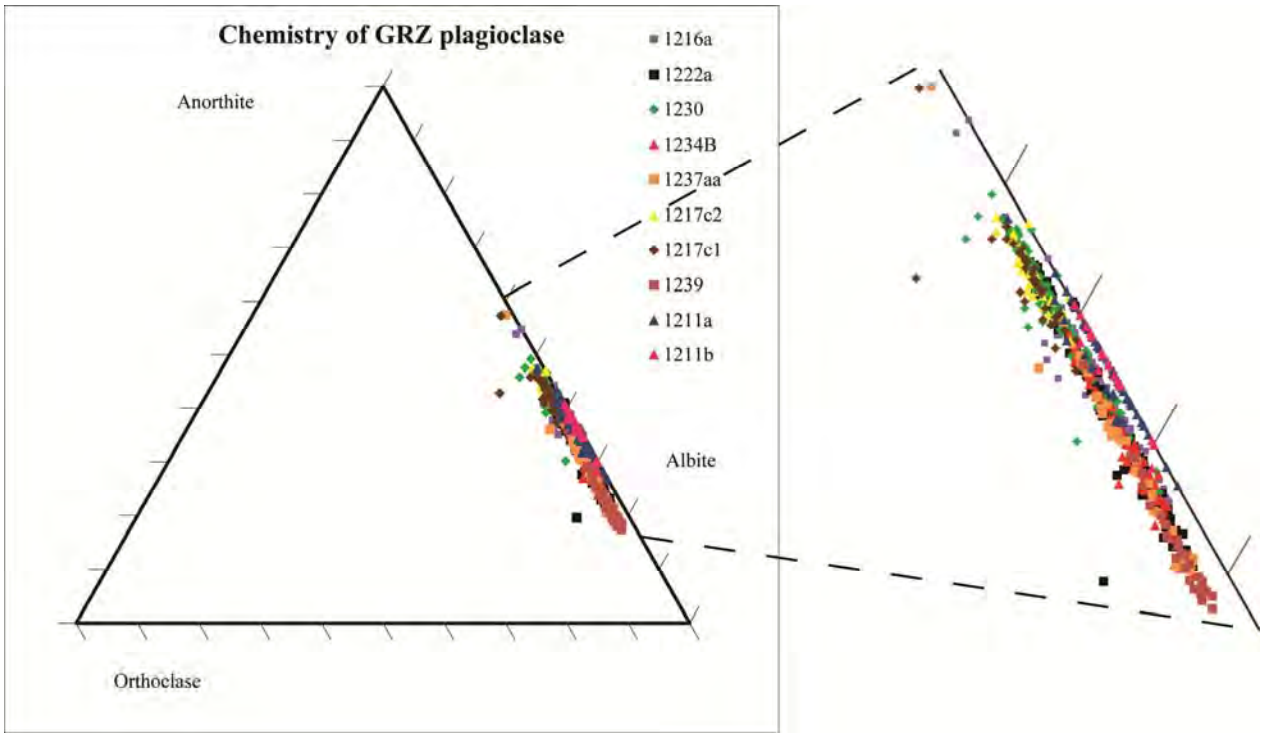

Figure 5.2.4: Variation of plagioclase between samples within domain 3

Transects PV1222a-T4 and PV1230-T1 are representative partially recrystallized samples. PV1222a presents anorthite content variation from neoblasts to relict grains with a transition from ~25% X_{An} to ~45% X_{An}, respectively (Fig 5.2.5). PV1230-T1 also displays variation in anorthite content with a range of ~25% - ~45% X_{An} due to the analysis of relict plagioclase (Fig 5.2.6).

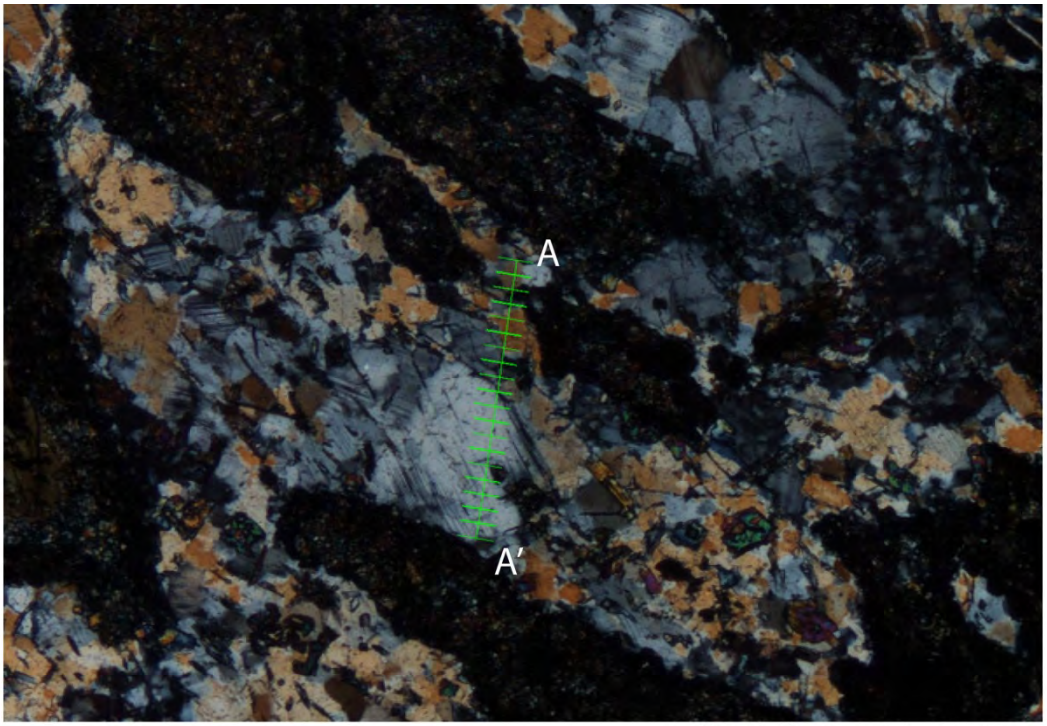

PV1222a-T4. Base of photo is 4.4mm

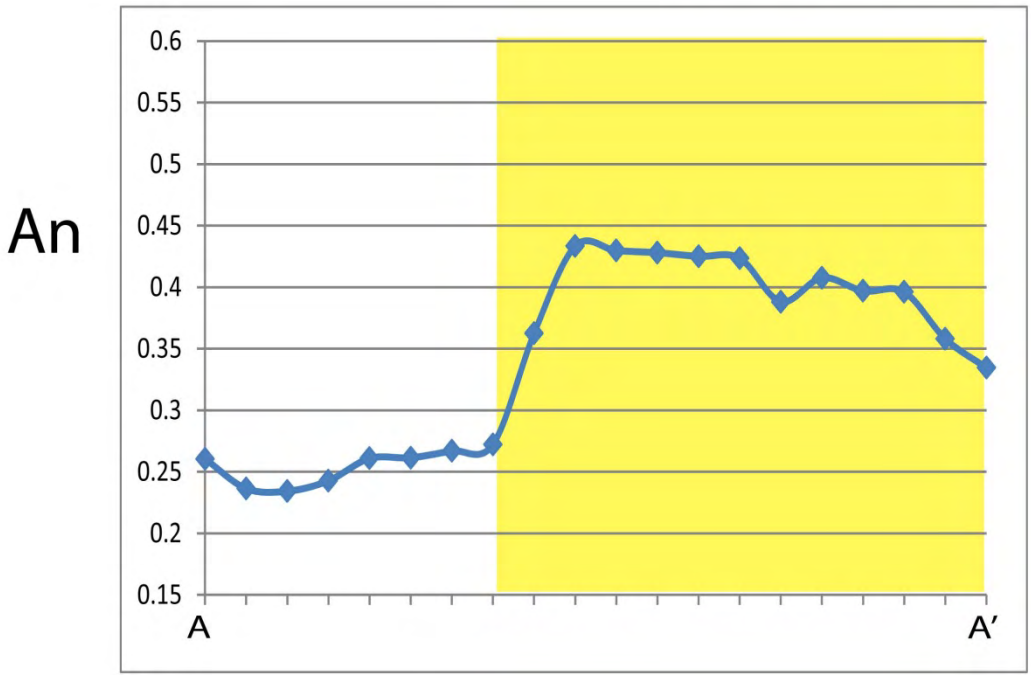

Figure 5.2.5: Transects within sample PV1222a. Variations in anorthite content from neoblast to relict plagioclase grains. Highlighted region represents relict plagioclase.

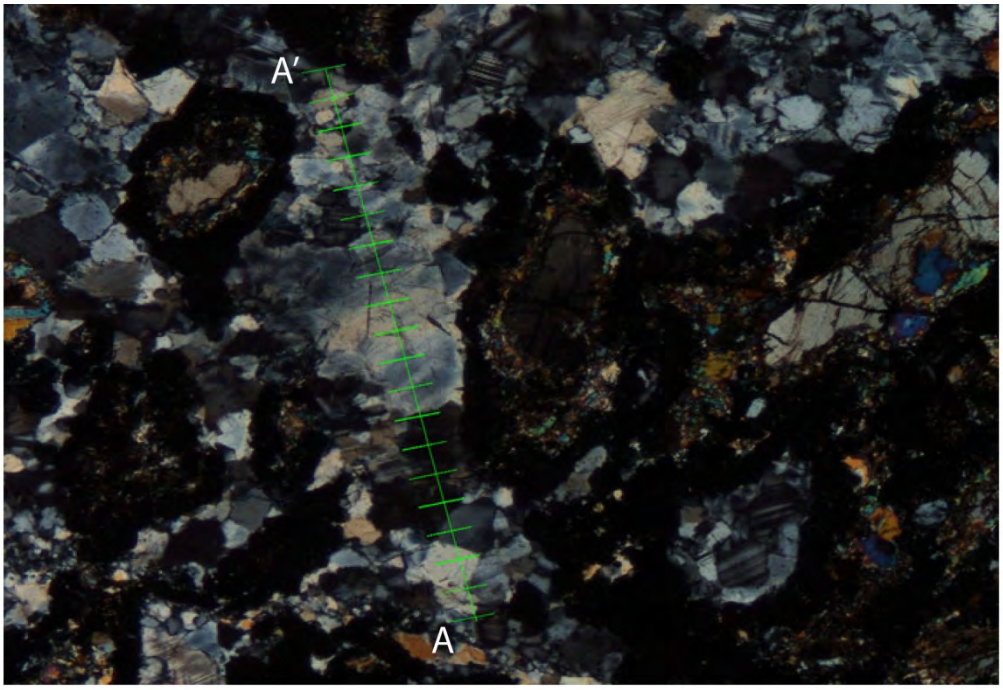

PV1230-T1. Base of photo is 4.4mm

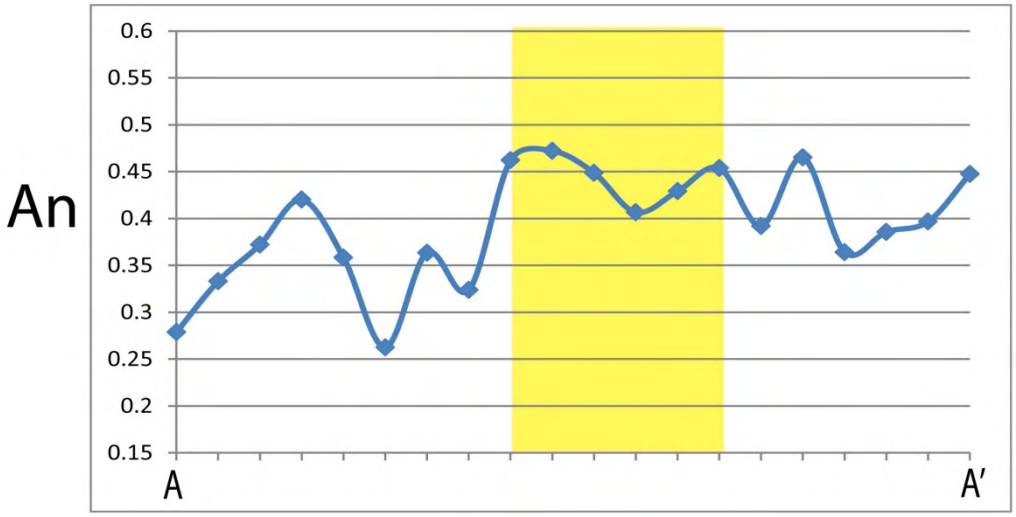

Figure 5.2.6: Transect within sample PV1230. Variations of anorthite content within sample PV1230 with a range of ~20% X_{An}. Highlighted region represents the relict plagioclase.

Representative transects of extensively recrystallized samples are PV1239-T1, PV1216a-T6 and PV1211a-T2. All samples display a maximum range of ~15% X_{An} and do not show variation between different plagioclase grain sizes. Sample PV1239 transect is located at the intersection of two dykes and displays homogenised X_{An} (<15% variation) (Fig 5.2.7). These dykes are highlighted to display their position relative to the transect, although no analysis of them has occurred.

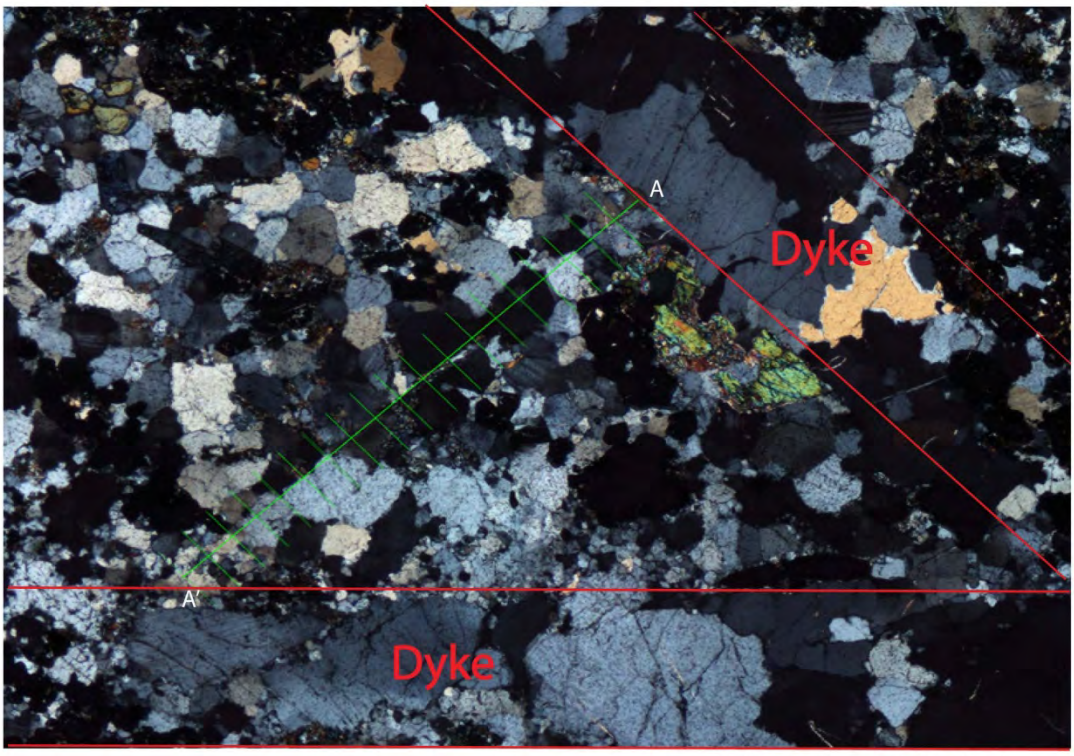

PV1239-T1. Base of photo is 4.4mm

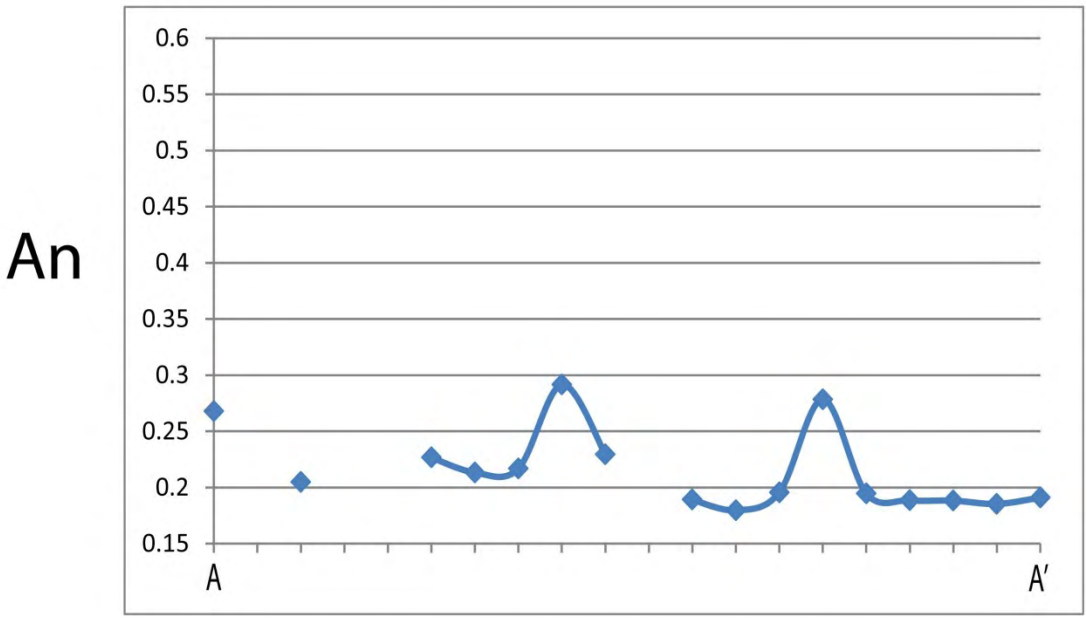

Figure 5.2.7: Transect of sample PV1239 at the intersection of two dykes with ~10% variation in X_{An} content.

Sample PV1216a was used as a control within chapter 4 to show the dyke and garnet grain size relationship. This sample shows varied plagioclase grain size with little variation in X_{An} content (<10%) (Fig 5.2.8).

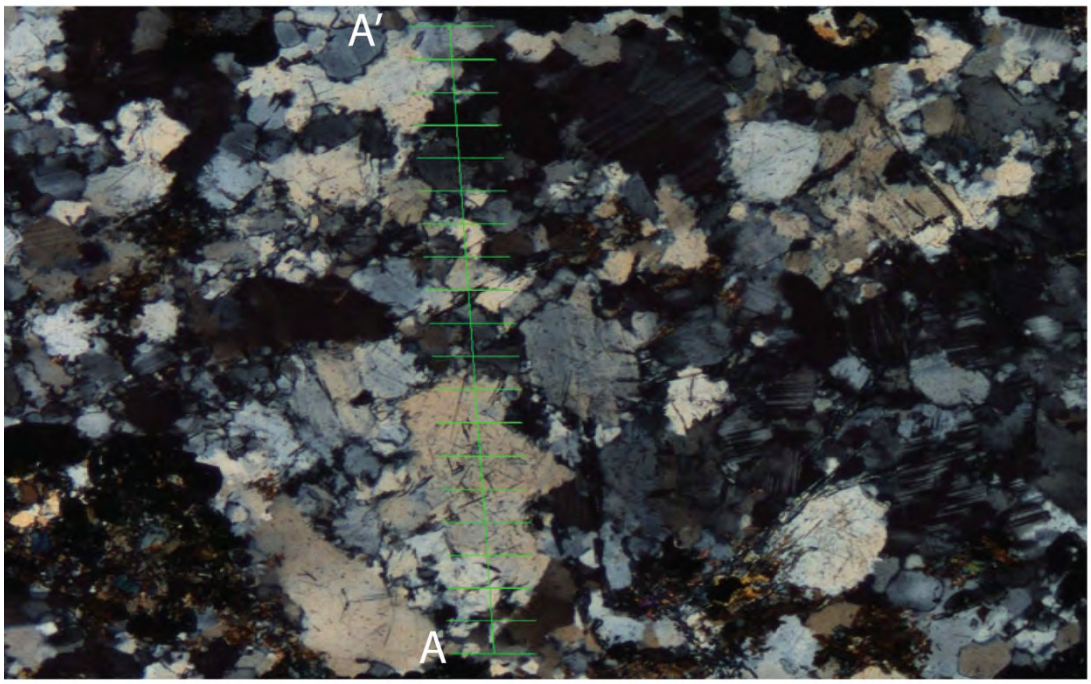

PV1216a-T6. Base of photo is 4.4mm

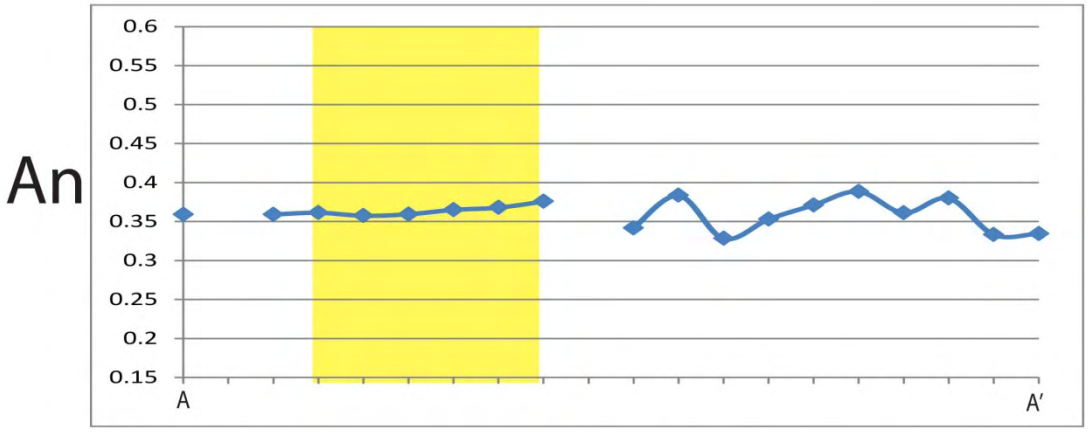

Figure 5.2.8: Transect within sample PV1216a. Highlighted region represents 'relict' plagioclase and the overall anorthite content varies by <10%.

Sample PV1211a is a paired shear zone sample and displays homogenised X_{An} content within the less deformed, extensively recrystallized region (Fig 5.2.9).

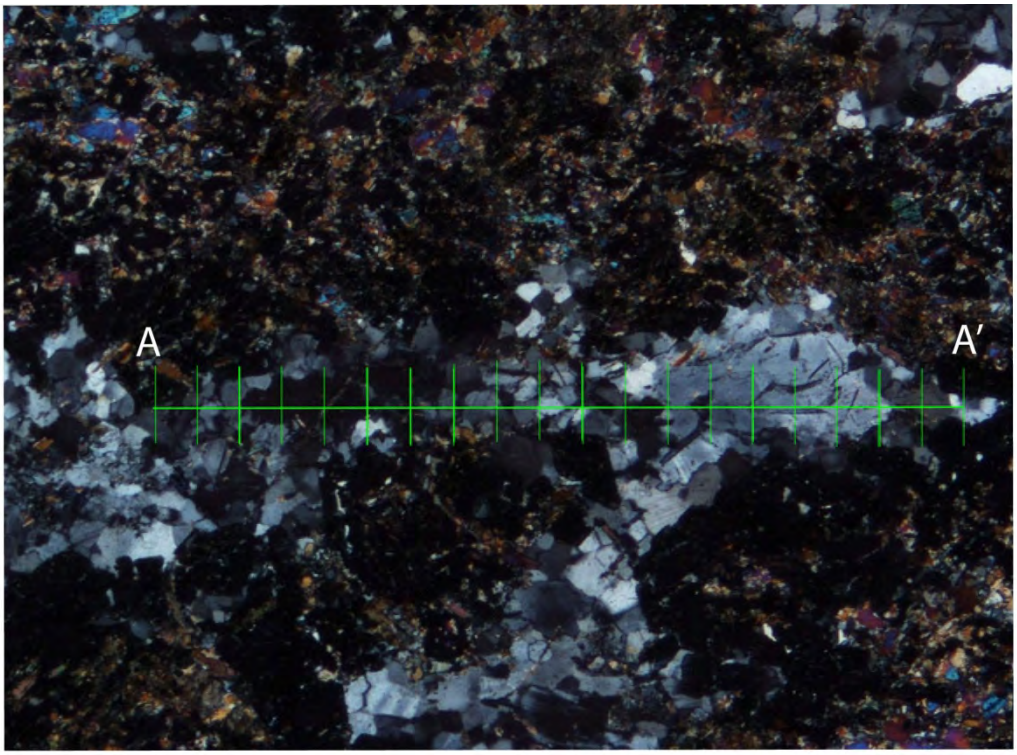

PV1211a-T2 Base of photo is 4.4mm

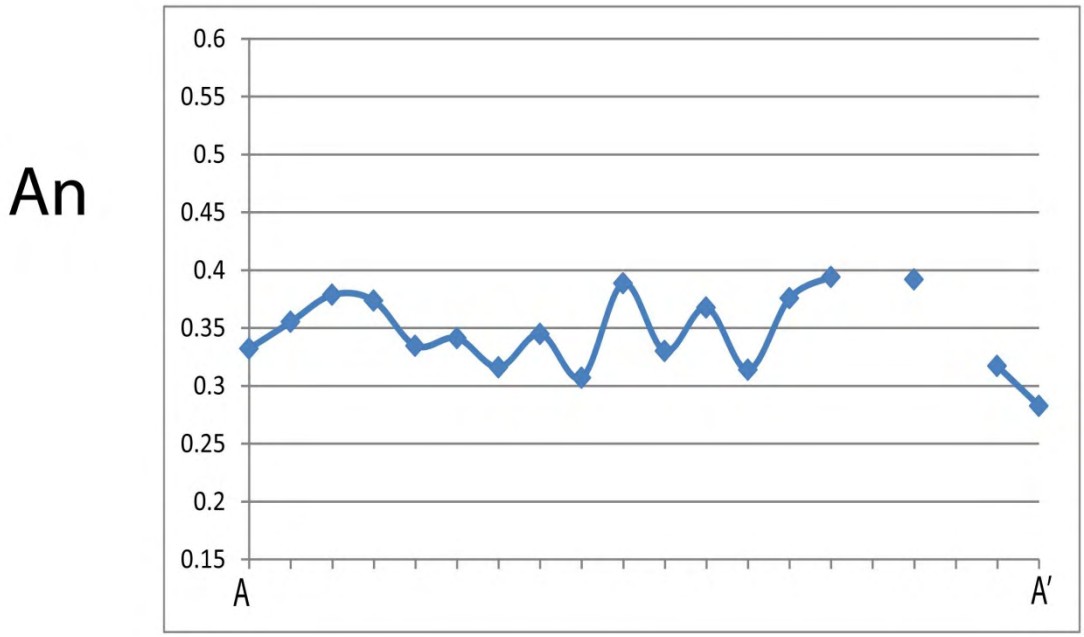

Figure 5.2.9: Less deformed zone within paired shear zone sample PV1211a. Homogenised X_{An} content with <10% variation.

Domain 4 (D3 shear zone) displays ~10% variation within samples and a maximum variation of 20% between samples. Four transects are displayed on a ternary diagram of Anorthite-Albite-Orthoclase with each transect displaying about 10% variation, excluding PV1211a-T3 (Fig 5.1.10).

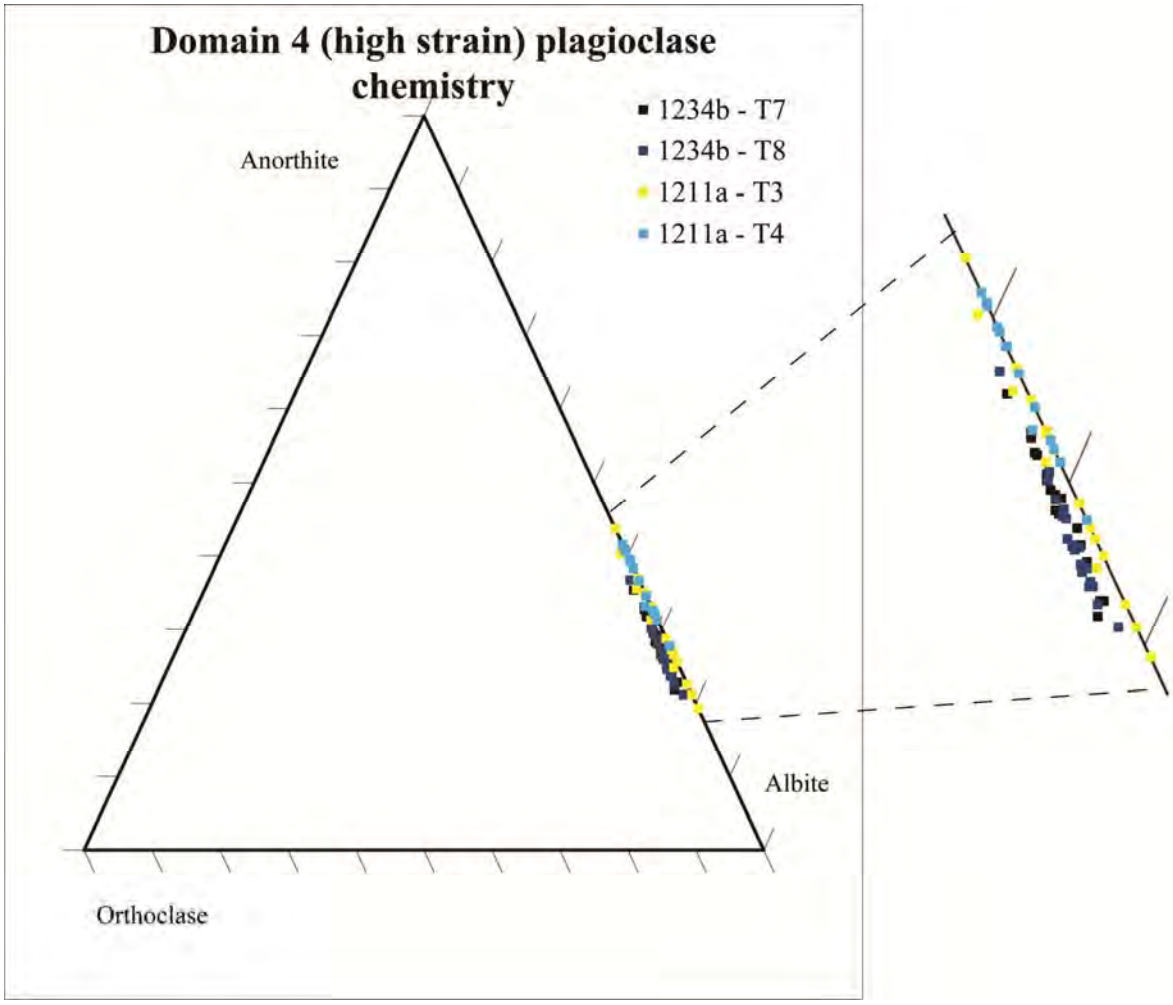

Figure 5.1.10: Variation of plagioclase within shear zone

Analysed plagioclases within shear zones have a homogenised grain size and X_{An} content (~10% variation). PV1234b –T7 is a representative transect of an analysed shear zone and X_{An} content varies by ~10% (Fig 5.1.11).

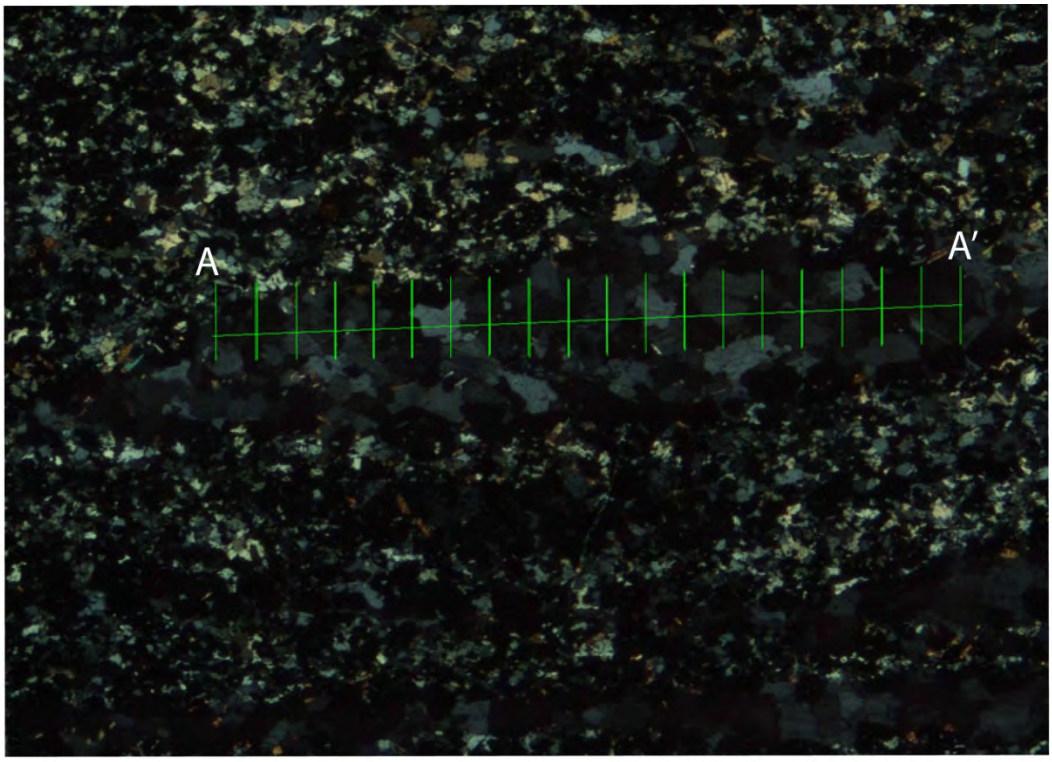

PV1234b-T7. Base of photo is 4.4mm

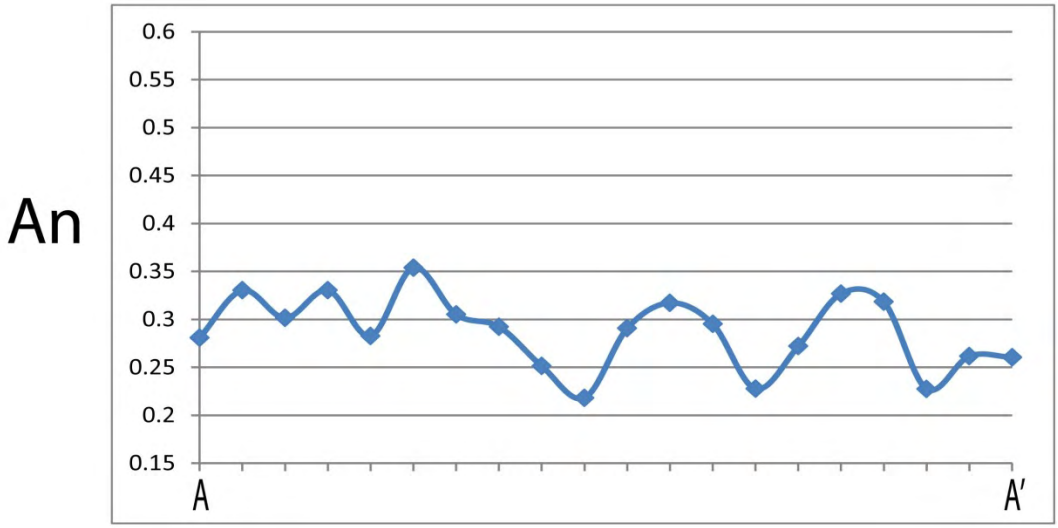

Figure 5.1.11: Homogeneous X_{An} content within the shear zone of PV1234b.

5.2.2 Garnet mineral chemistry

Tables 5.2, 5.3 and 5.4 present the Almandine, Pyrope and Grossular compositions of garnet within the three domains. Domain 2 (dyke) contains the lowest standard deviation of garnet between all domains. Samples PV1234b and PV1239 (extensively recrystallized) display the lowest standard deviation within domain 3 (GRZ). Domain 4 has a varied standard deviation between the three garnet end-members and displays a higher standard deviation to domain 3.

Table 5.2: Range of Almandine composition within domains

Domain	**Sample**	**Alm Content**			
		Min	Max	Avg.	St.Dev
Domain 2: Dyke	PV1217a	42.88	44.23	43.48	0.69
	PV1217b	47.56	49.57	48.51	0.80
	PV1217c2	46.99	47.94	47.46	0.67
Domain 3: GRZ: Partially Recrystallized	PV1237aa	44.67	50.33	47.10	1.76
	PV1217c2	41.81	48.95	45.13	2.06
	PV1217a	37.52	43.51	40.12	2.47
	PV1217b	39.86	44.96	42.77	1.71
	PV1217c1	39.18	44.27	41.28	1.71
Domain 3: GRZ: Extensively Recrystallized	PV1234b	48.35	54.61	50.89	1.33
	PV1239	44.77	51.32	47.18	1.56
Domain 4: D3 Shear Zone	PV1234b	44.57	56.09	47.34	2.83

Table 5.3: Range of Pyrope composition within domains

Domain	**Sample**	**Prp Content**			
		Min	Max	Avg.	St.Dev
Domain 2: Dyke	PV1217a	31.94	33.75	32.55	1.04
	PV1217b	26.63	29.37	28.12	1.22

	PV1217c2	23.31	26.20	24.75	2.04
Domain 3: GRZ: Partially Recrystallized	PV1237aa	23.02	31.51	26.92	2.58
	PV1217c2	21.05	32.30	27.61	3.18
	PV1217a	26.49	39.65	33.38	5.01
	PV1217b	26.55	32.80	30.37	2.16
	PV1217c1	32.32	38.08	34.86	1.80
Domain 3: GRZ: Extensively Recrystallized	PV1234b	21.37	26.33	23.82	1.48
	PV1239	19.29	31.75	28.65	2.49
Domain 4: D3 Shear Zone	PV1234b	24.50	30.44	27.52	1.56

Table 5.4: Range of Grossular composition within domains

Domain	**Sample**	**Grs Content**			
		Min	Max	Avg.	St.Dev
Domain 2: Dyke	PV1217a	23.38	24.71	23.97	0.68
	PV1217b	21.85	25.61	23.37	1.28
	PV1217c2	26.82	28.76	27.79	1.37
Domain 3: GRZ: Partially Recrystallized	PV1237aa	20.00	31.00	25.99	3.33
	PV1217c2	20.90	35.14	27.26	4.41
	PV1217a	22.16	30.76	26.50	3.30
	PV1217b	22.24	33.59	26.86	3.83
	PV1217c1	21.52	26.47	23.87	2.07
Domain 3: GRZ: Extensively Recrystallized	PV1234b	21.80	29.37	25.29	2.30
	PV1239	20.35	32.11	24.17	2.41
Domain 4: D3 Shear Zone	PV1234b	15.04	24.96	25.14	3.07

Within domain 2 (cf. Chapter 4), two garnets have been categorised as dyke or wall rock garnet which have been plotted onto an Almandine – Pyrope – Grossular + Spessartine ternary diagram (Fig 5.2.12). There is a chemical difference between the two garnets as dyke garnets are more Grossular + Spessartine rich, whereas wall rock garnets are more Pyrope + Almandine rich.

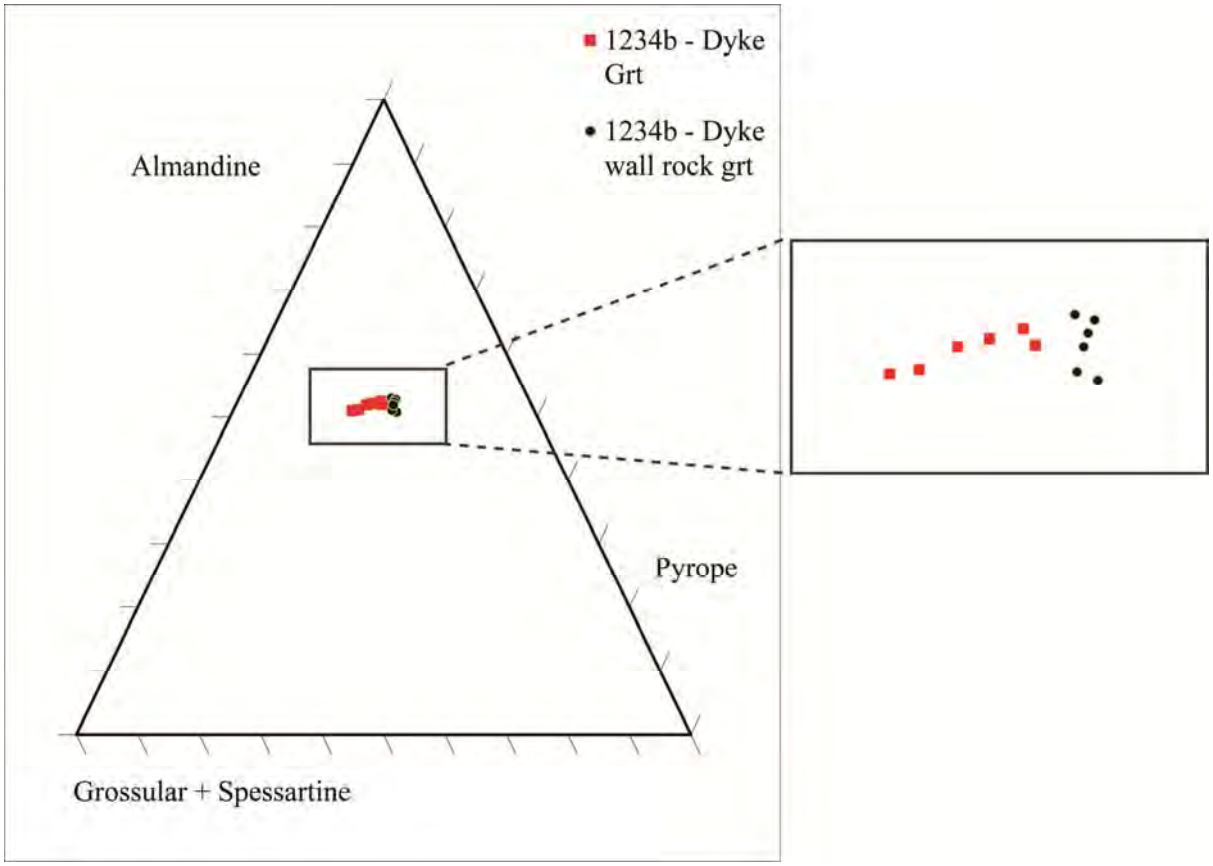

Figure 5.2.12: Ternary diagram of analysed dyke and wall garnet within PV1234b. Dyke garnet are more Grossular + Spessartine rich whereas wall rock garnet are more Pyrope + Almandine rich.

Garnet reaction zone garnet can be further segregated (cf. Chapter 4) into inclusion rich or inclusion poor growth phases and therefore garnet from domain 3 have been analysed to distinguish between these phases. The inclusion-poor regions are Grossular-rich, while the inclusion-rich growths contain higher proportions of Almandine and Pyrope (Fig 5.2.13).

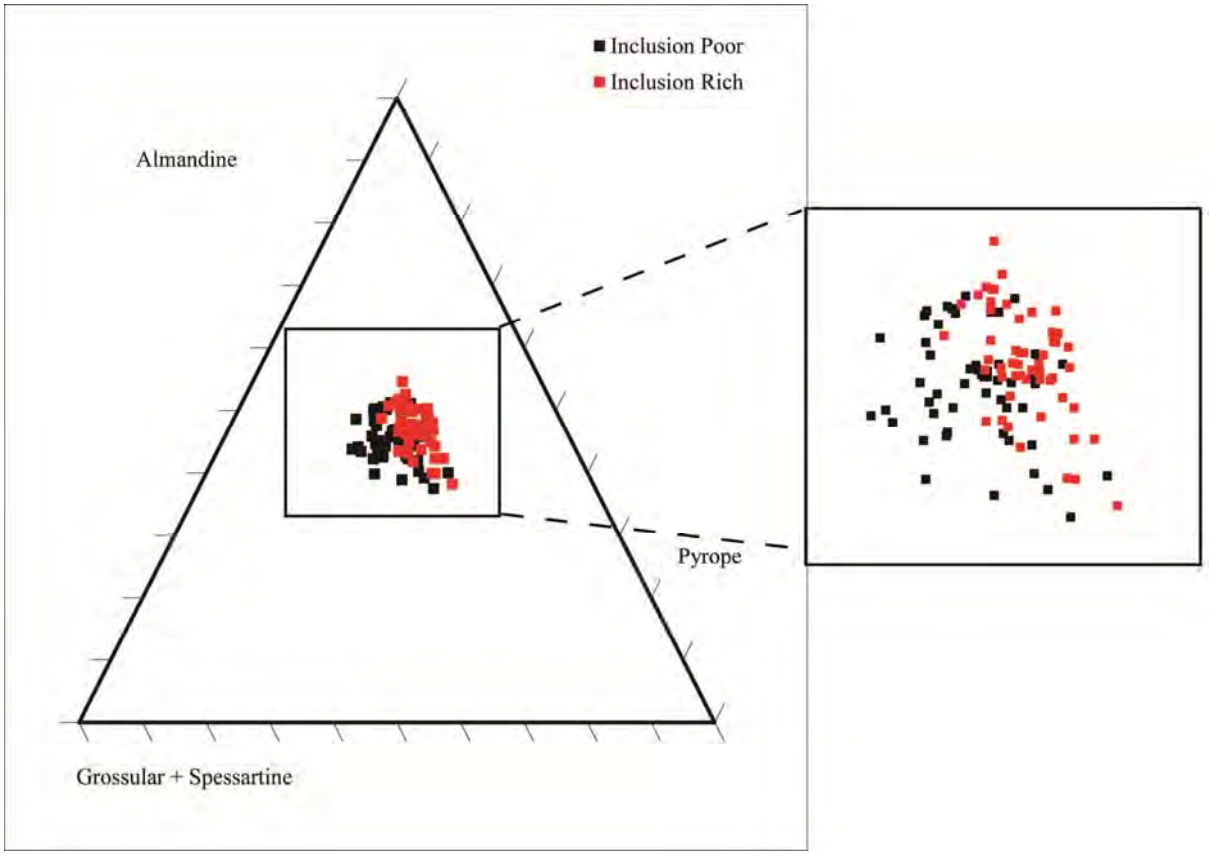

Fig 5.2.13: Ternary Diagram of Almandine-Pyrope-Grossular-Spessartine plotting garnet inclusion poor and inclusion rich regions.

5.3 Discussion

Published electron microprobe (EMP) data of plagioclase and garnet within reaction zones has been collated and is presented in table 5.5 and table 5.6 (Clarke et al., 2000; Daczko and Halpin, 2009; Daczko et al., 2002; Hollis et al., 2004; Stowell et al., 2010). These published data are compared with this study where appropriate. Published data ~~(Clarke et al., 2000; Daczko and Halpin, 2009; Daczko et al., 2002; Hollis et al., 2004; Stowell et al., 2010)~~ and analysed plagioclase from different domains within the ten samples, plot in the Oligoclase to Labradorite fields using an Anorthite – Albite – Orthoclase diagram (Fig 5.3.14). Whereas published dat~~um~~ show compositions ranging from Andesine – Oligoclase. All garnet data from domain 2, 3 and literature have been plotted onto an Almandine-Pyrope-Grossular-Spessartine ternary diagram (Fig 5.3.15).

Table 5.5: Anorthite, albite and orthoclase values from published plagioclase EMP analyses

Reference	**Sample ID**	**Anorthite (X_{An})**	**Albite (X_{Ab})**	**Orthoclase (X_{Or})**
Daczko et al., 2002	Dan18 – Garnet Reaction zones and symplectite textures	**0.24**	0.75	0.01
Stowell et al., 2010	05NZ11a – Gabbroic Gneiss	**0.26**	0.74	0
Clarke et al., 2000	9635a – Garnet Reaction Zone	**0.24**	0.74	0.02
Clarke et al., 2000	9637d – Garnet Reaction Zone	**0.25**	0.73	0.02
Hollis et al., 2004	DS08C – WFO	**0.21**	0.77	0.02
Daczko and Halpin, 2009	LG4051 – Dyke	**0.28**	0.69	0.03
Daczko and Halpin, 2009	LG4051 – Garnet Reaction Zone	**0.35**	0.64	0.01

Table 5.6: Garnet core analysis from published EMP data

Reference	**Sample ID**	**Almandine (X_{Alm})**	**Pyrope (X_{Pyp})**	**Grossular (X_{Grs})**	**Spessartine (X_{Sps})**
Daczko et al., 2002	Dan18 – Garnet Reaction zones and symplectite textures	34.32	33.41	31.21	1.06
Stowell et al., 2010	05NZ11a – Gabbroic Gneiss	49.00	20.96	26.63	3.41
Clarke et al., 2000	9635a – Garnet Reaction Zone	40.11	29.31	30.12	0.47
Clarke et al., 2000	9637d – Garnet Reaction Zone	44.07	29.73	25.18	1.02
Hollis et al., 2004	DS08C – WFO	50.20	28.06	20.73	1.02
Daczko and Halpin, 2009	LG4051 – Dyke	36.17	40.04	22.63	1.17
Daczko and Halpin, 2009	LG4051 – Garnet Reaction Zone	38.36	39.57	21.70	0.37

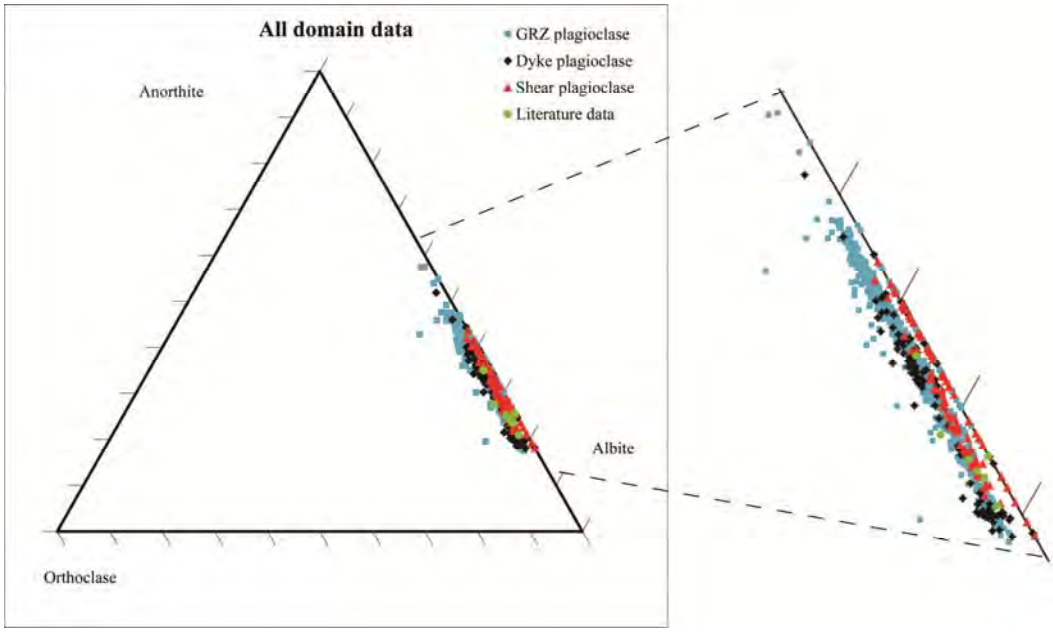

Figure 5.2.14: Plagioclase composition of all analysed samples compared to literature data. Literature data ranges from Andesine to Oligoclase.

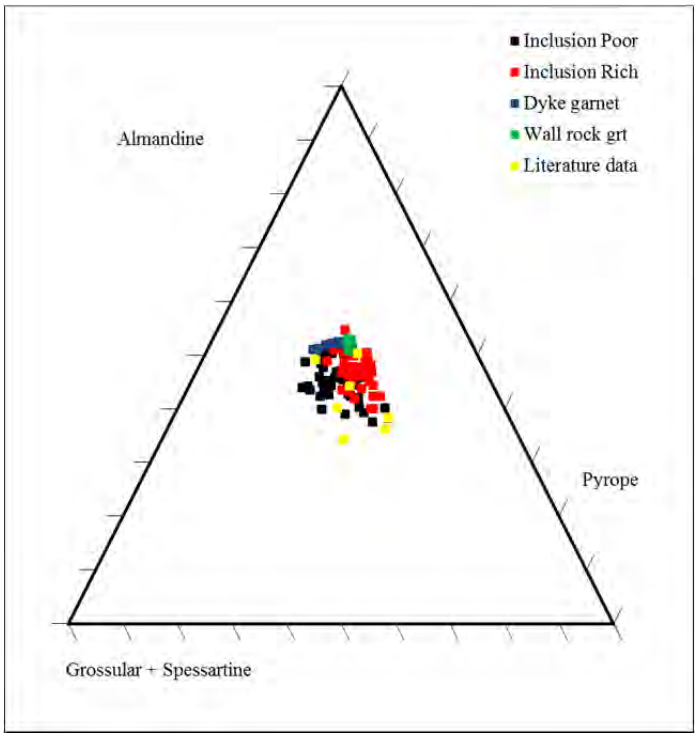

Figure 5.2.15: Garnet composition. Data plotted include data produced in this study and data from the previous work (see text for references).

Previous studies have also classified plagioclase as oligoclase to andesine which confirms the values obtained with the SEM-EDS. Obtained garnet data also supports the literature data.

Although it is critical to explain the changes occurring in the formation of paired shear zones, no detailed analysis of chemical variation with reference to the dyke had been performed before this work. Previous studies within Granodiorites within South Tyrol, Italy (Mancktelow and Pennacchioni, 2005; Pennacchioni and Mancktelow, 2007) observed a similar phenomenom of localised shearing due to the interaction of the host rock with a dyk Mancktelow and Pennacchioni (2005) concluded paired shear zones formed due to a rheological contrast, therefore strengthening of the rheology is a pre-cursor for paired shear zones and understanding what changes occur to result in this strengthening is essential.

The slight variations observed in plagioclase chemistry within domain 2 (dyke) vary slightly between samples (~20% variation in X_{An}). This is confirmed with dyke garnet major element chemistry as it is homogenous (low standard deviation). Schroter et al. 2004 who studied trace elements of the dioritic gneiss, concluded the felsic dykes are derived from partial melting of this unit. Diorite has slightly varied compositions in outcrop (cf. Chapter 2), therefore this is a possible reason for the slight chemical variation found within the felsic dykes (plagioclase and dyke garnet) (Schroter et al., 2004).. Assuming that all dykes originate from a similar melt, the temperature of the melt within the dyke would be similar as well. Consequently, the observed variation in the degree of feldspar and garnet recrystallization as seen in domain 3 cannot be the result of variations in dyke temperature but is more likely a result from the duration a fracture acted as an open melt conduit.

Within domain 3 the transformation of hbl-granulite to garnet granulite occurred under static conditions as garnet granulite assemblage's pseudomorphs the S1 assemblage (cf. Chapter 4). Static recrystallization occurs within a deformation free environment and will result in the rearrangement of dislocations in low energy configurations, subgrain formation, movement of grain boundaries, grain growth and nucleations of new low dislocation density grains (neoblasts) resulting in a reduction of energy (Heilbronner and Tullis, 2012; Humphreys and Hatherly, 1995). The duration of heating under static conditions will directly influence the degree of recrystallization (Herwegh et al., 2008). Therefore if the melt conduit is open for long enough, this will result in the reduction of dislocations and the coarsening of recrystallised grains (Heilbronner and Tullis, 2012). The duration will influence the degree of recrystallization and therefore microstructures in partially or extensively recrystallised garnet reaction zones. Partially recrystallised garnet reaction zones contain plagioclase relict (igneous) and neoblasts (metamorphic) grains with variable X_{An} and also display varied

garnet chemistry between inclusion poor and inclusion rich growths. Variable garnet chemistry within partially recrystallized samples is a result of the reactant; more Grossular rich inclusion-poor growths are due to a plagioclase reactant whereas more Almandine & Pyrope inclusion-rich regions are due to the pyroxene reactant. The reactant affecting the composition is further supported by wall rock garnet analyses as they are more enriched in Pyrope as it is replacing clinopyroxene. Extensively recrystallised GRZs are largely devoid of relict plagioclase grains, exhibiting mainly newly grown grains. These show a more homogeneous X_{An} due to higher diffusion (Rosenberg and Stunitz, 2003). Garnet composition supports the decrease in chemical variance as extensively recrystallised samples also display lower standard deviations of analysed garnet, removing variations from inclusion poor/rich growths. This homogenised chemistry is the result of grain coarsening, reducing the interfacial free energy (Heilbronner and Tullis, 2012). Both the grain coarsening and increased garnet abundance (cf. chapter 4) will increase the strength of the microstructure.

Domain 4, D3 shear zone samples have undergone dynamic recrystallization (syn-tectonic) which results in crystal plastic deformation, decrease in grain size by strain-induced grain boundary migration, sub-grain rotation and nucleations of grains (Bestmann et al., 2005; Rosenberg and Stunitz, 2003; Shigematsu, 1999). Paired shear zone samples preserve a grain size reduction (Montesi and Hirth, 2003; Shigematsu, 1999) due to the recrystallization weakening and the formation of small grains. This process results in homogenisation of X_{An} due to the high abundance of nucleations. Garnet termed post-D3 (cf. Chapter 4) within these high strain zones displays heterogeneous chemistry, supporting this conclusion that they are later growths.

5.4 Summary

As observed in chapter 4, dykes have a similar mineralogy, therefore representing similar magmas and temperature to drive the recrystallization of the gneiss. This is further supported by a very low variation of major element chemistry within the dyke. Consequently the duration of the activity of the magma conduit (dyke) results in a) the garnet reaction zone and b) different degrees of recrystallization within garnet reaction zones. If this conduit is open for long enough, static recrystallization will result in extensive recrystallization, grain coarsening, increased garnet abundance, homogenisation of X_{An} and garnet chemistry. As observed in chapter 4, the most extensive recrystallization is observed closest to the dyke and decreases away from the dyke. Both grain coarsening and the higher abundance of garnet will

result in rheological strengthening of the highly recrystallized garnet reaction zone. D3 strain (shearing) has subsequently localised on the outer regions of the garnet reaction zones where a rheological contrast between highly recrystallized and moderately recrystallized garnet reaction zones exist. This location of rheologically soft and hard regions results in the localization of strain: thus formation of paired shear zones. This scenario is in accordance to the observation (cf. Chapter 4) that paired shear zones are only formed in garnet reaction zones that exhibit a high degree of recrystallization close to the dyke.

Chapter 6:

Trace Element Mineral Chemistry: Laser Ablation Inductively Coupled Plasma Mass Spectrometry (LA-ICP-MS)

6.1 Introduction

Chapters 4 and 5 have identified petrographic and chemical variations between domains 2, 3 and 4. Domain 2 (dyke) consists of a similar mineralogy between samples with varied plagioclase chemistry and contains two types of garnet, wall-rock and dyke garnet. Domain 3 (garnet reaction zone) comprises different degrees of recrystallization with reference to the dyke; 1) Partially recrystallized, resulting in heterogeneous plagioclase and garnet chemistry and 2) extensively recrystallized resulting in the homogenisation of plagioclase and garnet chemistry. Domain 4 (shear zone) includes homogeneous plagioclase chemistry and heterogeneous garnet chemistry (later growths. cf. chapter 4). A prediction developed from chapters 4 and 5 is that dykes are sourced from partial melting of the dioritic gneiss with slight variations and the products of metamorphic reactions are affected by what they locally replace.

To investigate this hypothesis, trace elements have been analysed from two key samples, PV1222a and PV1234b. PV1222a is a partially recrystallized garnet-granulite and PV1234b is a paired shear zone sample, both analysed with the LA-ICP-MS at Macquarie University, Sydney. Spot analysis was undertaken at 30 - 50µm diameter within different runs, in order to analyse different grain sizes. Data was processed using GLITTER for processing time-resolved signals. Rare earth element (REE) plots have been normalised using the values of Sun & McDonough (1989) and data has been excluded if the laser ablated through inclusions. All analysed data are within 1 sigma error of published values for the BCR-2 standard (cf. chapter 3).

Rare earth element (REE) fractionation is very useful in identifying the history of a mineral and inferring petrographic processes (Rollinson, 1993). The main aim of this chapter is to understand if the REE patterns mimic the major element chemistry variations identified in chapter 5.

Chondrite normalised REE patterns have been completed for domains 2, 3 and 4. Plagioclase, dyke and wall rock garnet have been analysed within domain 2 (dyke). Domain 3 (GRZ), comprises analysis of S1 hornblende, relict (S1) and recrystallized pyroxene, plagioclase and garnet. Analysed late garnet growths established from chapter 4 have been analysed within domain 4 (D3 high strain) as recrystallized garnets were too small to analyse within this domain. Complete tables of all major element data and end member calculations are available in Appendix C. As well as trace element data, lower limit of detection (LLD) (for 99% confidence) and 1σ error which are calculated on a single analysis basis. Appendix C is arranged in the same order as presented in this chapter.

6.2 Results

6.2.1 Domain 2

Domain 2 (dyke) comprises of an enriched light REE (LREE) signature within sample PV1234b (~8 chondrite normalised) and depleted LREE within sample PV1222a (~0.1 chondrite normalised) (Fig 6.2.1). This corresponds with the major element plagioclase end-member, anorthite as PV1234b is enriched in X_{An} (~32%) while PV1222a is depleted in X_{An} (~23%). Both samples show a positive Eu anomaly, typical of plagioclase (Fig 6.2.1). A large proportion of analyses within the heavy REE (HREE) are below detection limits.

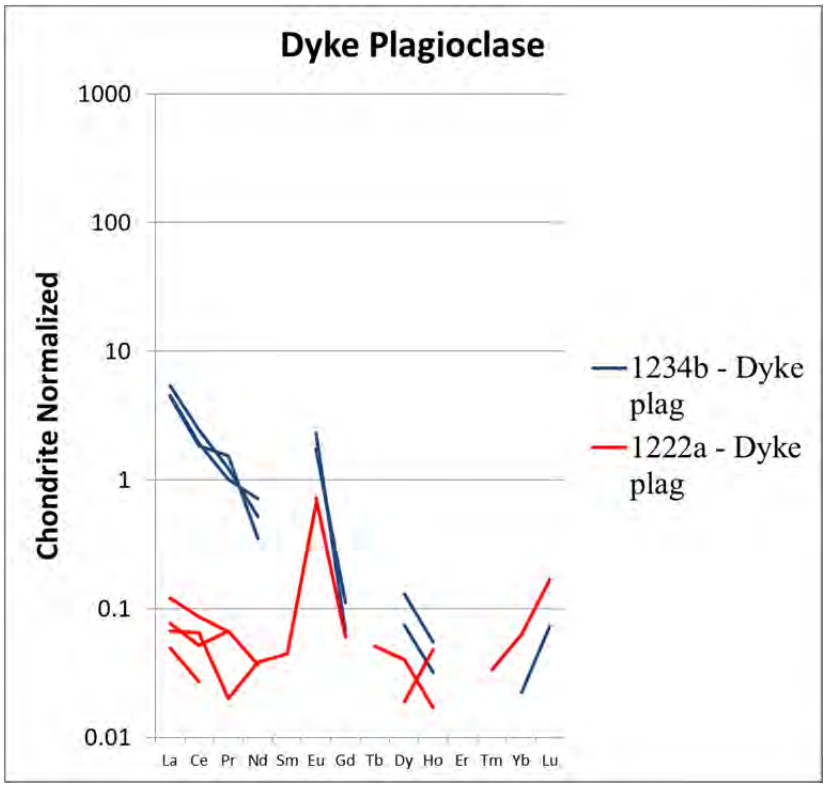

Figure 6.2.1: Varied dyke plagioclase composition between samples PV1234b and PV1222a. PV1234b is enriched in LREE and PV1222a is depleted in LREE. Both samples show a Eu anomaly.

Dyke and wall rock garnet have also been analysed within this domain (Fig 6.2.2). Dyke garnet grains are depleted in LREE (~0.01 chondrite normalised) and enriched in HREE (PV1234b - ~100 chondrite normalised and PV1222a - ~30 chondrite normalised). The wall rock garnets analysed are more enriched in LREE (~0.1 chondrite normalised) and are further depleted in HREE (~5 chondrite normalised) within sample PV1234b. Major element end-member calculations show wall rock garnets are more enriched in Pyrope (~26% X_{Pyp}) as oppose to dyke garnet (~22% X_{Pyp}).

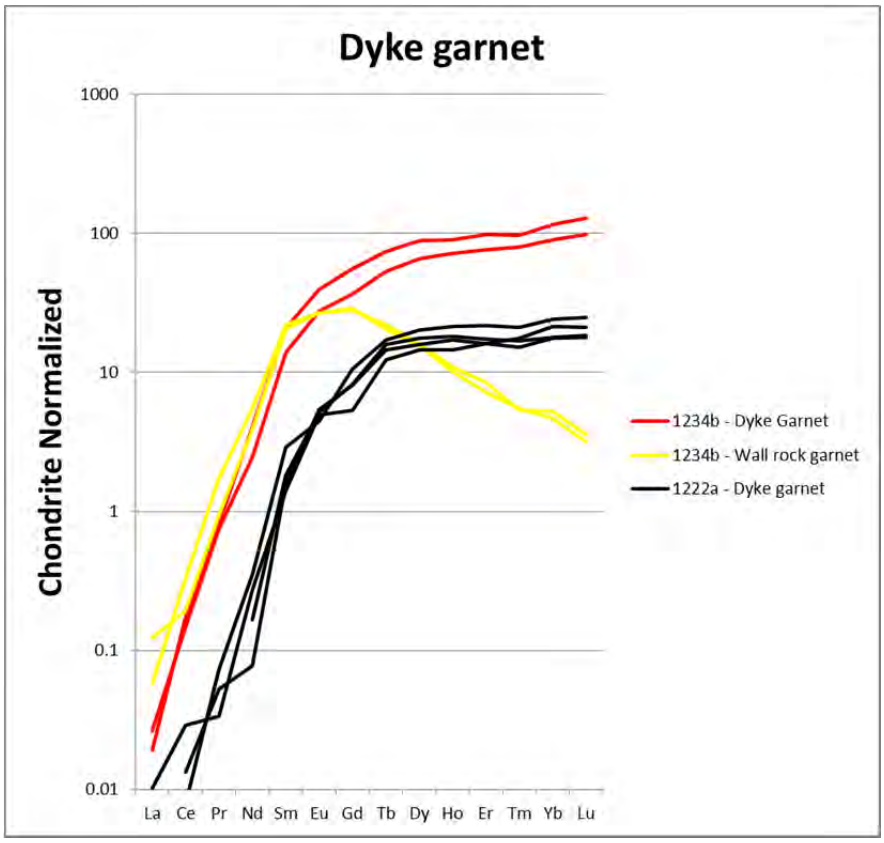

Figure 6.2.2: Dyke and wall rock garnet REE signatures. Both samples of dyke garnet are enriched in HREE whereas the wall rock garnet analysed in PV1234b is depleted in HREE.

6.2.2 Domain 3

Clinopyroxene, hornblende, metamorphic garnet and plagioclase trace elements have been analysed within domain 3 (GRZ). Clinopyroxene has been categorised as S1 or recrystallized from chapter 4 and in both settings the REE pattern is similar within a sample, although recrystallized cpx is more depleted in all REE (Fig 6.2.3). In addition, the HREE pattern of recrystallized clinopyroxene is slightly more depleted than S1 grains. PV1222a is more enriched in the HREE whereas PV1234b is more depleted in the HREE with one analysis containing a slight Eu anomaly, possibly reflecting the ablation of a plagioclase inclusion. Recrystallized grains are also more enriched in Enstatite (Mg) and more depleted in Ferrosilite (Fe).

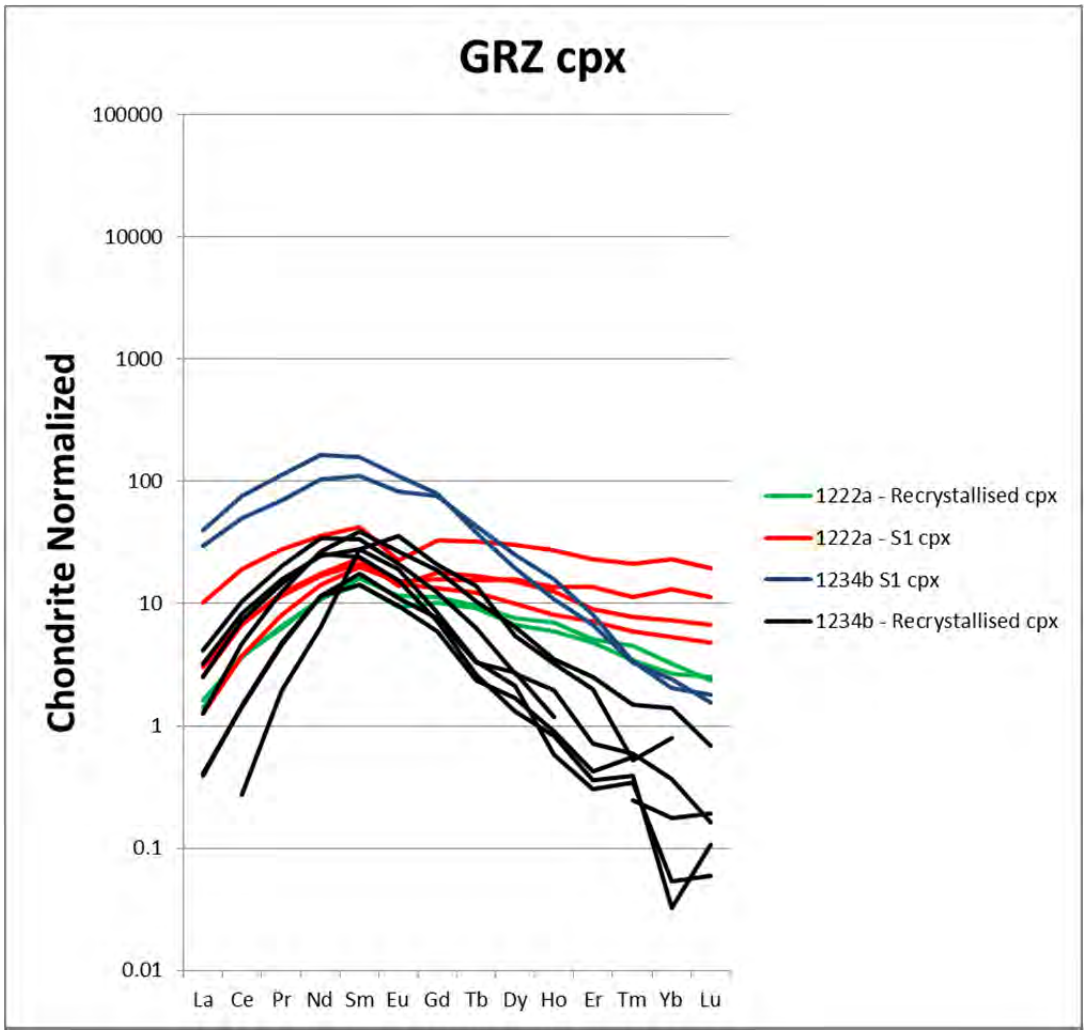

Figure 6.2.3: REE of relict S1 and recrystallized clinopyroxene from PV1222a and PV1234b. Recrystallized cpx has a similar pattern to the relict S1 grain although it is slightly more depleted in all REE.

Hornblende (S1 minerals) have been analysed within PV1234b and displays an enriched middle rare earth (~80 chondrite normalised) and depleted HREE pattern (~5 chrondrite normalised) (Fig 6.2.4).

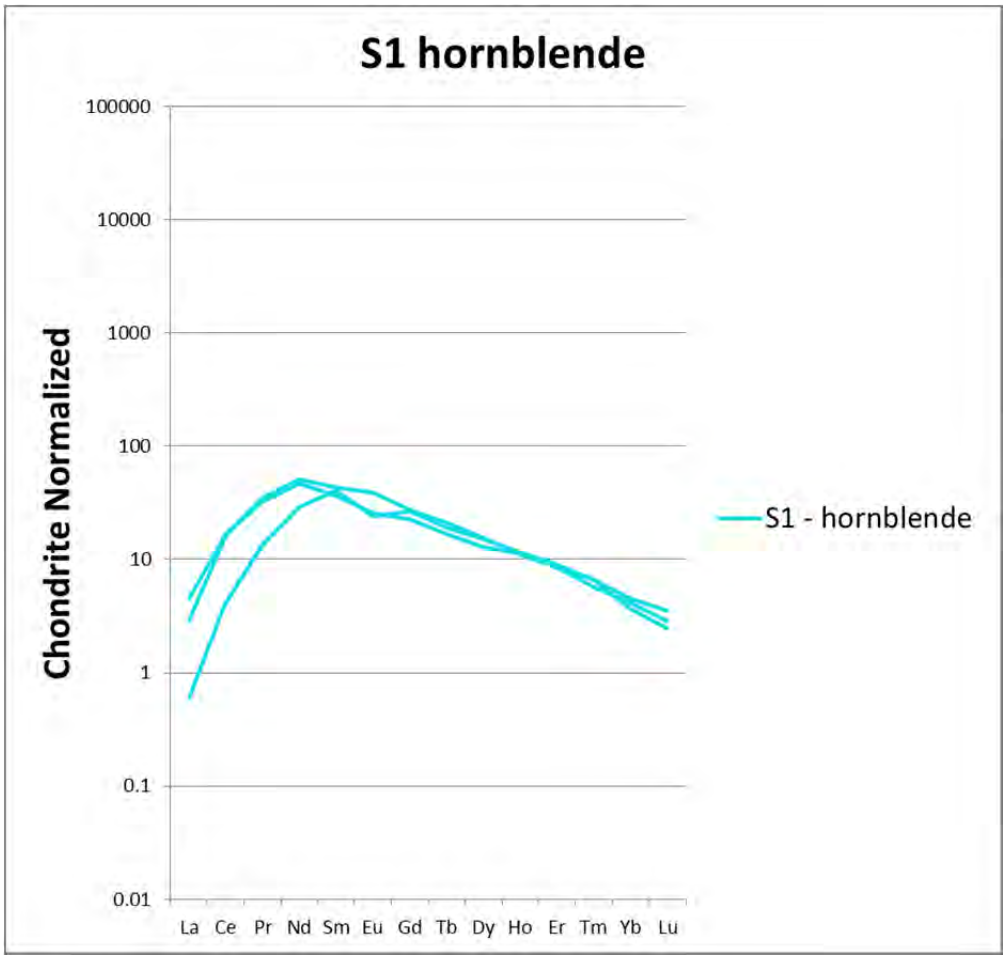

Figure 6.2.4: REE signature of hornblende enriched in middle rare earth elements and depleted in heavy rare earth.

Relict S1 and recrystallized plagioclase grains have been analysed, although no variation was observed and therefore plagioclase has not been categorised as S1 or recrystallized within this chapter. Plagioclase within domain 3 displays similar trace element patterns in all analysed samples. It is enriched in the LREE (~1 – 10 chondrite normalised) with a characteristic Eu anomaly and depleted in the HREE (Fig 6.2.5). PV1234b displays more variation in the abundance of LREE trace elements (~0.5 – 10 LREE range chondrite normalised). This corresponds with a higher variation in X_{An} with a range of 18% – 39% X_{An} whereas PV1222a ranges from 37% – 42% X_{An}. Note that some analyses of HREE are below the detection limit.

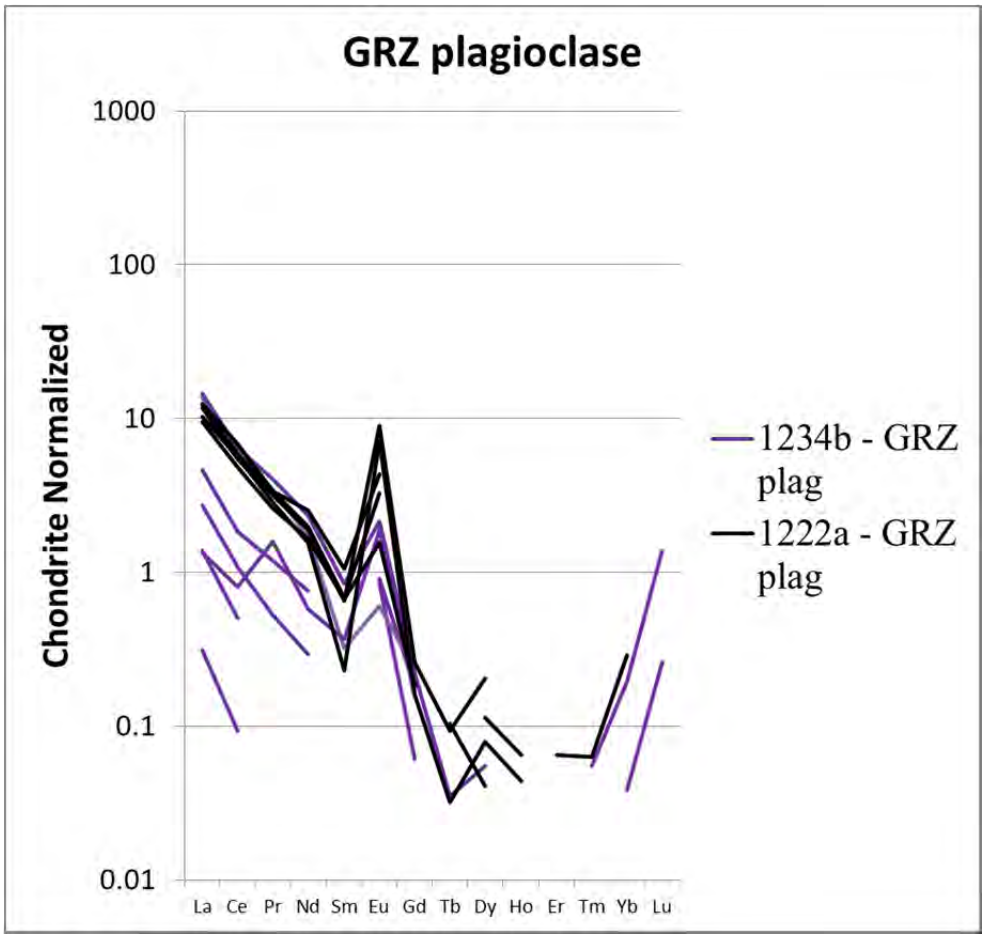

Figure 6.2.5: REE signature of plagioclase within the GRZ. All analyses have a similar pattern, enriched in LREE, with a characteristic Eu anomaly and depleted HREE.

Garnet reaction zone garnet within domain 3 have a similar pattern to the dyke garnet (enriched HREE), although they are generally further depleted in the mid to heavy rare earth elements (Fig 6.2.6). Both samples PV1222a and PV1234b have similar patterns, enriched HREE signature (~20 - 60 chondrite normalised), excluding the two depleted HREE analyses within PV1234b which display a Eu anomaly (Fig 6.2.6). There is no significant difference in major element analysis.

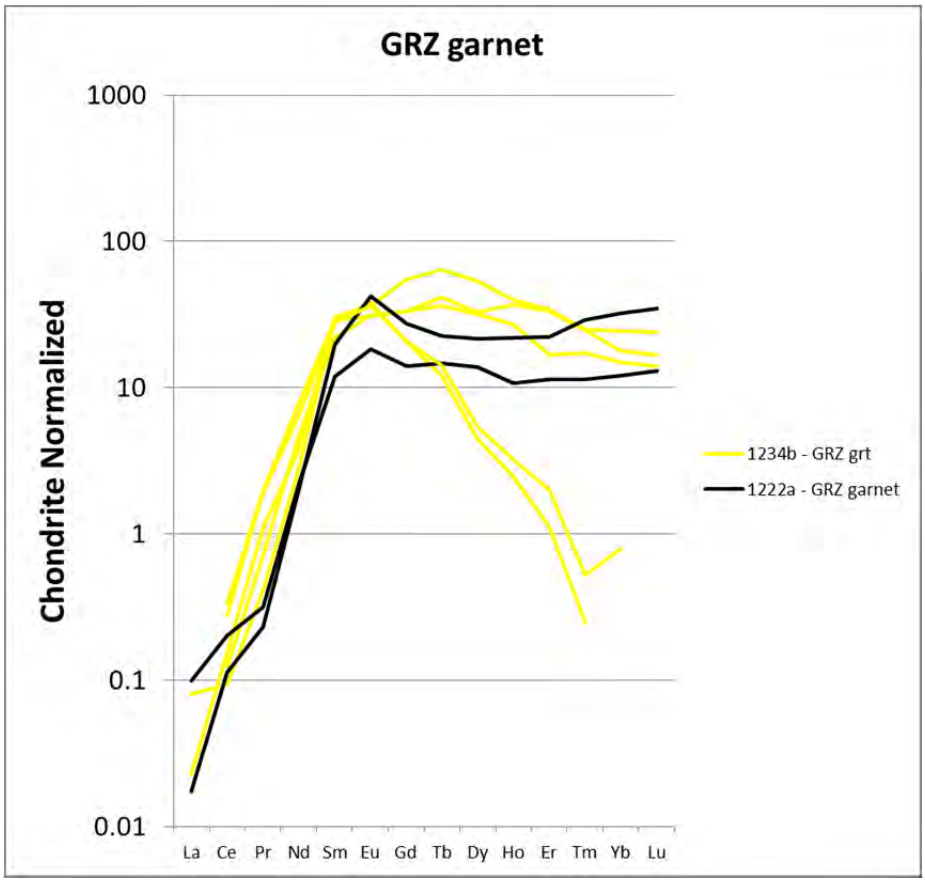

Figure 6.2.6: REE signature of metamorphic garnet and dyke garnet within PV1222a and PV1234b. Both GRZ garnet samples display a similar pattern of enriched HREE excluding two analyses within PV1234b.

6.2.3 Domain 4

Domain 4 (D3 high strain zone) garnet grains show a depleted LREE (~0.08 – 0.1 chondrite normalised) and a further depleted HREE pattern (~7 - 20 chondrite normalised) compared to dyke garnet with a slight Eu anomaly (Fig 6.2.7). There is no significant difference in major elements when comparing post-D3 garnet and garnet reaction zone garnet.

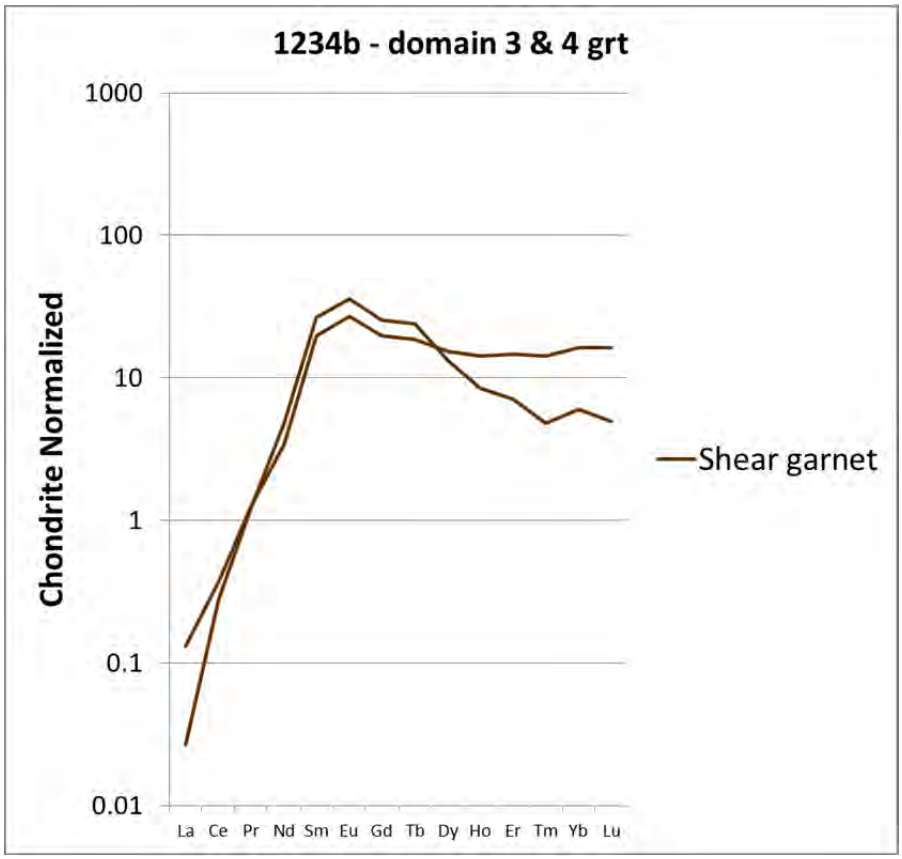

Figure 6.2.7: D3 shear zone garnet. Analysed samples are depleted in LREE contain a slight Eu anomaly, consistent with plagioclase and are depleted in the HREE.

Light to middle rare earth elements ($(La/Sm)_N$) have been plotted against Eu* (Eu* = $Eu_N/\sqrt{(Sm_N.Gd_N)}$; subscript N indicates chondrite-normalized) to determine if plagioclase or other minerals are affecting the trace element patterns of recrystallized grains (Fig 6.2.8). Figure 6.2.8 presents data on S1 cpx, GRZ cpx, GRZ grt and post-D3 grt. Clinopyroxene within sample PV1222a displays no change in Eu from S1 to recrystallized cpx whereas PV1234b displays a slight increase in Eu from S1 to recrystallized cpx. Garnet reaction zone garnet within PV1222a displays an increase in Eu anomaly (line 1) as well as post-D3 grt within PV1234b (line 3). PV1234b garnet reaction zone garnet displays no significant increase in Eu (line 2).

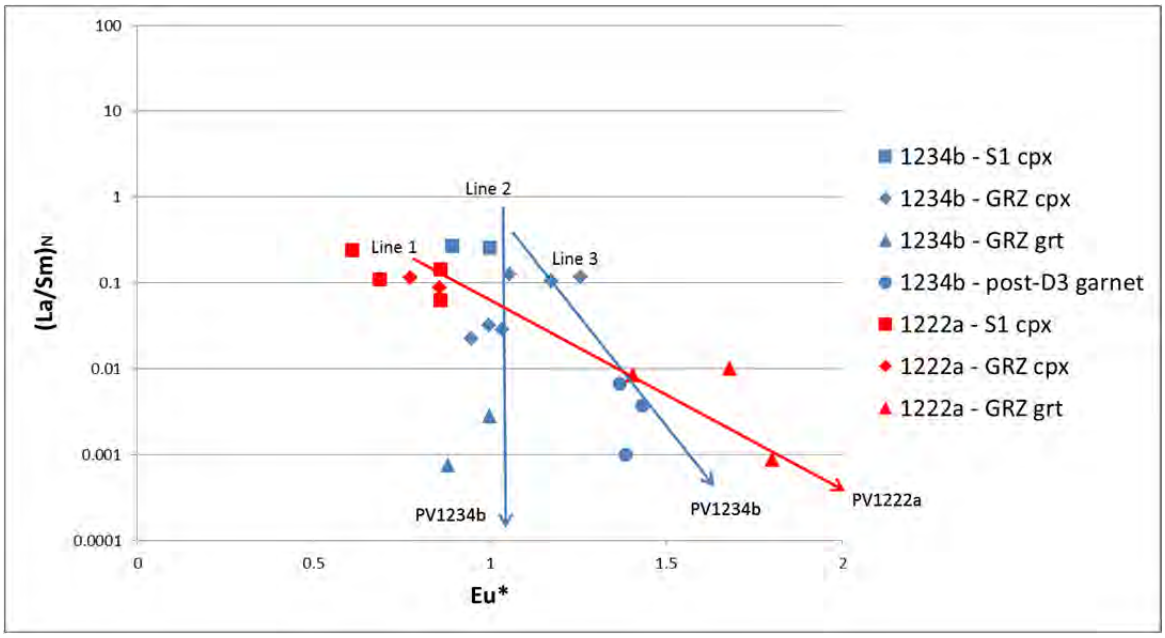

Figure 6.2.8: Variation of $(La/Sm)_N$ vs Eu* [$Eu^* = Eu_N/\sqrt{(Sm_N*Gd_N)}$; subscript N indicates chondrite-normalized] presenting an increase in Eu for GRZ grt within PV1222a and post-D3 grt within PV1234b. Recrystallised cpx show no or little variation due to plagioclase (Eu).

Heavy rare earth elements $(Lu/Gd)_N$ have also been plotted against Eu* (Fig 6.2.9). S1 and GRZ cpx, GRZ grt and post-D3 grt minerals are displayed. Similar patterns are observed to figure 6.2.7, supporting the trends of LREE vs Eu*.

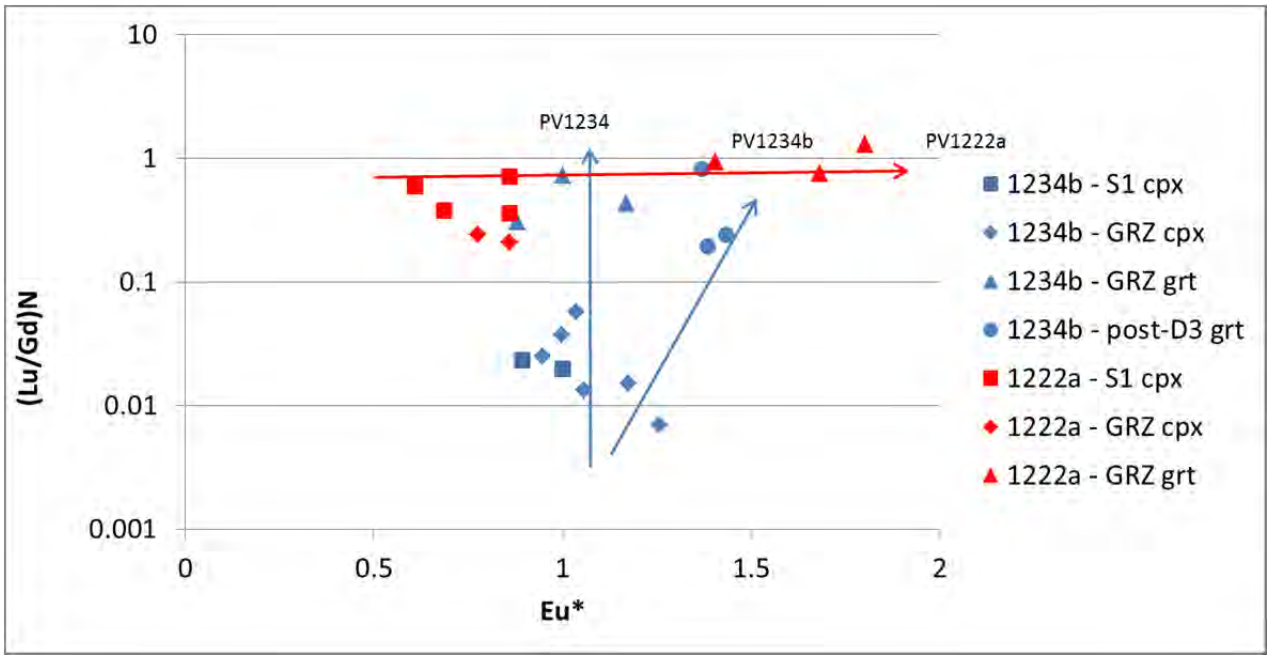

Figure: 6.2.9: Variation of $(Lu/Gd)_N$ vs Eu* [$Eu^* = Eu_N/\sqrt{(Sm_N*Gd_N)}$; N indicates chondrite-normalized] presenting an increase in Eu for GRZ grt within PV1222a and post-D3 grt within PV1234b. Recrystallised cpx show no or little variation due to plagioclase (Eu).

6.3 Discussion

Trace element variation within domain 2 (dyke) displays different signatures in the LREE pattern of plagioclase, likely due to subtly different silicate liquid compositions. This is further supported through major element analysis with different anorthite content between the two samples, supporting the conclusion from chapter 5; variation is the result of partial melting of slight variants of the dioritic gneiss (Schroter et al., 2004). Dyke garnet grains display similar trace element patterns (enriched HREE due to high partition co-efficient (Rollinson, 1993)), whereas wall rock garnet display depleted HREE signatures. Wall rock garnet are more enriched in Pyrope (Mg end-member), suggesting garnet is replacing clinopyroxene (observed through petrography), inferring the reactant influences this depleted HREE signature. This variation between wall and dyke garnet supports the garnet chemistry from chapter 5 and the conclusion that recrystallized minerals are affected by their reactant.

Minerals analysed within domain 3 (garnet reaction zones) consist of S1 relicts (in partially recrystallized samples) and recrystallized minerals, in order to see any relationships between the reactant and product phases.

Plagioclase displays slight variation between samples and no variation between S1 and recrystallized grains. This is consistent with the conclusion from chapter 5: garnet reaction zone or shear zone plagioclase has been recrystallized at different degrees and nucleates or grows from S1 plagioclase, resulting in similar REE patterns. This supports the proposal that precursor minerals play a major role on the trace element pattern of recrystallized grains.

Garnet, if replacing plagioclase, is predicted to have an increased amount of Eu. Garnet grains in sample PV1222a display a Eu anomaly (Fig 6.2.6)~~. T~~he involvement of plagioclase as a reactant in the development of GRZ garnet ~~is supported within figures 6.2.8 and 6.2.9; displaying GRZ garnet increase in Eu.~~ In contrast, garnet within PV1234b does not show these features and tends to mimic the REE pattern of clinopyroxene (Fig 6.2.9). This supports clinopyroxene as the main reactant. Post-D3 garnet grains in the shear zones are further depleted in HREE, displaying Eu enrichment observed in figures 6.2.8 and 6.2.9. This supports the observations that these garnets are texturally replacing plagioclase (cf. chapter 4).

Pyroxene trace element patterns do not significantly vary between S1 and recrystallized grains; although the overall abundance of REE decreases during recrystallization (Fig 6.2.3). This suggests another mineral is competing for the REE. Garnet neoblasts are growing at the same time as the recrystallized grains and this is likely the competing mineral. Clinopyroxene within sample PV1234b is more depleted in the HREE, with a Eu anomaly in some analyses. Clinopyroxene within this sample also displays a slight increase in Eu (Figs 6.2.8 & 6.2.9). This indicates plagioclase may have been ablated as an inclusion or that the growth of the S1 and recrystallized clinopyroxene within PV1234b was affected by the reactant plagioclase (Fig 6.2.8 & 6.2.9). In contrast clinopyroxene from PV1222a has not been affected by the reactant plagioclase as it is more enriched in the HREE, most likely replacing S1 clinopyroxene (Fig 6.2.8 & 6.2.9).

Hornblende analysed in sample PV1234b displays a pattern which is more enriched in HREE than cpx and textural analysis (cf. chapter 4) show it is a major reactant during development of garnet reaction zone textures. This supports plagioclase as the reactant during cpx recrystallization within PV1234b as its pattern is depleted in HREE.

Temperature, composition, replacements and partition coefficients can all affect trace element patterns (Rollinson, 1993). P-T increased during the transition to garnet granulite (Daczko

and Halpin, 2009), although it is argued that melt composition plays the major role on trace element partitioning (Rollinson, 1993). As concluded from chemical and trace element analysis, dykes are of a similar composition. Therefore the main factors affecting the trace element patterns within garnet granulites are the reactant minerals and partition coefficients. The main minerals being replaced during the transition to garnet granulite are hornblende, and clinopyroxene with plagioclase playing a minor role. Hornblende and clinopyroxene have similar patterns of enriched middle REE and depleted HREE. Therefore there is a budget of trace elements for GRZ garnet and recrystallized cpx. Garnet is up taking more of the HREE (due to its partition coefficient) from the more depleted hornblende or clinopyroxene. This replacement results in a slightly depleted HREE signature compared to dyke garnet where diffusion is high. In contrast, recrystallized clinopyroxene is more enriched in the middle REE and depleted in HREE; this signature is partly inherited from its precursor minerals (hornblende or S1 clinopyroxene) and the competition from garnet.

6.4 Summary

As concluded from chapters 4 & 5, domain 2 (dyke) has varied mineralogy and chemistry. This variation is seen within trace element analysis which supports the conclusion from Schroter~~, F.C.~~ et al. (2004) that the felsic dykes are due to the melting of the dioritic gneiss. Therefore, chapter 5 concluded the duration the melt conduit is open will result in different degrees of recrystallization. This recrystallization affects the trace element patterns depending on the precursor minerals. Therefore this chapter has concluded the main factors affecting trace element patterns within garnet reaction zones are a) the reactant mineral and partition coefficients and b) the timing of crystallization (i.e. later growths). Recrystallized minerals are competing against each other for trace elements from hornblende and clinopyroxene, resulting in a budget of trace elements. These trace elements are dispersed between garnet and recrystallized cpx and the degree of dispersion depends greatly on the partition coefficient of each mineral. This results in the observed trace element patterns within garnet reaction zones.

Chapter 7: SEM – Electron Back-scatter Diffraction (EBSD)

7.1 Introduction

Chapter 4 observed varied microstructures related to dyke influence and categorised the gabbroic gneiss into 4 distinct domains. Chapters 5 and 6 aimed to provide chemical and trace element data to support these observations from chapter 4. These chapters concluded: 1) garnet pseudomorphs S1 hornblende from the two-pyroxene-hornblende assemblage, 2) Garnet reaction zones vary in the degree of recrystallization, chemistry and trace elements and 3) some garnets within the D3 high strain zone appear to be post-D3 through observations and trace element analysis. Predictions developed from these chapters are: 1) garnet reaction zone recrystallization occurred under static conditions and any lattice preferred orientation (LPO) would be therefore expected to mimic the orientation of their pre-cursor phase regardless of the degree of recrystallization; this would be the case if there is a crystallographic information "transfer" between reactant and product; and 2) post-D3 garnet will have a different preferred orientation to the syn-D3 garnet.

In order to examine these hypotheses, three key samples have been analysed by SEM-EBSD at Macquarie University, Sydney. These key samples are PV1222a (partially recrystallized GRZ), PV1216a (extensively recrystallized GRZ) and PV1234b (paired shear zone). The approach involved EBSD analysis of small areas (~0.5mm²) during the day in order to choose where an overnight high resolution large area map (~5mm²) should be run. The main aim of this chapter will be to understand what factors affect the crystallographic orientation during the different deformation histories (D1, D2 and D3) leading to paired shear zones.

Pole figures and contour pole figures of crystallographic orientations for hornblende, orthopyroxene, clinopyroxene, garnet and plagioclase have been plotted. Since hornblende, pyroxene, garnet and feldspar have different crystal systems, different sets of pole figures have been plotted for these. For garnet (cubic) {100}, {110}, and {111} pole figures are shown, for feldspar (triclinic) <100>, <010> and <001> and for hornblende, clinopyroxene, orthopyroxene (monoclinic) {100}, {110} and {111} pole figures.

Band contrast maps, displaying in grey scale the quality of indexing (darker for poor indexing), euler angle maps to display the deviation (0 - 10°) from one grain to another and phase maps are displayed to show different textures and phase relationships.

Garnet reaction zones provide a rare opportunity to study the role the precursor phase has on the growth and nucleation of garnet (Padron-Navarta et al., 2008). It is stated that the orientation of garnet under static conditions will be similar to the reactant (hornblende) (Spiess et al., 2007). Therefore EBSD is a powerful method to determine if recrystallization has occurred without deformation (static) or syn-deformation (dynamic).

7.2 Results

As explained within chapter 3, noise reduction has been undertaken with the software Tango within HKL Channel 5. After noise reduction has occurred, representative pole figures are presented within this chapter. Appendix D consists of filtered data of band contrast, euler angles, phases and pole figures for all completed EBSD maps, as well as subsets from large maps. Domain 1 (two-pyroxene-hornblende gneiss) and domain 3 (garnet reaction zone) have been analysed within sample PV1222a. Table 7.1 displays band contrast, all euler angles and phases for domain 1 (Opx-Cpx-Hbl-gneiss) within PV1222a.

Garnet granulite has formed through the reaction of hornblende + pyroxene + plagioclase → Garnet + pyroxene + quartz + H_2O (Schroter et al., 2004). Therefore the orientation of the original host assemblage will be analysed in order to see what the original orientation relationships between different phases are.

Table 7.1: Band contrast, euler angles and phases for domain 1

Band Contrast. Different grey scales indicate different orientations. Dark areas and lines are where the system could not identify the orientation. This is either caused by scratches, holes and/or grain boundaries. There is no significant deformation within individual grains. However, the difference in grain size is nicely depicted.	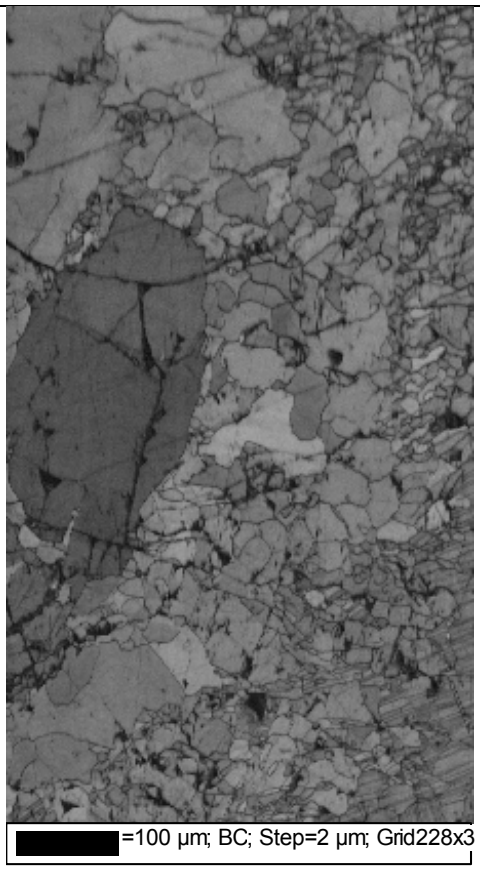
All Euler angle map displaying variation of orientation by different colours. Note the feldspar twinning seen as stripes of orange and lilac.	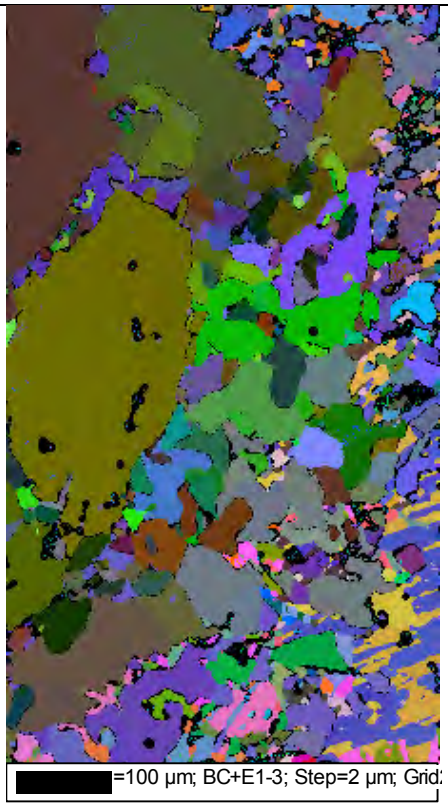

Phases. Green – Hbl Yellow – cpx Blue – anorthite Grey – Opx White – Ilmenite + Rutile + quartz	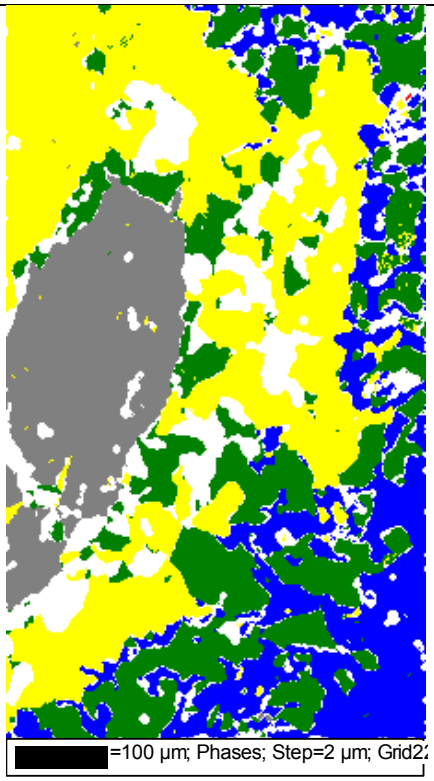

As orthopyroxene is within the original phase, the orientation has been measured and displayed on a pole figure with the planes {100}, {010} and {001}. Orthopyroxene (Fig 7.2.1) shows one grain aligned with the foliation at {010} and {001} with the {100} plane being perpendicular to the foliation. Clinopyroxene (Fig 7.2.2) within this sample displays a preferred orientation, aligned with the foliation in the plane {001} (similar to orthopyroxene) with the two other planes displaying variations in their alignment.

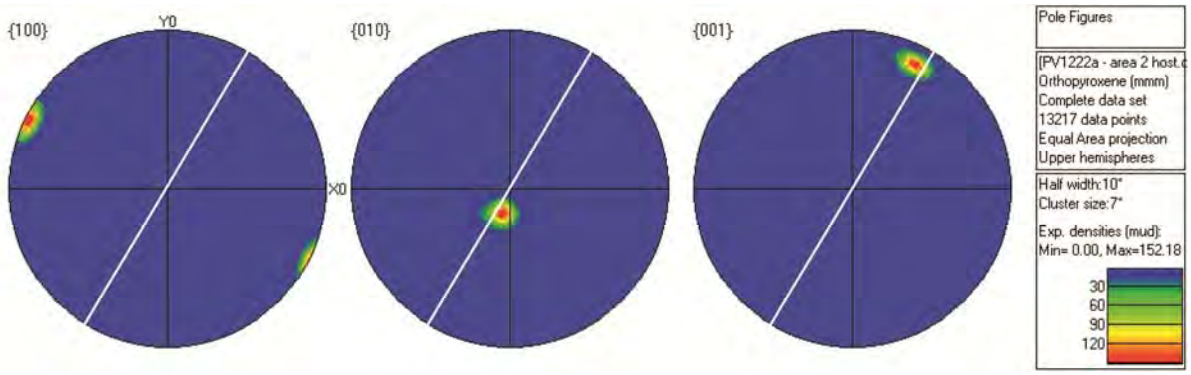

Figure 7.2.1: Contour plot of orthopyroxene, preferred alignment in the {001} and {010} planes

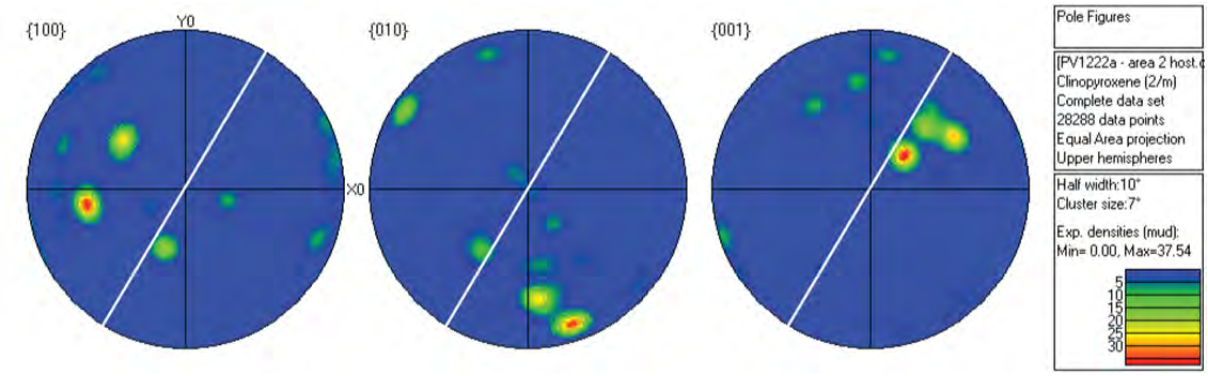

Figure 7.2.2: Contour plot of clinopyroxene, preferred alignment in the {001} plane.

Hornblende displays a strong preferred orientation within all three planes {100}, {010} and {001} (Fig 7.2.3/4). Hornblende has a preferred orientation within the plane {001} along the foliation (Fig 7.2.4) and also displays slight variation in the planes {100} and {010} (Daczko et al., 2001b). Hornblende mimics statically the clinopyroxene and orthopyroxene orientation.

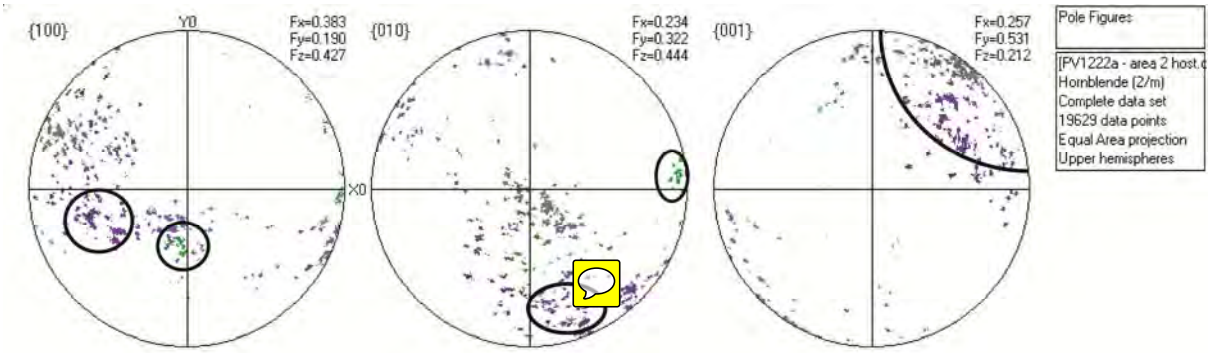

Figure 7.2.3: Scatter pattern of hornblende poles to the {100}, {010} and {001} with two preferred orientations. Different colours represent different euler angles.

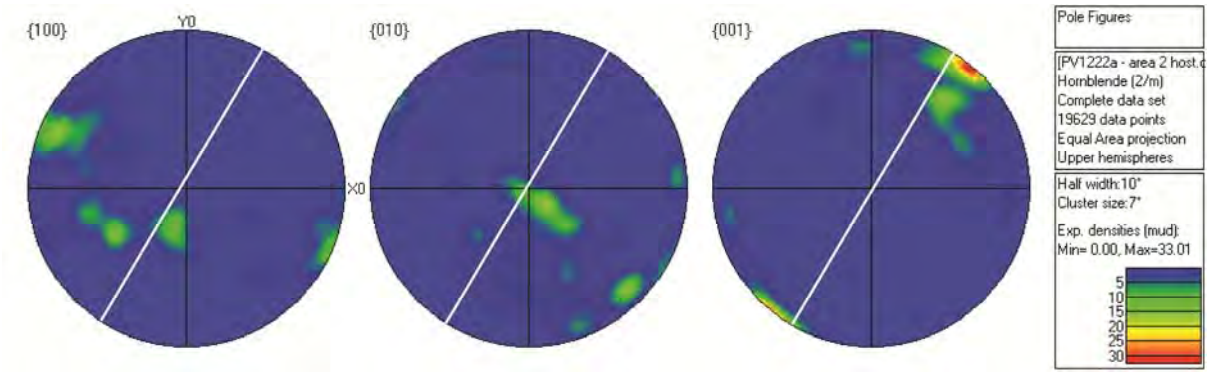

Figure 7.2.4: Contour plot showing LPO of hornblende to the {100}, {010} and {001} with two preferred orientations. White line indicates S1 foliation.

The garnet granulite in PV1222a has also been analysed and band contrast, all euler and phase analysis are within table 7.2. This area has been analysed as it transitions to garnet granulite, providing an opportunity to measure pre-cursor mineral effects on orientation during this transition. Garnet granulite consists of a garnet-clinopyroxene-orthopyroxene-quartz assemblage and will present garnet, orthopyroxene and clinopyroxene relationships.

Table 7.2: Band contrast, all euler and phases for domain 3 within PV1222a

Band Contrast – Different grey scales representing different orientations.	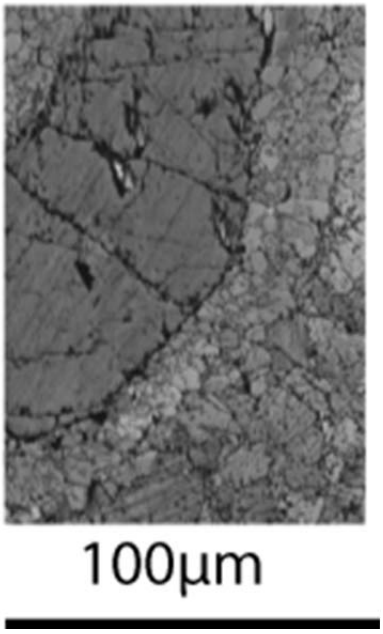	
Band Contrast and all Euler. Different colours represent different orientations. Bright red area is a Grt grain that is defined by 10 degree boundaries to its neighbours.	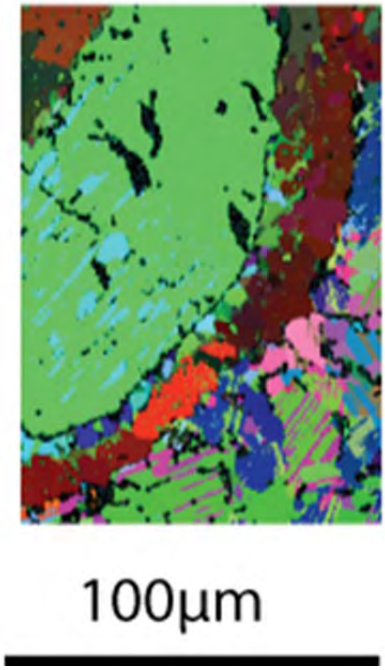	

Phases. Yellow – cpx Blue – anorthite Red - Almandine Grey – Opx Yellow – Cpx White – Ilmenite + quartz + rutile	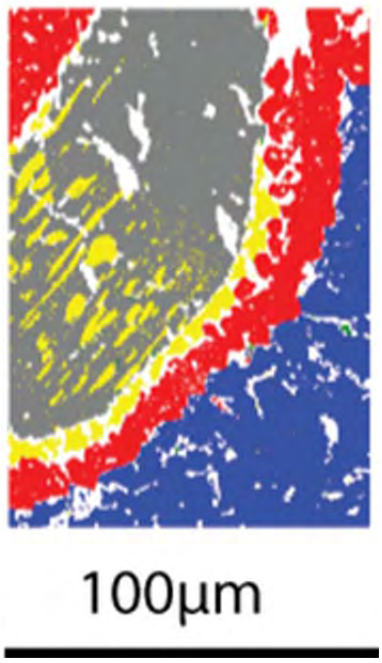

Orthopyroxene displays an orientation along the foliation within the plane {010} and {001}. {100} is perpendicular to the foliation (Fig 7.2.5).

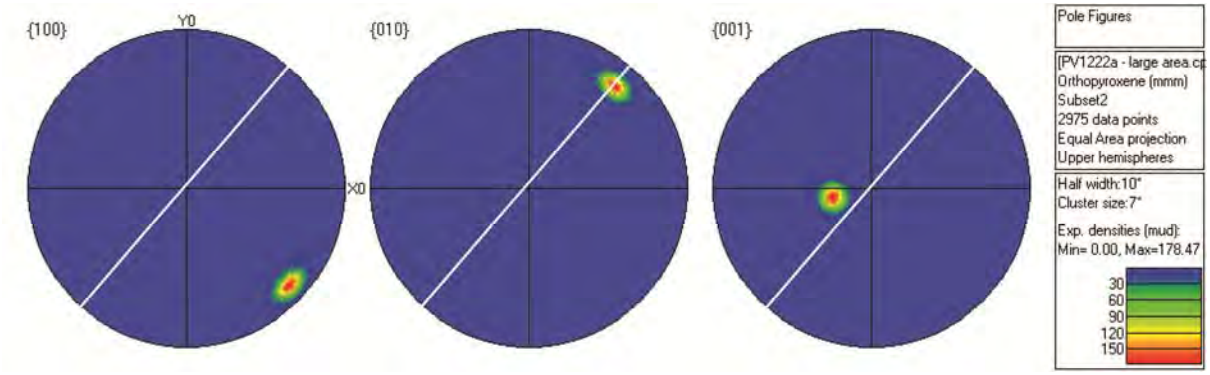

Figure 7.2.5: Alignment of an orthopyroxene grain aligned to the foliation (white line).

Clinopyroxene displays a preferred orientation within the plane {010}, aligned with the foliation. The plane {100} is perpendicular to the foliation and {001} is aligned to the foliation (Fig 7.2.6). This is mimicking the orientation of orthopyroxene.

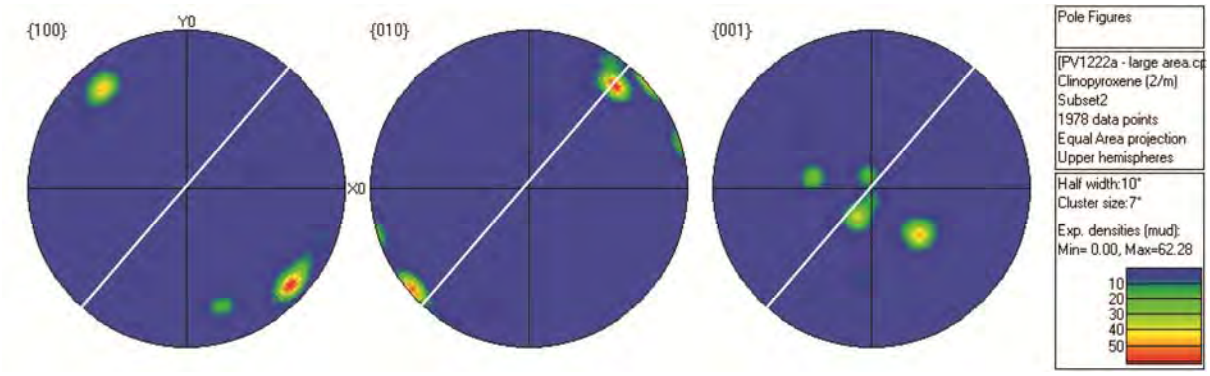

Figure 7.2.6: clinopyroxene alignment to the NE. White line indicates S1 foliation.

Garnet within PV1222a also displays a preferred orientation. Interestingly, the garnet orientation is dominated by one single orientation with a systematic spread. Within the family of planes {100} and {110}, there is a preferred orientation aligned with the foliation (Fig 7.2.7/8). Garnet is cubic and consists of more than three planes; therefore the family {100} consists of planes (100), (010) and (001). Family {111} displays variation with some inheritance of its orientation (Fig 7.2.8).

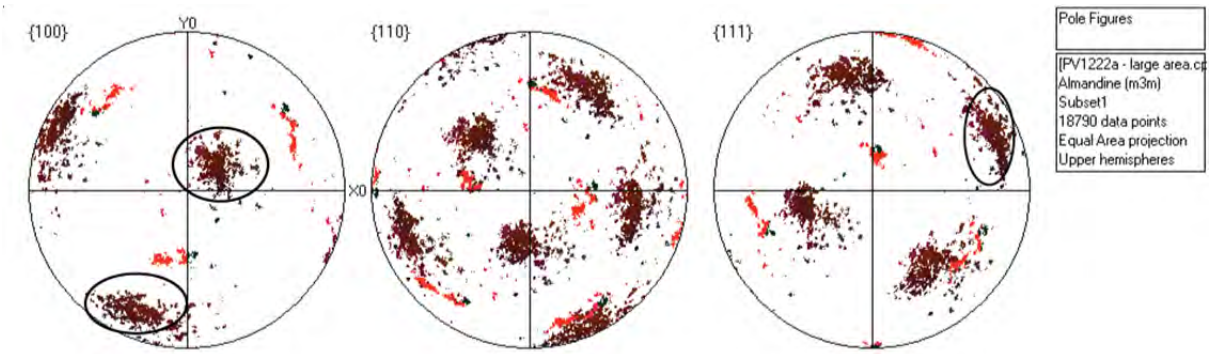

Figure 7.2.7: Scatter pattern of garnet poles to the {100}, {110} and {111}. Different colours represent different euler angles. Preferred orientations are present for garnets different planes. Circles represent some key preferred orientations.

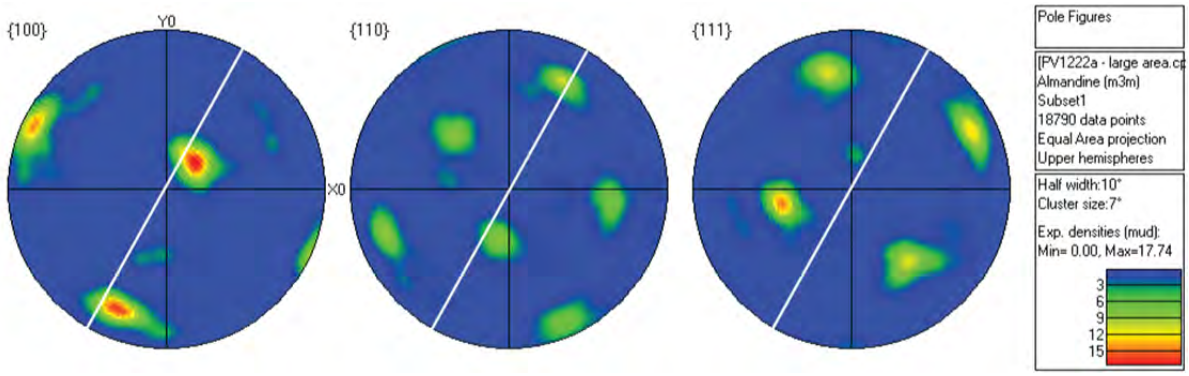

Figure 7.2.8: Contour plot of garnet poles to the {100}, {110} and {111}. Preferred orientations are present. White line represents S1 foliation.

PV1216a is an extensively recrystallized sample and garnet has been analysed and band contrast, euler angles, phases and IPF images for this domain are within table 7.3. This sample has undergone further recrystallization (concluded from chapter 4) and is therefore a key sample to understand if this sample has undergone further static recrystallization or dynamic recrystallization.

Table 7.3: Band contrast, all euler and phases for domain 3 within PV1216a

Band Contrast – Different grey scales represent different orientations. Base of photo is 3000µm.	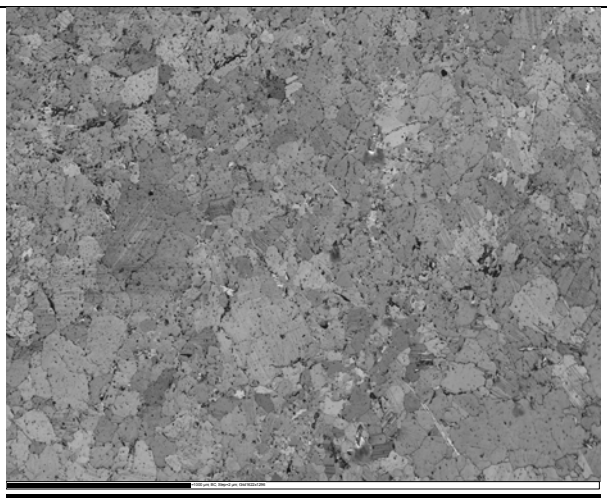

Band Contrast and all Euler – Different colours represent different orientations. Base of photo is 3000µm.	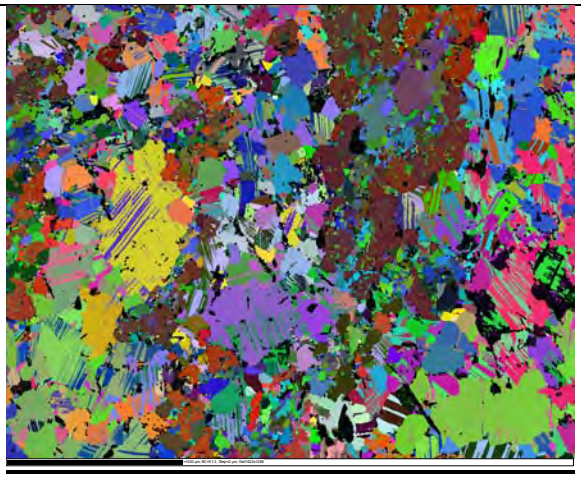
Phases. Yellow – cpx Blue – anorthite Red – Almandine Purple – Quartz Green – Hornblende White – Ilmenite + Quartz + Rutile Base of photo is 3000µm.	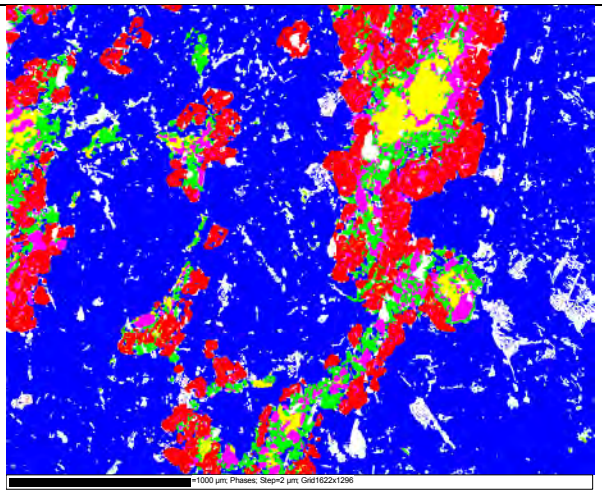
IPF colouring – Colour scheme is generated from three primary colours from an inverse pole figure (IPF). Changes in colour of each grain represent changes in orientations. There are clusters of different orientations. Base of photo is 3000µm.	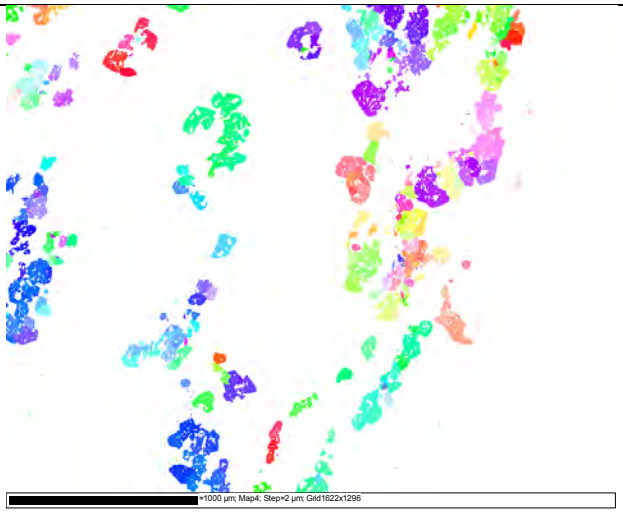

Clinopyroxene within this sample has undergone a high degree of recrystallization. There is a preferred orientation within the plane {001} with the foliation (Fig 7.2.9). Plane {010} is affected by the foliation with slight alignment and the plane {100} is perpendicular to the foliation.

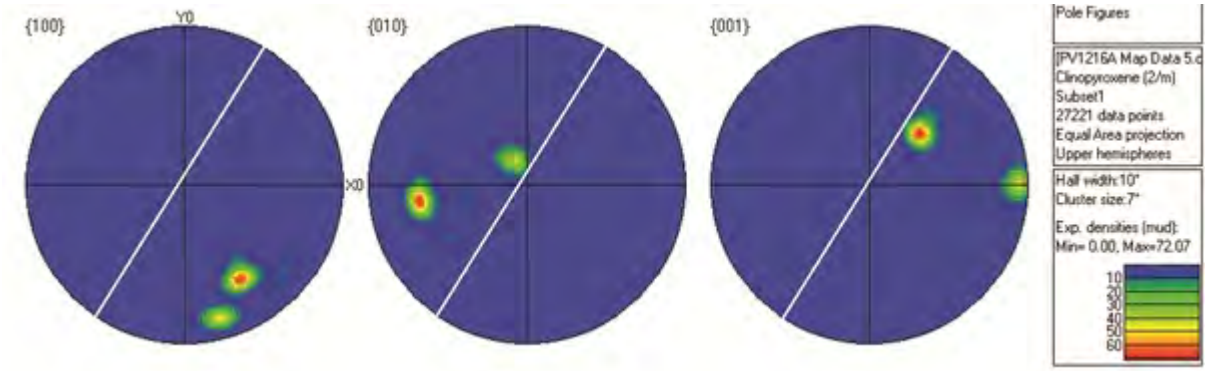

Figure 7.2.9: Contour plot of clinopyroxene. Preferred orientation within the plane {001}. White line indicates S1 foliation.

Garnet within this sample displays a preferred orientation aligned to the S1 foliation within {100} and {111} (Fig 7.2.10/11). Family {110} displays no preferred orientation with the foliation (Fig 7.2.11). There is spread within the data due to the different garnet cluster orientations observed in the IPF figure (table 7.3).

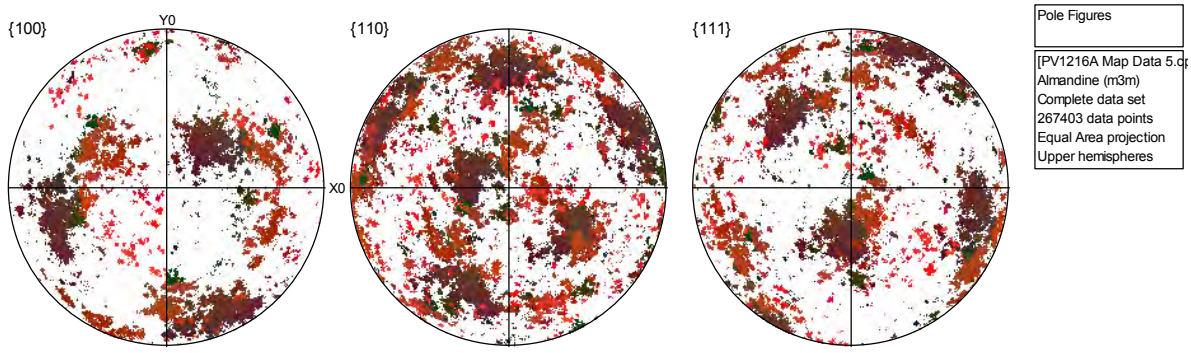

Figure 7.2.10: Scatter pattern of garnet poles to the {100}, {110} and {111}. Preferred orientations are within the three families.

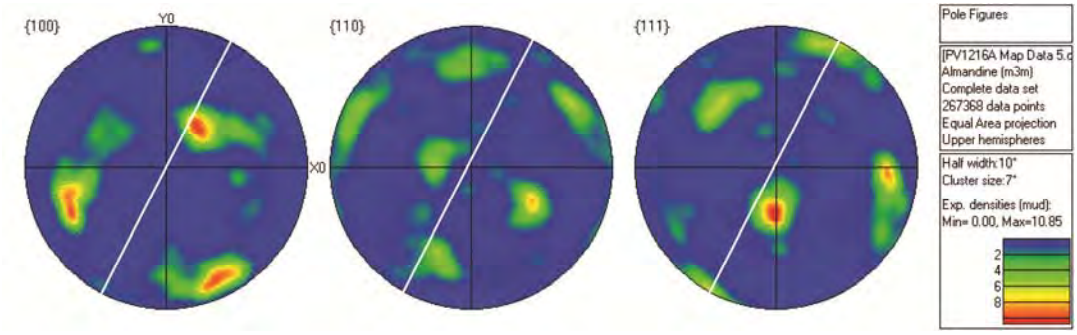

Figure 7.2.11: Contour plot of garnet poles {100}, {110} and {111}. Preferred orientations are present. Note preferred orientation within {100} and {111}. White line indicates S1 foliation.

Sample PV1234b is a paired shear zone sample. Garnet analysis has been undertaken within the D3 shear zone and band contrast, euler angles and phases are observed in table 7.4. This sample has been further deformed by mylonitic shear zones with possible later garnet growth (post-D3) concluded from Chapter 4.

Table 7.4: Band contrast, all euler and phases for domain 4 within PV1234b

Band Contrast – Different grey scales represent different orientations. Base of photo is 4000µm.	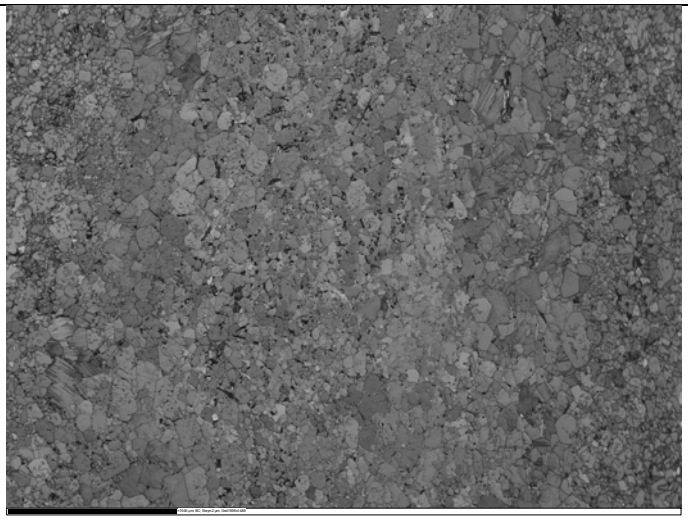
Band Contrast and all Euler – Different colours represent different orientations. Base of photo is 4000µm.	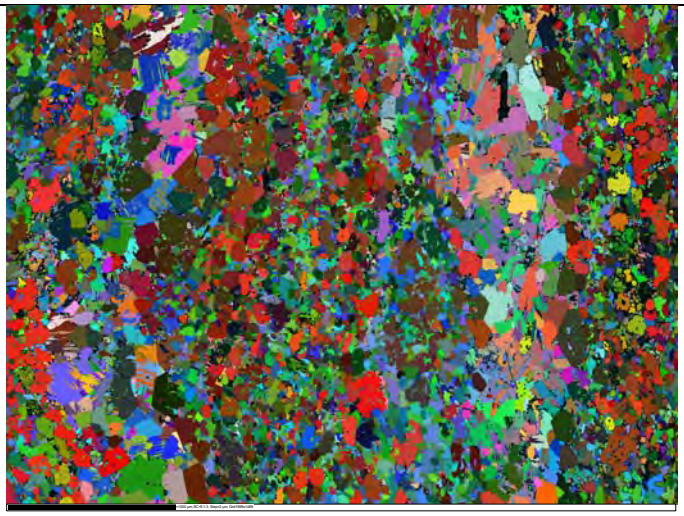

Phases. Green – Hbl Yellow – cpx Blue – anorthite Grey – Opx Aqua – Rutile Purple – Kyanite White – Quartz + Ilmenite Base of photo is 4000µm.	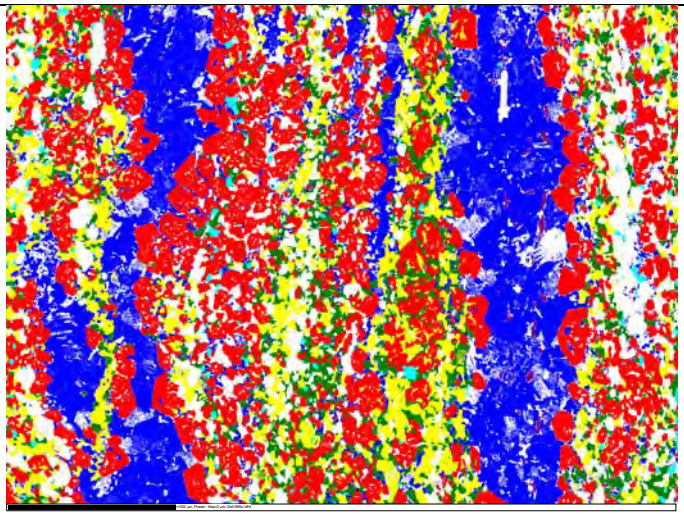

Plagioclase within the high strain zone has been analysed and plotted onto scatter and contour plots with the directions <100>, <010> and <001> (Fig 7.2.12/13). There are preferred orientations, most obvious within the contour plot as clusters (Fig 7.2.13).

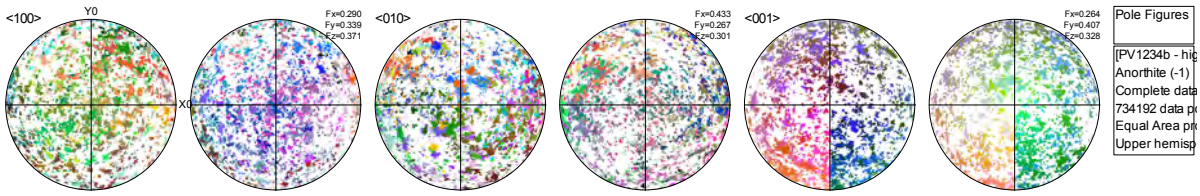

Figure 7.2.12: Scatter plot of plagioclase directions <100>, <010> and <001>

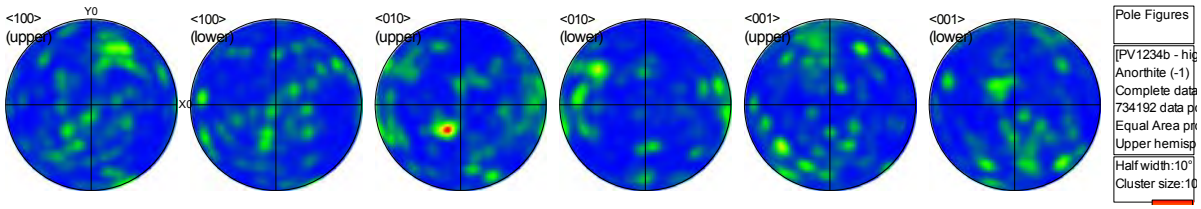

Figure 7.2.13: Contour plot of plagioclase directions <100>, <010> and <001>. Preferred orientations are present

Syn-D3 garnet has also been analysed within the high strain zone and displays no preferred orientation (Fig 7.2.14/15). This garnet has an average grain area of 3527µm .

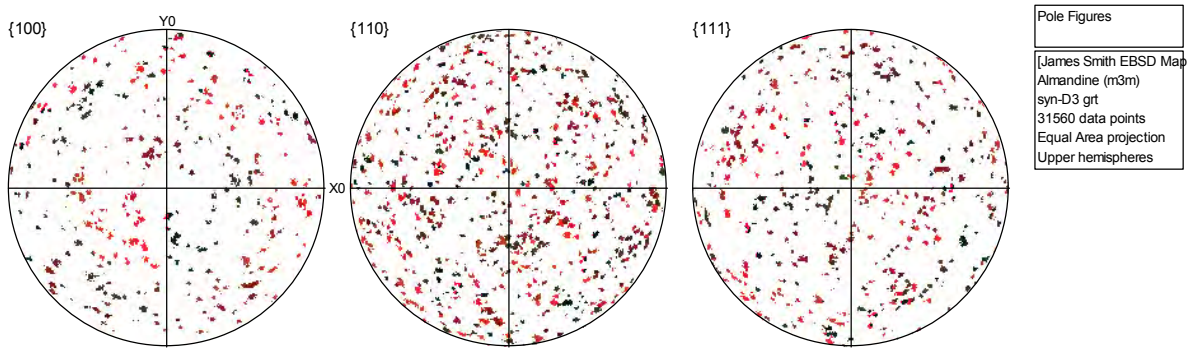

Figure 7.2.14: Scatter plot of syn-D3 garnet. Different colours represent different euler angles.

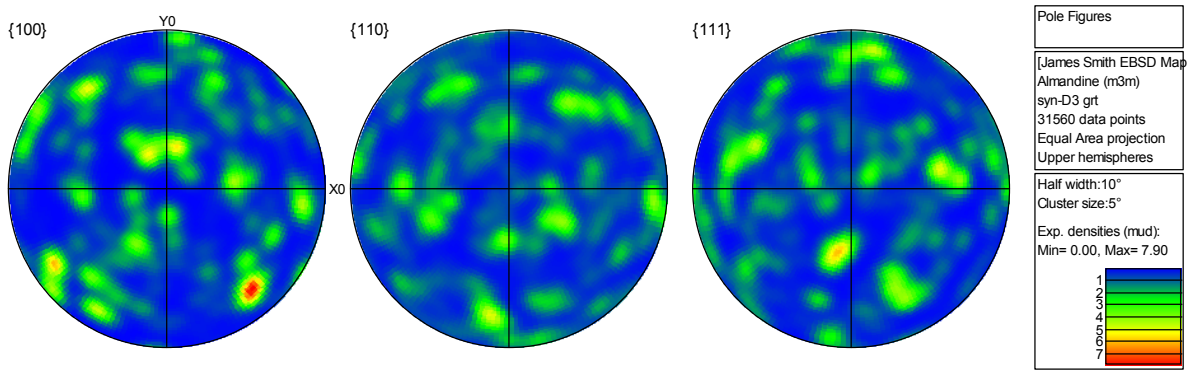

Figure 7.2.15: Contour plot of syn-D3 garnet. No preferred orientation.

The post-D3 garnet observed in chapter 4 have been analysed and plotted onto pole figures. There is some preferred orientation, most obvious in the contour plot (Fig 7.2.16/17). These garnets have an average grain area of 20491µm .

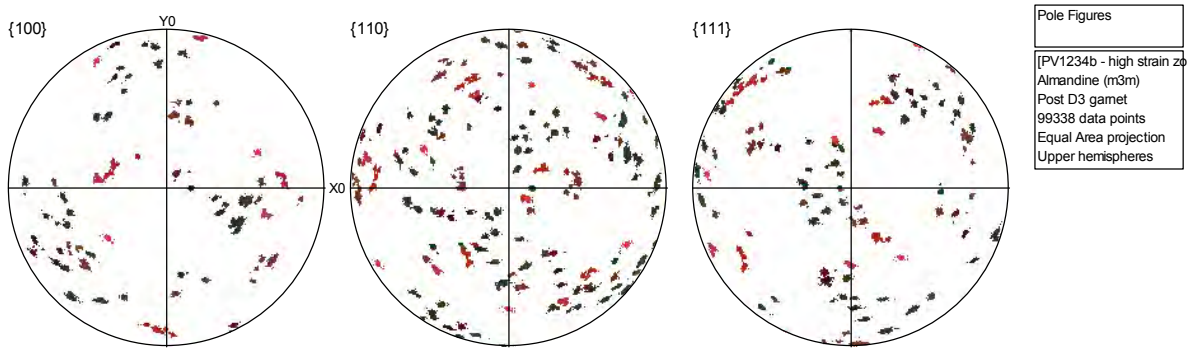

Figure 7.2.16: Scatter plot of post-D3 garnet within PV1234b

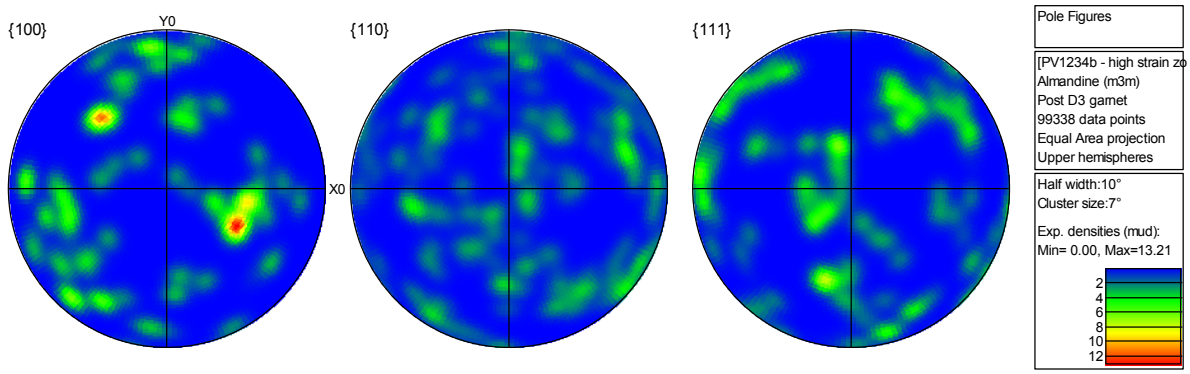

Figure 7.2.17: Contour plot of post-D3 garnet within PV1234b

7.3 Discussion

SEM-EBSD has been undertaken on similar garnet granulites within the Jijal complex northern Pakistan. This study concluded pre-cursor phases have a strong relationship with the orientation of the garnet during the transition to garnet granulite (Padron-Navarta et al., 2008). Padron-Navarta et al. (2008) termed epitaxy to be the control on the precursor and recrystallized mineral alignment. Garnet has grown epitaxially upon crystallographic orientation {001} and {010} hornblende planes. Clinopyroxene and orthopyroxene planes within the garnet granulite of PV1222a display alignment with the foliation, likely to affect the precursor hornblende with an alignment also of {010} or {001}. This indicates hornblende rotates ~~aligned to~~ the foliation and always displays alignment within either {010} or {001} which garnet grows epitaxially upon. S1 clinopyroxene and orthopyroxene also display this rotation along the foliation.

Recrystallized garnet always display a preferred orientation aligned to the foliation within a plane in the family {100} with rotation occurring in between the other two families ({111} and {110}). Therefore garnets LPO is inherited from the precursor foliation (due to solid state deformation) which affects the orientation and nucleation of minerals under static conditions (Spiess et al., 2007). This orientation is still observed within extensively recrystallized sample PV1216a. This preferred orientation shows further recrystallization has occurred due to the longer interaction with the melt conduit under static conditions and not due to syn-deformation (dynamic recrystallization).

The high strain zone within sample PV1234b indicates the different types of deformation garnet and plagioclase have encountered. Plagioclase displays preferred orientation within the high strain zone which indicates crystal plastic deformation. Crystal plastic deformation results in a domain collectively accommodating the imposed deformation and results in the preferred orientation of minerals (Arul Kumar and Mahesh, 2012). Whereas syn-D3 garnet does not display any preferred orientation within this high strain zone and this indicates grain boundary sliding has occurred resulting in large rotations of the garnet grains causing randomly orientated grains (Bestmann and Prior, 2003). Post-D3 garnet displays some preferred orientations, supporting the conclusions from previous chapters; these garnets are replacing plagioclase. Although phase maps indicate garnet is growing epitaxially from syn-D3 garnet and plagioclase grains, resulting in some preferred orientations.

7.4 Summary

SEM-EBSD supports the conclusion from chapters 4, 5 and 6 that the formation of garnet reaction zones is under static conditions. Preferred orientation due to the precursor minerals will only be found under static conditions, therefore longer heat influence results in further recrystallization and not further deformation. The high strain zone has been deformed by dynamic recrystallization and EBSD has determined plagioclase for up taking the most deformation. Plagioclase has accommodated most of the strain through crystal plastic deformation (displays preferred orientation) and garnet deforms by grain boundary sliding (no preferred orientation) accommodated by feldspar deformation. As the post-D3 garnet displays some preferred orientations, it has replaced plagioclase and syn-D3 garnet, supporting it is a later growth.

Chapter 8: Summary and Conclusion

This study investigated the potential rheological and chemical variations of the gabbroic gneiss required to result in a paired shear zone. Figure 8 presents the developed model for paired shear zone formation. Domains 1 – 4 are represented within figure 8, presenting a time sequence with domains 2 and 3 being contemporaneous as dykes cause garnet reaction zones. Domain 1 (Fig 8a) is the well foliated S1 two-pyroxene-hornblende assemblage of the original high temperature rock, with a developed corona texture. Figure 8b displays felsic dykes (domain 2) with a similar mineral assemblage, cutting domain 1. These dykes can be open with melt flowing through or collapsed, preventing melt movement. Major and trace element analysis showed that there are subtle differences in the major and trace element chemistry between different dykes. This is interpreted as the result of a slightly varied melt source for the suite of dykes observed. K-feldspar abundance increases close to the dyke, indicating partial melting of the gabbroic gneiss. Therefore dehydration melting has resulted in the transition from hornblende granulite to garnet granulite (Fig 8b). Garnet pseudomorphing hornblende from the S1 assemblage under static conditions is supported by EBSD, where the precursor minerals effect the orientation of garnet. This replacement is further supported by trace element analysis, indicating the precursor mineral also affects the trace element pattern. Figure 8b presents two types of garnet reaction zones. 1) A partially recrystallized GRZ located within figure 8b at A and B and 2) Extensively recrystallized within figure 8b C and D. This poses the question, why are there different degrees of recrystallization? As they have a similar composition and source, the difference in microstructure must be due the time the dyke is open and melt is moving through. Partially recrystallized garnet reaction zones can be located at the outer regions of garnet reaction zones with a long dyke influence or close to a collapsed dyke (short interaction). This lower degree of static recrystallization is indicated by the presence of an S1 assemblage and varied major element chemistry within plagioclase and garnet. Extensively recrystallized regions have a different textural setting with no S1 assemblage present and are seen within all studied paired shear zones close to the dyke. EBSD analysis of extensively recrystallized reaction zones displays a preferred orientation with the foliation, supporting further static recrystallization. This degree of recrystallization generally increases towards dykes of longer interaction as well as increased garnet abundance. Longer dyke interaction is further supported by the extensively recrystallization at two dyke intersections (Fig 8b C). This recrystallization corresponds with the major element chemistry, homogenising at areas of

extensive static recrystallization. This recrystallization results in a rheological contrast with a trend of decreasing recrystallization away from the dyke. Figure 8c represents the two different textural settings, 1) a collapsed dyke resulting in partial recrystallization and the presence of an S1 assemblage and 2) an extensively recrystallized region close to the dyke, resulting in localized strain on the outer regions of the garnet reaction zone. Therefore the degree of static recrystallization plays a major role on paired shear zone formation. The duration of dyke influence and recrystallization is a required pre-cursor for paired shear zone development as this results in stress localization at interfaces of different rheology (soft – hard). Garnet is a hard material and this increase in abundance due to extensive recrystallization causes a stronger bulk rock and subsequently localised strain.

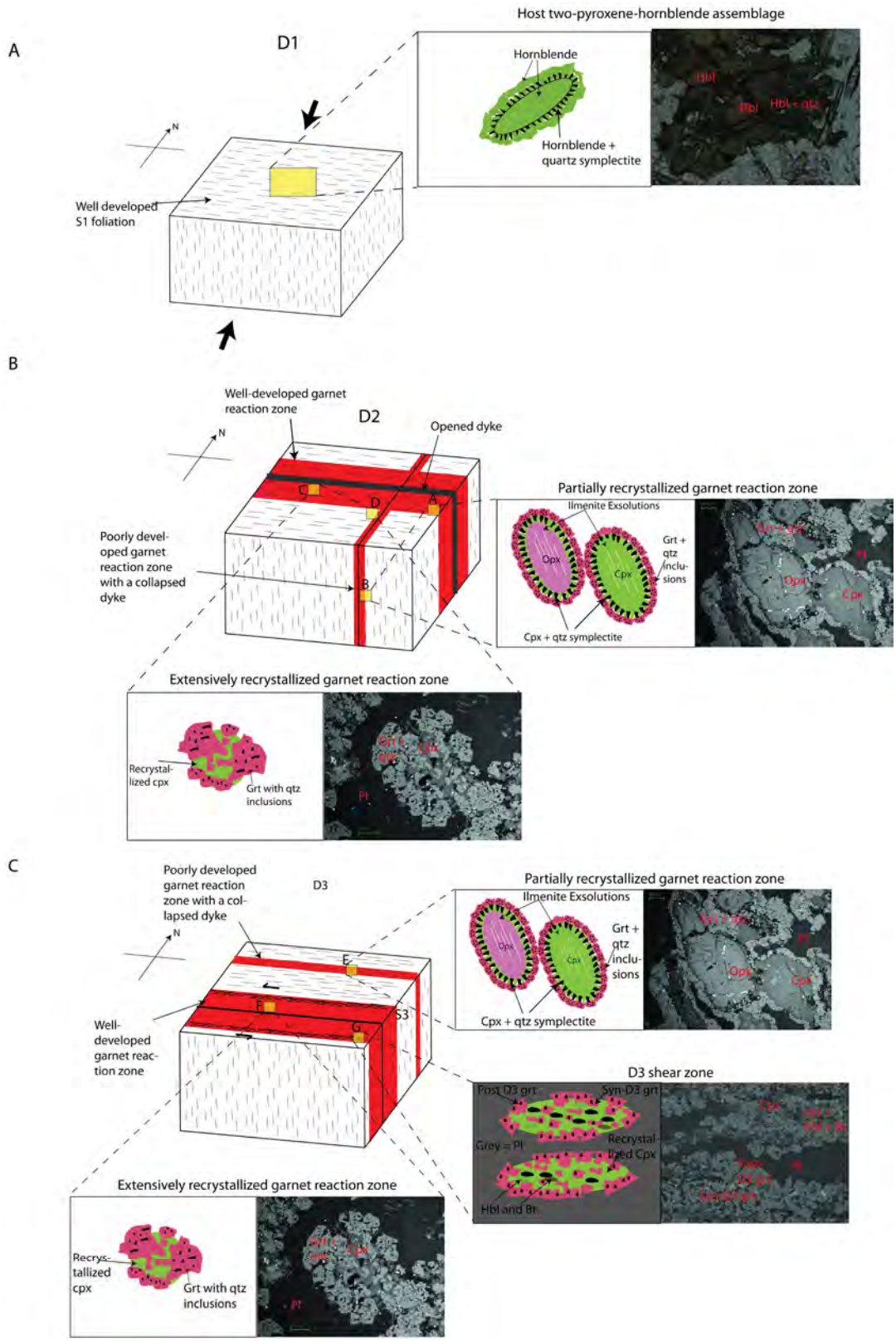

Figure 8: Proposed model for paired shear zone development. A, B and C represent three different deformation events. D1 resulted in the S1 gneissic foliation of two-pyroxene-hornblende gneiss. D2 resulted in felsic dykes and garnet reaction zone formation with different degrees of recrystallization and D3 resulted in east-striking mylonitic shear zones which can sometimes be localised as a paired shear zone. Modified from Clarke et al. (2000).

Chapter 9: Future Research

- Detailed petrographic analysis for collapsed structures
    - Cut more thin sections of ‘collapsed dyke’ garnet reaction zones
- Obtain Electron Microprobe (EMP) data for supporting SEM-EDS data
- Further analysis of samples with the LA-ICP-MS
    - In order to further constrain trend of minerals
- Melt microstructures within the dioritic gneiss
    - This unit has not been focused on during this thesis due to time constraints. Can look for evidence of melt-microstructures to support the proposed melt source for the dykes.
- Large mylonitic zones within the gabbroic and dioritic gneiss
    - Possible fluid influxes?

References

Allibone, A. H., Milan, J. A., Daczko, N. R., and Turnbull, I. M., 2009, Granulite facies thermal aureoles and metastable amphibolite facies assemblages adjacent to the Western Fiordland Orthogneiss in southwest Fiordland, New Zealand: J. metamorphic Geol., v. 27, p. 349-369.

Arul Kumar, M., and Mahesh, S., 2012, Banding in single crystals during plastic deformation: International journal of plasticity v. 36, p. 15-33.

Bestmann, M., Piazolo, S., Spiers, C. J., and Prior, D. J., 2005, Microstructural evolution during initial stages of static recovery and recrystallization: new insights from in-situ heating experiments combined with electron backscatter diffraction analysis: Journal of structural geology, v. 27, p. 447-457.

Bestmann, M., and Prior, D. J., 2003, Intragranular dynamic recrystallization in naturally deformed calcite marble: diffusion accommodated grain boundary sliding as a result of subgrain rotation recrystallization: Journal of structural geology, v. 25, p. 1597-1613.

Blattner, P., 1976, Replacement of hornblende by garnet in granulite facies assemblages near Milford Sound, New Zealand: Contributions to mineralogy and petrology, v. 55, p. 181-190.

-, 2005, Transport of low-aH_2O dehydration products to melt sites via reaction-zone networks, Milford Sound, New Zealand: J. metamorphic Geol., v. 23, p. 569-578.

Blattner, P., and Black, P. M., 1980, Apatite and Scapolite as Petrogenetic Indicators in Granolites of Milford Sound, New Zealand: Contrib. Mineral. Petrol., v. 74, p. 339-348.

Borthwick, V. E., and Piazolo, S., 2010, Post-deformational annealing at the subgrain scale: Temperature dependent behaviour revealed by in-situ heating experiments on deformed single crystal halite: Journal of Structural Geology, v. 32, p. 982-996.

Bradshaw, J. D., 1989a, Cretaceous Geotectonic patterns in the New Zealand region: tectonics, v. 8, no. 4, p. 803-820.

-, 1989b, Early Cretaceous vein-related garnet granulite in Fiordland, southwest New Zealand: a case for infiltration of mantle-derived CO_2-rich fluids[1]: Journal of Geology, v. 97, p. 697-717.

Clarke, G. L., Daczko, N. R., Klepeis, K. A., and Rushmer, T., 2005, Roles for fluid and/or melt advection in forming high-P mafic migmatites, Fiordland, New Zealand J. metamorphic Geol., v. 23, p. 557-567.

Clarke, G. L., Klepeis, K. A., and Daczko, N. R., 2000, Cretaceous high-P granulites at Milford Sound, New Zealand: metamorphic history and emplacement in a convergent margin setting: J. metamorphic Geol., v. 18, p. 359-374.

Daczko, N. R., Clarke, G. L., and Klepeis, K. A., 2001a, Transformation of two-pyroxene hornblende granulite to garnet granulite involving simultaneous melting and fracturing of the lower crust, Fiordland, New Zealand: J. metamorphic Geol., v. 19, p. 549-562.

Daczko, N. R., and Halpin, J. A., 2009, Evidence for melt migration enhancing recrystallization of metastable assemblages in mafic lower crust, Fiordland, New Zealand: J. metamorphic Geol., v. 27, p. 167-185.

Daczko, N. R., Klepeis, K. A., and Clarke, L. G., 2001b, Evidence of Early Cretacous collisional-style orogenesis in northern Fiordland, New Zealand and its effects on the evolution of the lower crust: Journal of Structural Geology, v. 23, p. 693-713.

Daczko, N. R., Stevenson, A. J., Clarke, L. G., and Klepeis, K. A., 2002, Successive hydration and dehydration of high-P mafic granofels involving clinopyroxene-kyanite symplectites, Mt Daniel, Fiordland, New Zealand: Journal of metamorphic Geology, v. 20, p. 669-682.

Deer, W. A., Howie, R. A., and Zussman, J., 1992, An introduction to the rock-forming minerals, Essex, Longman Group.

Garrido, C. J., Bodinier, J., Burg, J., Zeilinger, G., Hussain, S. S., Dawood, H., Chaudhry, M. N., and Gervilla, F., 2006, Petrogenesis of mafic garnet granulite in the lower crust of the Kohistan Paleo-arc Complex (Northern Pakistan): Implications for intra-crustal differentiation of island arcs and generation of continental crust Journal of petrology, v. 47, no. 10, p. 1873-1914.

Gibson, I. L., and Walker, P. L., 1963, Some composite rhyolite/basalt lavas and related composite dykes in eastern Iceland.

Harte, B., Hunter, R. H., and Kinny, P. D., 1993, Melt geometry, movement and crystallization, in relation to mantle dykes, veins and metasomatism Philosophical transactions: physical sciences and engineering, v. 342, no. 1663, p. 1-21.

Heilbronner, R., and Tullis, J., 2012, The effect of static annealing on microstructures and crystallographic preferred orientations of quartzites experimentally deformed in axial compression and shear Geological Society of London, v. 200, p. 191-218.

Herwegh, M., Berger, A., Ebert, A., and Brodhag, S., 2008, Discrimination of annealed and dynamic fabrics: Consequences for strain localization and deformation episodes of large-scale shear zones: Earth and Planetary Science v. 276, p. 52-61.

Hollis, J. A., Clarke, G. L., Klepeis, K. A., Daczko, N. R., and Ireland, T. R., 2004, The regional significance of Cretaceous magmatism and metamorphism in Fiordland, New Zealand, from U-Pb zircon geochronology J. metamorphic Geol., v. 22, p. 607-627.

Holness, M. B., and Sawyer, E. W., 2008, On the Pseudomorphing of Melt-filled Pores During the Crystallization of Migmatites Journal of Petrology, v. 49, no. 7, p. 1343-1363.

Humphreys, F. J., 2001, Review: Grain and subgrain characterisation by electron backscatter diffraction: Journal of materials science v. 36, p. 3833-3854.

Humphreys, F. J., and Hatherly, M., 1995, Recrystallization and related annealing Phenomena, Oxford Pergamon.

Jessel, M. W., Siebert, E., Bons, P. D., Evans, L., and Piazolo, S., 2005, A new type of numerical experiment on the spatial and temporal patterns of localization of deformation in a material with a coupling of grain size and rheology: Earth and Planetary Science, v. 239, p. 309-326.

Kleinschrodt, R., and McGrew, A., 2000, Garnet plasticity in the lower continental crust: implications for deformation mechanisms based on microstructures and SEM-electron channeling pattern analysis Journal of structural geology, v. 22, p. 795-809.

Mancktelow, N. S., and Pennacchioni, G., 2005, The control of precursor brittle fracture and fluid-rock interaction on the development of single and paired ductile shear zones: Journal of Structural Geology, v. 27, p. 645-661.

Montesi, L. G. J., and Hirth, G., 2003, Grain size evolution and the rheology of ductile shear zones: from laboratory experiments to postseismic creep: Earth and Planetary Science, v. 211, p. 97-110.

Mortimer, N., Tulloch, J. A., Spark, R. N., Walker, W. N., Ladley, E., Allibone, A., and Kimbrough, D. L., 1999, Overview of the Median Batholith, New Zealand: a new interpretation of the geology of the Median Tectonic Zone and adjacent rocks: Journal of African Earth Sciences, v. 29, no. 1, p. 257-268.

Muramoto, M., Michibayashi, K., Ando, J., and Kagi, H., 2011, Rheological contrast between garnet and clinopyroxene in the mantle wedge: An example from Higashi-akaishi peridotite mass, SW Japan: Physics of the Earth and Planetary Interiors v. 184, p. 14-33.

Norman, M. D., Griffin, W. L., Pearson, N. J., Garcia, M. O., and O'Reilly, S. Y., 1998, Quantitative analysis of trace element abundances in glasses and minerals: a comparison of laser ablation inductively coupled plasma mass spectrometry, solution inductively coupled plasma mass spectrometry, proton microprobe and electron microprobe data: Journal of Analytical Atomic Spectrometry, v. 13, p. 477-482.

Oliver, G. J. H., 1977, Feldspathic hornblende and garnet granulites and associated anorthosite pegmatites from doubtful sound, Fiordland, New Zealand: Contrib. Mineral. Petrol., v. 65, p. 111-121.

Padron-Navarta, J. A., Garrido, C. J., Sanchez-navas, A., Tommasi, A., Sanchez-Vizcaino, V. L., Gomez-pugnaire, M. T., and Hussain, S. S., 2008, Oriented growth of garnet by topotactic reactions and epitaxy in high-pressure, mafic garnet granulite formed by dehydration melting of

metastable hornblende-gabbronorite (Jijal Complex, Kohistan Complex, north Pakistan) Journal of metamorphic Geology, v. 26, p. 855-870.

Pennacchioni, G., and Mancktelow, N. S., 2007, Nucleation and initial growth of a shear zone network within compositionally and structurally heterogeneous granitoids under amphibolite facies conditions: Journal of Structural Geology v. 29, p. 1757-1780.

Piazolo, S., Bestmann, M., Prior, D. J., and Spiers, C. J., 2006, Temperature dependent grain boundary migration in deformed-then-annealed material: Observations from experimentally deformed synthetic rocksalt Tectnophysics, v. 427, p. 55-71.

Prior, D. J., Wheeler, J., Peruzzo, L., Spiess, R., and Storey, C., 2002, Some garnet microstructures: an illustration of the potential of orientation maps and misorientation analysis in microstructural studies: Journal of Structural Geology, v. 24, p. 999-1011.

Ranalli, G., 1995, Rheology of the earth, London, Chapman & Hall.

Rollinson, H., 1993, Using geochemical data: evaluation, presentation, interpretation, Essex, Pearson Education Limited.

Rosenberg, C. L., and Stunitz, H., 2003, Deformation and recrystallisation of plagioclase along a temperature gradient: an example from the Bergell tonalite Journal of structural geology, v. 25, p. 389-408.

Rushmer, T., 1993, Experimental high-pressure granulites-some applications to natural mafic xenolith suites and Archean granulite terranes Geology, v. 21, p. 411-414.

Schroter, F. C., Stevenson, J. A., Daczko, N. R., Clarke, G. L., Pearson, N. J., and Klepeis, K. A., 2004, Trace element partioning during high-P partial melting and melt-rock interaction: an example from northern Fiordland, New Zealand: Journal of metamorphic Geology, v. 22, p. 443-457.

Shigematsu, N., 1999, Dynamic recrystallization on deformed plagioclase during progressive shear deformation: Tectnophysics, v. 305, p. 437-452.

Spiess, R., Groppo, C., and Compagnoni, R., 2007, When epitaxy controls garnet growth: J. metamorphic Geol., v. 25, p. 439-450.

Stowell, H., Tulloch, A., Zuluaga, C., and Koenig, A., 2010, Timing and duration of garnet granulite metamorphism in magmatic arc crust, Fiordland, New Zealand: Chemical Geology, v. 273, p. 91-110.

Sun, S.-s., and McDonough, W. F., 1989, Chemical and isotopic systematics of oceanic basalts: implications for mantle composition and processes Geological Society of London, v. 42, p. 313-345.